# Theoretical analysis of hybrid nanofluid flow by various stretching surfaces



QUAID-I-AZAM UNIVERSITY

ISLAMABAD

By

## Nadeem Abbas

### Department of Mathematics

Quaid-i-Azam University

Islamabad, Pakistan

2021

# Theoretical analysis of hybrid nanofluid flow by various stretching surfaces

By

## Nadeem Abbas

Supervised By

## Prof. Dr. Sohail Nadeem

### Department of Mathematics

Quaid-i-Azam University

Islamabad, Pakistan

2021

# Theoretical analysis of hybrid nanofluid flow by various stretching surfaces

By

## Nadeem Abbas

A DISSERTATION SUBMITTED IN THE PARTIAL FULFILLMENT OF THE REQUIREMENT

FOR THE DEGREE OF

### DOCTOR OF PHILOSOPHY

IN

MATHEMATICS

## Supervised by
## Prof. Dr. Sohail Nadeem

### Department of Mathematics
## Quaid-i-Azam University
## Islamabad, Pakistan
## 2021

# Author's Declaration

I, **Nadeem Abbas,** hereby state that my PhD thesis titled **Theoretical analysis of hybrid nanofluid flow by various stretching surfaces** is my own work and has not been submitted previously by me for taking any degree from the Quaid-I-Azam University Islamabad, Pakistan or anywhere else in the country/world.

At any time if my statement is found to be incorrect even after my graduate the university has the right to withdraw my PhD degree.

Name of Student: **Nadeem Abbas**

Date: **22-Feb-2021**

# Plagiarism Undertaking

I solemnly declare that research work presented in the thesis titled "**Theoretical analysis of hybrid nanofluid flow by various stretching surfaces**" is solely my research work with no significant contribution from any other person. Small contribution/help wherever taken has been duly acknowledged and that complete thesis has been written by me.

I understand the zero tolerance policy of the HEC and **Quaid-i-Azam University** towards plagiarism. Therefore, I as an Author of the above titled thesis declare that no portion of my thesis has been plagiarized and any material used as reference is properly referred/cited.

I undertake that if I am found guilty of any formal plagiarism in the above titled thesis even afterward of PhD degree, the University reserves the rights to withdraw/revoke my PhD degree and that HEC and the University has the right to publish my name on the HEC/University Website on which names of students are placed who submitted plagiarized thesis.

Student/Author Signature

Name: **Nadeem Abbas**

# Theoretical analysis of hybrid nanofluid flow by various stretching surfaces
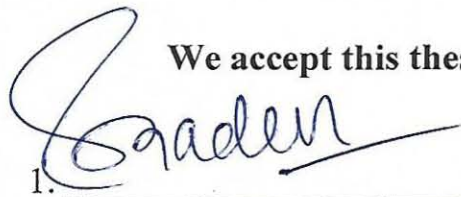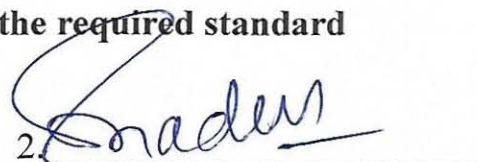
By

## Nadeem Abbas

CERTIFICATE

A THESIS SUBMITTED IN THE PARTIAL FULFILLMENT OF THE
REQUIREMENTS FOR THE DEGREE OF THE

## DOCTOR OF PHILOSOPHY IN MATHEMATICS

We accept this thesis as conforming to the required standard

1. _____

**Prof. Dr. Sohail Nadeem**
(Chairman)

2. _____

**Prof. Dr. Sohail Nadeem**
(Supervisor)

3. _____

**Dr. Rahmat Ellahi**
(External Examiner)

4. _____

**Dr. Muhammad Awais**
(External Examiner)

Department of Mathematics & Statistics,
Faculty of Basics Applied Sciences
International Islamic University, Islamabad.

Department of Mathematics, COMSATS
University Islamabad, Attock Campus,
Attock.

## Department of Mathematics
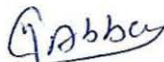## Quaid-I-Azam University
## Islamabad, Pakistan
## 2021

# Certificate of Approval

This is to certify that the research work presented in this thesis entitled **Theoretical analysis of hybrid nanofluid flow by various stretching surfaces** was conducted by **Mr. Nadeem Abbas** under the kind supervision of **Prof. Dr. Sohail Nadeem**. No part of this thesis has been submitted anywhere else for any other degree. This thesis is submitted to the Department of Mathematics, Quaid-i-Azam University, Islamabad in partial fulfillment of the requirements for the degree of Doctor of Philosophy in field of Mathematics from Department of Mathematics, Quaid-i-Azam University Islamabad, Pakistan.

Student Name: **Nadeem Abbas**                          Signature:_____

External committee:

a) **External Examiner 1**:                                Signature:_____

   Name: **Prof. Dr. Rahmat Ellahi**

   Designation: Associate Professor

   Office Address: Department of Mathematics & Statistics, Faculty of Basics Applied Sciences International Islamic University, Islamabad.
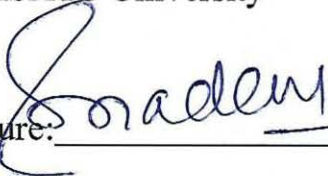
b) **External Examiner 2**:                                Signature:_____

   Name: **Dr. Muhammad Awais**

   Designation: Assistant Professor

   Office Address: Department of Mathematics, COMSATS University Islamabad, Attock Campus, Attock.
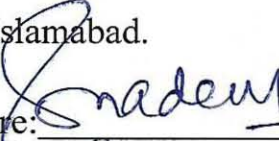
c) **Internal Examiner**                                    Signature:_____

   Name: **Prof. Dr. Sohail Nadeem**

   Designation: Professor

   Office Address: Department of Mathematics, QAU Islamabad.

   **Supervisor Name:**                                    Signature:_____
   **Prof. Dr. Sohail Nadeem**
   **Name of Dean/ HOD**                                   Signature:_____
   **Prof. Dr. Sohail Nadeem**

*This Thesis is dedicated to the Ideal personalities of my life,*

# *My Parents and Teachers*

*Your memories will remain alive in our hearts forever.*

## In the Name of Allah,
### The Most Gracious, The MostMerciful

# Acknowledgement

*"The will of the God will never take you where Grace of God will not protect"*

Although it is just my name mentioned on the cover, many people have contributed to this research in their own way and for that I want to give them special thanks. My first and foremost gratitude and thanks go to **Almighty Allah** for making me enable to proceed in this desertation successfully. Sure, all praise is for HIMwho created us as best of HIS creations and grant us strength, health. Knowledge, ability and opportunity to achieve our goals. I also express my sincere gratitude to **Holy Prophet Hazrat Muhammah S. A. W.** for guide us to right path by HIS teachings of patience, motivation and immense knowledge.

No research is possible without infrastructure and requisite materials and resource. At the very outset, I express deepest thanks to **Qauid-I-Azam University** for all the academic support to complete my degree as a PhD students.

I owe my gratitude to my esteemed surpervisor **Prof. Dr. Sohail Nadeem** for providing me this great opportunity to do my doctoral programed under his guidance and to learn from his research expertise. His support and advise helped me in all the time of research and writing of this thesis.

# Contents-

# Chapter 01

## Introduction

In the recent years, boundary layer flow and heat transfer analysis over a stretching surface have achieved a lot of success because of its numerous applications in the field of industries, engineering and technology due to their applications, namely, melt-spinning, wire drawing, assembly of rubber and plastic sheets, extrusion, the hot rolling, glass–fiber production, which may be an electrolyte etc. The filaments and polymer sheets are assembled with continuous extrusion of the polymer from a die to a windup roller that exists for away from the limited distance in the industry. In the past era, Crane [1] pioneered boundary layer flow caused by the stretching surface. Carragher and Crane [2] highlighted that the temperature contrast among the surrounding liquid and surface was relative to the control of the settled point. The conduct of Newtonian nanofluids could be valuable in assessing the chance of heat transfer improvement in different procedures of these industries. Wu [3] studied the boundary layer flow of water entry of twin wedges through a numerical scheme. Micropolar fluid flow at convective stretching sheet was debated by Haq et al. [4]. Ramesh [5] explored the results of slip effects with the convective conditions of peristaltic flow in a porous medium. Ramesh [6] also investigated the impression of inclined MHD in the inclined asymmetric channel. Gireesha et al. [7] investigated the Hall impact with MHD nanofluid and also worked on irregular heat consumption/generation. Gireesha et al. [8] deliberated the impressions of Hall and thermal radiation impacts at porous medium in the existence of suspension of fluid particles. Mahanthesh [9] explored the influence of dusty liquid with Hall effects at the stretching sheet. Gireesha et al. [10] analyzed the Hall effects on nano-material fluid at linear stretching sheet under the Hall effects. Gireesha et al. [11] examined the dusty fluid flow with Hall impacts under the nonlinear radiation at the stretching plate. Shalini and Mahanthesh [12] explained the nanomaterial dusty fluid with Rayleigh-Benard convection without/with Coriolis force. Recently, few investigators have discussed the behavior of fluid at various stretching surfaces under various assumptions at sheet see Refs. [13-15].

Within the past few protracted times, researchers have confronted a substantial problem of thermal efficiency in numerous industrial and engineering applications. Advance technology such as microfluidics, optical, chemical synthesis, high speed microelectronics, transportation, microsystems including electrical components and mechanical bears high thermal loads. In

such days, cooling specific systems is a key problem. The rate of heat transfer is typically boosted by adding the region accessible for heat transfer. An assist approach is to utilize a thermally viable liquid, which is regularly dispersed interior conventional heat transfer liquids, such as water, propylene glycol, ethylene glycol, etc. Heat transfer is the most important these days due to an energy crisis in the whole world. Choi [16] was the first person who worked on nanofluid. He used the nanoparticles in the base fluids. Before this idea, several authors analyzed the heat transfer rate enhancement, but Choi [16] achieved heat transfer rate more than two times as compared to conventional flow because of low thermal conductivity. Lee et al. [17] used oxide nanoparticle. The properties of the nanofluids were discussed by Das et al. [18]. They additionally brought a physical and chemical method for synthesizing nanofluids and also defined the methods for making a stable suspension of nanoparticles with the base fluids. They also analyzed the stagnation point flow at the convective stretching sheet. Mixed convection of nanomaterial fluid flow at porous wedge explored by Ellahi et al. [19]. Usman et al. [20] elaborated the effects of nanofluid flow within the nearness of the time-dependent warm conductivity and nonlinear radiations. Sheikholeslami et al. [21] worked on the nanofluid model under the assumptions of thermal radiations and natural convection flow at porous medium. Most interesting research on nanofluids can be seen in the Refs. [23-25].

In the Hybrid nanofluids, the study of heat transfer are more prominent and useful ways to enhance because of their lot of applications namely, biomedical, defence, generator cooling, automobile radiators and welding etc. At the mechanical level, there are positive highlights like chemical soundness and tall thermal usefulness, which empowers them to implement useful as compared to nanofluids. Suspension of two nanosized particles having base fluids namely hybrid nanofluid has been studied experimentally. In the early time, hybrid nanofluid flow analyzed experimental and numerical results by Suresh et al. [26-27]. They concluded that hybrid nanofluid gets more heat transfer rate as compared to ordinary fluid because improve the thermal conductivity of the liquid due to adding solid nanoparticles. The flow of hybrid nanofluid with multiwall/spherical silica nanotubes has discussed by Baghbanzadeh et al. [28]. Esfe et al. [29] studied the MWCNTs with base fluid and their characteristics of thermal conductivity. Hayat and Nadeem [30] analyzed the flow behavior of the hybrid nanoparticles with base fluid at a stretching surface. Muhammad and Nadeem [31] achieved the effects of the ferromagnetic nanomaterial with base fluid. Theoretical and analytically performance of the hybrid nanofluid has initiated by the investigators [32-34].

Normally, Newtonian liquids are weak to project engineering arrangement like as suspended particles, liquid having materials comprising fibrous organization. Micropolar fluid theory may describe the internal movement and deforming of these substances which are called micropolar fluids and was explored by Eringen [35]. He analyzed the jumped conditions and imitative the constitutive equations. Non-Newtonian fluid models are useful for studying in polymer suspension fluid actions, colloidal solutions, biological fluids, messy liquids, etc. Micropolar fluid through radiation impressions is evaluated by Alla et al. [36] in the occurrence of porous medium. These initiative results are taken much attracted to the researchers. Magnetized micropolar fluid over a stretching disk was pioneered by Rauf et al. [37]. They also worked out to gain the results of thermal radiation. The stagnation flow of a micropolar fluid under the assumptions of stretching surface with buoyancy and radiation effects has explored by Haq et al. [38]. Pal and Mandal [39] have pioneered thermal radiation and MHD in the occurrence of non-uniform heat sink or source of the micropolar fluid. Influences of electrical magnetic hydrodynamics and Hall current of micropolar fluid are discussed by Shah et al. [40]. Recently, a few pieces of research have been studied to analyze the flow behavior of micropolar fluid for different flow assumptions, see Refs. [41-44].

Motivated from the above highlights, the aim of the presented study is to deliberate the boundary layer flow of hybrid nanofluid at stretching surfaces. This thesis consists of 8 chapters in which chapter one is the introductory chapter.

Three dimensional flow of hybrid nanofluid over a circular cylinder having sinusoidal radius variation is deliberated in chapter 2. The governing equation of motion for three dimensional flows is simplified under the assumption as of the boundary layer theory. Furthermore, the suitable similarity transformations are applied in developing a mathematical model simplification and non dimensionalization. The simplified model is solved through numerical scheme. The results of the solid nanoparticle concentrations, and thermal slip, dimensionalization saddle and nodal points are calculated at a surface of the cylinder and presented through graphs and tables. This chapter has been published in **''Results in Phy** **2018, 8: 829- 8 3 5** https://doi.org/10.1016/j.rinp.2018.01.024.

Three dimensional flow of based micropolar hybrid nanofluid over a circular cylinder is discussed in chapter 3. The flow due to the stagnation point at a stretching surface is modeled in term of partial differential equations. The simplified model is solved through numerical scheme.

The influence of magnetic hydrodynamics, thermal and velocity slip, solid nanoparticle concentrations, Nusselt number and skin frictions presented through graphs and tables. This chapter has been published in ''Canadian Journal of -3P9h9y's'ics, https://doi.org/10.1139/cjp-2018-0173.

Steady of 3D stagnation point flow of hybrid nanofluid over a moving surface having anisotropic slip is analyzed in chapter 4. No slip condition is replaced through the partial slip condition. Such anisotropic slip happens in geometrically striated surface and super hydrophobic stripes. Using the experimental values, we have discussed the hybrid nanofluid theoretically for boundary layer flow due to stagnation point flow. The mathematical model is considered under the flow behavior. The boundary layer approximation and similarity transformations are applied on mathematical model. The dimensionless model further solved through numerical scheme. The effects on a moving surface with anisotropic slip are presented in term of graphs and tables. This chapter has been published in ''Physica alA: Stat Mechanics and its Applications, 2020, 5 5 4 ( 1 5 ) : https2/d4i0r2/10.1016/j.physa. 2019.124020.

Computational analysis of water based $Cu - Al_2O_3/H_2O$ flow over a vertical wedge is presented in chapter 5. Two kinds of solid nanoparticles with base fluid at vertical Riga wedge is studied. Thermal and velocity slip impacts on vertical Riga wedge are investigated in the current study. We discussed both the unsteady and steady cases. The water has low thermal conductivity. We added the nanoparticle $Cu$ and $Al_2O_3$ which increases the thermal conductivity of the base fluid. This phenomena increase the heat transfer rate at the surface Riga plate. Partial differential equations are reduced into an ordinary differential equation by means of dimensionless similarity variables. The resulting ordinary differential equations are further elucidated through numerical and perturbation methods. Thickness of momentum boundary layer is declined because of the solid nanoparticle rises in all cases of $\xi = 0$, $(2i\xi)^0$, $(2i\xi)^1$ and $(2i\xi)^n$. This chapter has been published in ''Advances in Mechar Engineering, 2020, 20-0197(11): 1 –1 0. https://doi.org/10.1177/1687814020968322

The steady of based micropolar hybrid nanofluid at a Riga curved surface is analyzed in chapter 6. Two diverse varieties of the nanoparticles are studied at the curved surface. The effects of thermal and velocity slip on the curved surface are discussed. The governing equations of the motions for the micropolar hybrid nanofluid flow are simplified under the assumptions of boundary layer theory. The system of differential equations is simplified and

4

dimensionalized. Furthermore, the dimensionalized system is solved by a numerical procedure. The results of the thermal and velocity slip, curvature parameter, micro rotation parameter, and solid nanoparticle concentration at the curved surface are highlighted in graphs and tables. This chapter has been published in **'' P h y s i c a   A :   S t a t i s t i c a l   M e c h a n i c s   a n d   i t s   A p p l i c a t i o n s ,  2 0 2 0 , 551(1): 1 2 4 0 8 3 ''** https://doi.org/10.1016/j.physa.2019.124083.

Flow of micropolar hybrid nanofluid at the curved surface is analyzed in chapter 7. Stagnation point flow with Yamada-Ota and Xue models properties are applied on the hybrid nanofluid. The system under the flow suppositions has established and dimensionless through similarity transformations. Furthermore, the results of the dimensionless system built through numerical procedure. This chapter has been published in **'' P h y s i c a   A :   S t a t i s t i c a l   M e c h a n i c s   a n d   i t s   A p p l i c a t i o n s ,  2 0 2 0 ,   5 4 2  ( 5 ) :  1 2 3 5 1 2 ''** https://doi.org/10.1016/j.physa. 2019.123512.

Flow of hybrid nanofluid at the moving needle is analyzed in chapter 8. Two different nanoparticles are discussed, namely: SWCNT and MWCNT with base fluid pure water. The system under the flow assumptions has developed and dimensionless through similarity transformations. Furthermore, the results of the dimensionless system built through the numerical procedure. The effects of the governing parameters are discussed through tables and graphs. This chapter has been published in **" The European Physical Journal Plus, 2020, 135(2): 145 ''** https://doi.org/10.1140/epjp/s13360-020-00185-2.

# Nomenclature

| | |
|---|---|
| $V, W$ | Velocity components, $m/s$ |
| $\mu_{hnf}$ | Dynamic viscosity of Hybrid Nanofluid, $kg/ms$ |
| $\nu_{hnf}$ | Kinematic viscosity of hybrid Nanoluid, $m^2/s$ |
| $\rho_{hnf}$ | Density of Hybrid Nanofluid, $kg/m^3$ |
| $\alpha_{hnf}$ | Thermal diffusivity of Hybrid Nanofluid |
| $k_{hnf}$ | Thermal conductivity of Hybrid Nanoflui |
| $p$ | Pressure, $kg/ms^2$ |
| $\rho c_{p_{hnf}}$ | Heat capacitance of Hybrid Nanofluid |
| $T$ | Temperature of the fluid |
| $t$ | Dimensional time, $s$ |
| $Nu$ | Nusselt number |
| $\Phi_1, \Phi_2$ | Nanoparticles concentration |
| $Ri$ | Richardson number |
| $\mu_{nf}$ | Dynamic viscosity of Nanofluid, $kg/ms$ |
| $\nu_{nf}$ | Kinematic viscosity of Nanoluid, $m^2/s$ |
| $\rho_{nf}$ | Density of Nanofluid, $kg/m^3$ |
| $\alpha_{nf}$ | Thermal diffusivity of Nanofluid |
| $k_{nf}$ | Thermal conductivity of Nanofluid |
| $\sigma$ | Dimensionless parameter |
| $\zeta$ | Dimensionless similarity variable |
| $\rho c_{p_{nf}}$ | Heat capacitance of Nanofluid |
| $M$ | Modified Hartman number |
| $Re$ | Reynolds number |
| Pr | Prandtl number |
| $X, Y, Z$ | Direction components |
| $R$ | Curvature (m) |
| $K$ | Micropolar parameter |
| $K_1$ | Curvature parameter |
| $a^*$ & $b^*$ | Stretching parameter |
| $\tau_{WX}$ & $\tau_{WY}$ | Shear stress |
| $F, G$ | Velocity profile (Dimensionless) |
| $N_1$ & $N_1$ | Micropolar profile |
| $H, Q$ | Micropolar profile (Dimensionless) |

# Chapter 02

## 3D stagnation flow of hybrid nanofluid over a circular cylinder sinusoidal radius variation

## 2.1  Introduction

In this chapter, analysis of 3D flow of hybrid nanofluid flow at circular cylinder with sinusoidal radius variation are discussed. The stagnation point flow is also discussed with saddle or nodal points. Thermal slip effects analyzed at the surface of circular cylinder with sinusoidal radius variation. The properties $Cu$ copper and $Al_2O_3$ aluminum with ordinary fluid are analyzed in this chapter. The governing equations of motion for three dimensional flows are simplified under the assumptions of boundary layer theory. The suitable similarity transformations are applied to develop a mathematical model  simplification and non dimensionlization. The simplified model is solved through a numerical technique. The results of skin friction, Nusselt number, solid nanoparticle concentration, thermal slip and saddle or nodal points are presented through graphs and tables. Surprisingly, the velocities along X- axis and Y- axis show increasing attitude towards $\Phi_2$ When the thermal slip is considereded. The significant amount of heat transfer is observed for the $Cu-Al_2O_3$/water with that of $Cu$/water at the both saddle and nodal points. For positive values of the thermal slip parameter, temperature for both nanofluid and hybrid nanofluid are declining.

## 2.2  Mathematical formulation

Three dimensional time independent flow of hybrid nanofluid towards circular cylinder is considered. The radius of the cylinder varies sinusoidally as seen in Fig. 2.1. At the each point $M$, $N$ and $O$ (maximum and minimum radii), there exists a stagnation point.  The attachment lines divide the flow, which passes through the side or through the cylinder at points $M$ to $N$ and $O$ to $N$. The uniform ambient temperature is $T_\infty$, the constant wall temperature at surface is  $T_w$. We initially investigated the boundary layer flow in the area of the nodal stagnation point $M$. With $M$ taken as the inception, we present a facilitate framework with $X$-axis in the upward way, $Y$ in the longitudinal direction and $Z$ normal to the surface. The velocities along $X-$ direction, $Y-$ direction and $Z-$ direction are represented as $U$, $V$ and $W$ respectively. We have chosen (see the Ref. [45])

$$u_e^* = a^*X, \qquad v_e^* = b^*Y,$$

where, $b^*$ and $a^*$ are free stream dependent constants. It might be noticed that the amounts $u_e^*$ and $v_e^*$ don't fulfill the condition of equation of continuity. There is no misfortune of generality in requiring that $|a^*| \geq |b^*|$ having $a^* > 0$ presents in case of plane stagnation flow and $a^* = b^*$ case for axisymmetric flow of stgantion. The flow of stream lines is given by the equation $X_e^* = \beta Y^{1/c}$ where $c = b^*/a^*$, and $\beta$ is a constant which presents a particular streamline. The attachment lines of the nodal stagnation point range is $0 < c < 1$ while the attachment lines of the saddle stagnation point range is $-1 < c < 0$. If $c = 0$ then flow is plane.
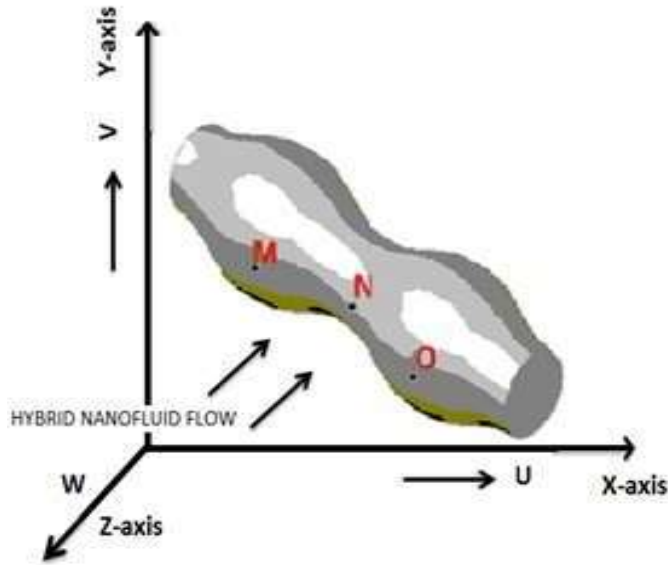


**Fig. 2.1:** Flow pattern of the physical model.

The ultimate flow narrating equations are

$$\frac{\partial U}{\partial X} + \frac{\partial V}{\partial Y} + \frac{\partial W}{\partial Z} = 0, \tag{2.1}$$

$$U\frac{\partial U}{\partial X} + V\frac{\partial U}{\partial Y} + W\frac{\partial U}{\partial Z} = a^{*2}X + v_{hnf}\frac{\partial^2 U}{\partial^2 Z}, \tag{2.2}$$

$$U\frac{\partial V}{\partial X} + V\frac{\partial V}{\partial Y} + W\frac{\partial V}{\partial Z} = b^{*2}Y + v_{hnf}\frac{\partial^2 V}{\partial^2 Z}, \tag{2.3}$$

$$U\frac{\partial T}{\partial X} + V\frac{\partial T}{\partial Y} + W\frac{\partial T}{\partial Z} = \alpha_{hnf}\frac{\partial^2 T}{\partial^2 Z}, \tag{2.4}$$

the boundary conditions are

$$U = 0, \quad V = 0, \quad W = 0, \ \gamma k_{hnf}\frac{\partial T}{\partial Z} = T - T_w, \ \text{when } Z = 0, \tag{2.5}$$

$$U \rightarrow u_e^*, \quad V \rightarrow v_e^*, \quad T \rightarrow T_\infty, \ \text{when } Z \rightarrow \infty. \tag{2.6}$$

8

Where, $T$, $U$, $V$ & $W$ are temperature and velocity element $X$, $Y$ and $Z$ directions.

## 2.3  Similarity transformations

Introducing the following transformable variables

$$U = a^* X F'(\zeta), \quad V = b^* Y G'(\zeta), \quad W = -\sqrt{a^* v_f}\,(F(\zeta) + cG(\zeta)),$$

$$T = T_\infty + (T_w - T_\infty)\Theta(\zeta), \qquad \zeta = Z\sqrt{\left(\frac{v_f}{a^*}\right)}. \tag{2.7}$$

By utilizing theses on the Eqs. (2.1)-(2.6), resultant equations are presented as

$$\frac{1}{(1-\Phi_1)^{2.5}(1-\Phi_2)^{2.5}\left[\left\{(1-\Phi_2)\left(1-\Phi_1+\Phi_1\frac{(\rho)_{s_1}}{(\rho)_f}\right)\right\}+\Phi_2\frac{(\rho)_{s_2}}{(\rho)_f}\right]}F''' + cG\,F''$$

$$- F'^2 + F\,F'' + 1 = 0, \tag{2.8}$$

$$\frac{1}{(1-\Phi_1)^{2.5}(1-\Phi_2)^{2.5}\left[\left\{(1-\Phi_2)\left(1-\Phi_1+\Phi_1\frac{(\rho)_{s_1}}{(\rho)_f}\right)\right\}+\Phi_2\frac{(\rho)_{s_2}}{(\rho)_f}\right]}G''' + FG''$$

$$+ cGG'' - cG'^2 + c = 0, \tag{2.9}$$

$$\frac{\frac{\kappa_{hnf}}{\kappa_f}}{Pr\left[\left\{(1-\Phi_2)\left(1-\Phi_1+\Phi_1\frac{(\rho C_p)_{s_1}}{(\rho C_p)_f}\right)\right\}+\Phi_2\frac{(\rho C_p)_{s_2}}{(\rho C_p)_f}\right]}\Theta'' + F\Theta' + cG\Theta' = 0, \tag{2.10}$$

$$F(0) = 0, \quad F'(0) = 0, \quad F'(\infty) \to 1, \tag{2.11}$$

$$G(0) = 0, \quad G'(0) = 0, \quad G'(\infty) \to 1, \tag{2.12}$$

$$\Theta(0) = 1 + \delta\frac{\kappa_{hnf}}{\kappa_f}\Theta'(0), \quad \Theta(\infty) \to 0. \tag{2.13}$$

Here, prime represents derivative with respect to $\zeta$, $\delta$ is the thermal slip parameter. $F(\zeta)$ and $G(\zeta)$ represent the velocity profiles along $X-$ and $Y-$ direction respectively, $\Theta$ represents the temperature profile. The quantities of interest for this chapter are $Nu_x$ ''Nusselt number'' and $C_{fX}$ and $C_{fY}$ ''skin friction coefficients'' along $X-$ and $Y-$ directions, respectively which are characterized mathematically as

$$C_{fX} = \frac{\tau_{WX}}{\rho_f U_W^2}, \qquad C_{fY} = \frac{\tau_{WY}}{\rho_f U_W^2}, \qquad Nu_x = \frac{Xq_W}{k_f(T_W - T_\infty)}, \tag{2.14}$$

here $\tau_{WX}$ and $\tau_{WY}$ are the shear stresses and $q_W$ is t surface heat flux which are

$$\tau_{WX} = [\mu_{hnf}\frac{\partial U}{\partial Z}]_{Z=0}, \tau_{WY} = [\mu_{hnf}\frac{\partial V}{\partial Z}]_{Z=0}, \tag{2.15}$$

$$q_W = -k_{hnf}\left(\frac{\partial T}{\partial Z}\right)_{Z=0}.$$

By engaging Eqs. (2.14) and (2.15), one can acquire the reduced form

$$\sqrt{Re_X}\, C_{fX} = \frac{F''(0)}{(1-\Phi_1)^{2.5}(1-\Phi_2)^{2.5}}, \tag{2.16}$$

$$(X/Y)\sqrt{Re_X}\, C_{fY} = \frac{cG''(0)}{(1-\Phi_1)^{2.5}(1-\Phi_2)^{2.5}}, \tag{2.17}$$

$$\frac{Nu_X}{\sqrt{Re_X}} = -\frac{k_{hnf}}{k_f}\Theta'(0). \tag{2.18}$$

**Table 2.1: Thermo-physical properties**

| Properties | Nanofluid | Hybrid nanofluid |
|---|---|---|
| Viscosity | $\mu_{nf} = \dfrac{\mu_f}{(1-\Phi)^{2.5}}$ | $\mu_{hnf} = \dfrac{\mu_f}{(1-\Phi_1)^{2.5}(1-\Phi_2)^{2.5}}$ |
| Heat capacity | $(\rho C_p)_{nf} = (1-\Phi)(\rho C_p)_f + \Phi(\rho C_p)_s$ | $(\rho C_p)_{hnf} = [\{(1-\Phi_2)(1-\Phi_1)(\rho C_p)_f\} + \Phi_1(\rho C_p)_{s_1}] + \Phi_2\rho(\rho C_p)_{s_2}$ |
| Thermal conductivity | $\dfrac{\kappa_{nf}}{\kappa_f} = \dfrac{\kappa_s + (n-1)\kappa_f - (n-1)\Phi(\kappa_f - \kappa_s)}{\kappa_s + (n-1)\kappa_f + \Phi(\kappa_f - \kappa_s)}$ | $\dfrac{\kappa_{hnf}}{\kappa_{bf}} = \dfrac{\kappa_{s_2} + (n-1)\kappa_{bf} - (n-1)\Phi_2(\kappa_{bf} - \kappa_{s_2})}{\kappa_{s_2} + (n-1)\kappa_{bf} + \Phi_2(\kappa_{bf} - \kappa_{s_2})}$ where $\dfrac{\kappa_{bf}}{\kappa_f} = \dfrac{\kappa_{s_1}+(n-1)\kappa_f-(n-1)\Phi_1(\kappa_f-\kappa_{s_1})}{\kappa_{s_1}+(n-1)\kappa_f+\Phi_1(\kappa_f-\kappa_{s_1})}$ |
| Density | $\rho_{nf} = (1-\Phi)\rho_f + \Phi\rho_s$ | $\rho_{hnf} = \{[(1-\Phi_2)(1-\Phi_1)\rho_f\} + \Phi_1\rho_{s_1}] + \Phi_2\rho_{s_2}$ |

**Table 2.2: Thermo-physical characteristics are delebrated.**

| Thermo-physical properties | Fluid phase (water) | $Al_2O_3$ | Cu |
|---|---|---|---|
| $C_p(j/kg)K$ | 4179 | 765 | 385 |
| $\rho(kg/m^3)$ | 997.1 | 3970 | 8933 |
| $k(W/mK)$ | 0.613 | 40 | 400 |
| $\alpha \times 107(m^2/s)$ | 1.47 | 131.7 | 1163.1 |

**Table. 2.3: Compression with existing literature for the values of $\sqrt{Re_X}\, C_{fX}$, $\sqrt{Re_X}\, C_{fY}$ and $\frac{Nu_X}{\sqrt{Re_X}}$ when δ=0.0 and $\Phi_2 = 0.0$.**

| | $\Phi_1$ | $\sqrt{Re_X}\, C_{fX}$ | | $\sqrt{Re_X}\, C_{fX}$ | | $\frac{Nu_X}{\sqrt{Re_X}}$ | |
|---|---|---|---|---|---|---|---|
| | | [46] | Present | [46] | Present | [46] | Present |
| Cu | 0.0 | 1.2681 | 1.2680 | 0.4993 | 0.4991 | 1.3301 | 1.3299 |
| | 0.1 | 1.9387 | 1.9387 | 0.7630 | 0.7627 | 1.6185 | 1.6183 |
| | 0.2 | 2.6968 | 2.6966 | 1.0617 | 1.0616 | 1.9293 | 1.9293 |

| $Al_2O_3$ | 0.0 | 1.2681 | 1.2678 | 0.4993 | 0.4991 | 1.3301 | 1.3298 |
|---|---|---|---|---|---|---|---|
| | 0.1 | 1.6482 | 1.6480 | 0.6487 | 0.6485 | 1.5726 | 1.5725 |
| | 0.2 | 2.1176 | 2.1175 | 0.8334 | 0.8333 | 1.8172 | 1.8171 |
| $TiO_2$ | 0.0 | 1.2681 | 1.2678 | 0.4993 | 0.4991 | 1.3301 | 1.3298 |
| | 0.1 | 1.6657 | 1.6656 | 0.6557 | 0.6556 | 1.4956 | 1.4955 |
| | 0.2 | 2.1530 | 2.1528 | 0.8477 | 0.8774 | 1.7386 | 1.7385 |

**Table. 2.4: Variation in skin friction coefficients**

| $\Phi_2$ | $Cu - Al_2O_2/water$ | | $Cu/water$ | |
|---|---|---|---|---|
| | $\sqrt{Re_X}\,C_{fX}$ | $(X/Y)\sqrt{Re_X}\,C_{fY}$ | $\sqrt{Re_X}\,C_{fX}$ | $(X/Y)\sqrt{Re_X}\,C_{fY}$ |
| **0.005** | 1.2688 | 0.3886 | 1.2767 | 0.3910 |
| **0.04** | 1.4538 | 0.4453 | 1.5033 | 0.4605 |
| **0.06** | 1.5623 | 0.4785 | 1.6340 | 0.5005 |
| **0.08** | 1.6731 | 0.5125 | 1.7664 | 0.5410 |

**Table 2.5. Variation in local Nusselt numbers**

| $\Phi_2$ | $\delta$ | $Cu - Al_2O_2/water$ $\dfrac{NU_X}{\sqrt{Re_X}}$ | $Cu/water$ $\dfrac{NU_X}{\sqrt{Re_X}}$ |
|---|---|---|---|
| **0.005** | 0.5 | 0.4572 | 0.4605 |
| **0.04** | - | 0.4804 | 0.4858 |
| **0.06** | - | 0.4930 | 0.4991 |
| **0.08** | - | 0.5052 | 0.5119 |
| - | 0.0 | 0.7869 | 0.8021 |
| - | 0.5 | 0.4804 | 0.4858 |
| - | 1.0 | 0.3457 | 0.3484 |
| - | 1.5 | 0.2701 | 0.2716 |

## 2.4   Results and discussion

In this analysis, the range of parameters are taken as $0.005 \leq \Phi_2 \leq 0.09$, $-0.5 \leq c \leq 0.5$, $0 \leq \delta \leq 1.5$ and $\Phi_1 = 0.1$(fixed). The physical circumstance is modeled in terms of differential equations while are solved by utilizing shooting method. The resulting consequences are expressed through graphs and tables. In detail, Table 2.1 reports the thermophysical characteristics of nanofluid and hybrid nanofluid, while, Table 2.2 provides the thermal physical properties of nanoparticles at 25°C. The variation of $\sqrt{Re_X}\,C_{fX}$, $\sqrt{Re_X}\,C_{fY}$ and $\frac{Nu_X}{\sqrt{Re_X}}$ are given in Table 2.3 when $\delta = 0.0$ and $\Phi_2 = 0.0$. It is also observed that our results matche with Refs. [46] which confirms the execution of the numerical scheme. It is also found that

$\sqrt{Re_X}\,C_{fX}$, $(X/Y)\sqrt{Re_X}\,C_{fY}$ and $\frac{Nu_X}{\sqrt{Re_X}}$ are accelerating a function of $\Phi_1$ for each Cu, $Al_2O_3$ and

$TiO_2$. Table 2.4 represents the variations of skin friction coefficients $\sqrt{Re_X}\,C_{fX}$ and $(X/Y)\sqrt{Re_X}\,C_{fY}$ for both the $Cu - Al_2O_3$/water and Cu/water. It is seen from Table 2.4 that the

$\sqrt{Re_X}\,C_{fX}$ and $(X/Y)\sqrt{Re_X}\,C_{fY}$ are improving function of $\Phi_2$ for each $Cu - Al_2O_3$/water and Cu/water. Similarly, Table 2.5 reports the variations in local Nusselt number for the higher values of both $\delta$ and $\Phi_2$ towards $Cu - Al_2O_3$/water and Cu/water.

Fig. 2.1 is a physical illustration of flow problem while Figs. 2.2-2.11 are used to explain the effects of involved parameters, namely $\delta$ and $\Phi_2$ on both Hybrid nanofluid and nanofluid flow along X and Y-axis under the different assumptions. Particularly, Figs. 2.2 and 2.3 reveal the distinction of velocity profiles for the distinct values of $\Phi_2$. For Hybrid nanofluid ($Cu - Al_2O_3$/water), thickness of boundary layer is developed for velocity profiles ($F'(\zeta)$ and $G'(\zeta)$) as compared to nanofluid (Cu/water) and the velocity profile reduces by growing $\Phi_2$ in the absence of thermal slip parameter $\delta = 0.0$. The effects of $\Phi_2$ on Hybrid nanofluid velocity along both X and Y-axis at saddle and nodal points is specified in Fig. 2.4 and Fig. 2.5 correspondingly. It is realized that velocities are growing function of $\Phi_2$ at both nodal and saddle points. The impact of $\Phi_2$ on both nanofluid and Hybrid nanofluid velocities along X and Y-axis when thermal slip effects are presented in Figs. 2.6 and 2.7. One can see from these figures that the velocities are increasing function of $\Phi_2$. The effect of $\Phi_2$ on nanofluid and Hybrid nanofluid on temperature at $\delta = 0.0$ is depicted in Fig. 2.8. It is noted that the growing values of $\Phi_2$ exceeds the temperature. The effects of $\Phi_2$ on temperature profile at both nodal and saddle points are given in Fig. 2.9. One can see that the temperature profile is swelling function $\Phi_2$ at both nodal and saddle points. The impacts of the $\Phi_2$ and $\delta$ on temperature profile are revealed in Figs. 2.10 and 2.11. The significant growth in temperature profile is revealed in Fig. 2.10, due to increasing values of the solid nanoparticle $\Phi_2$ for both Hybrid nanofluid and nanofluid. The temperature distribution shows decline curves via thermal slip parameter for ($Cu - Al_2O_3$/water) and (Cu/water). Fig. 2.11 is evident in this regard. Increment in solid nanoparticle accelerates the velocity flow that obviously increases the skin friction coefficient for both ($Cu - Al_2O_3$/water) Hybrid nanofluid and (Cu/water) nanofluid that depicts in Table 2.4. It is observed that non-dimensional heat transfer improves due to enhance in solid volume fractions, which is revealed in Table 2.5. From Table 2.5, it is pointed

that the non-dimensional rate of heat transfer through $Cu - Al_2O_3$/water is larger than that of Cu/water. The heat transfer rate improves significantly for the both $(Cu - Al_2O_3$/water) Hybrid nanofluid and (Cu/water) nanofluid which are seen in the Table 2.5.

## 2.5 Closing remarks

To report the flow properties of both Cu/water and $Cu - Al_2O_3$/water models, a comparative analysis is executed. The fluid flow is past a circular cylinder under the stagnation point assumption. The role of the thermal slip parameter is also taken into account. The summary of the presented work is itemized as follows:

- In the absence of thermal slip effect, the velocities along $X -$ axis and $Y -$ axis for Cu/water and $Cu - Al_2O_3$/water are decreasing function of $\Phi_2$.

- The velocities along X- axis and Y- axis shows increasing when $\Phi_2$ and thermal slip are considered increasing.

- The significant amount of heat transfer is observed for the $Cu - Al_2O_3$/water with that of Cu/water at the both saddle and nodal points.

- For positive values of the thermal slip parameter, temperature of the both nanofluid and Hybrid nanofluid are declining function.

**Fig. 2.2**
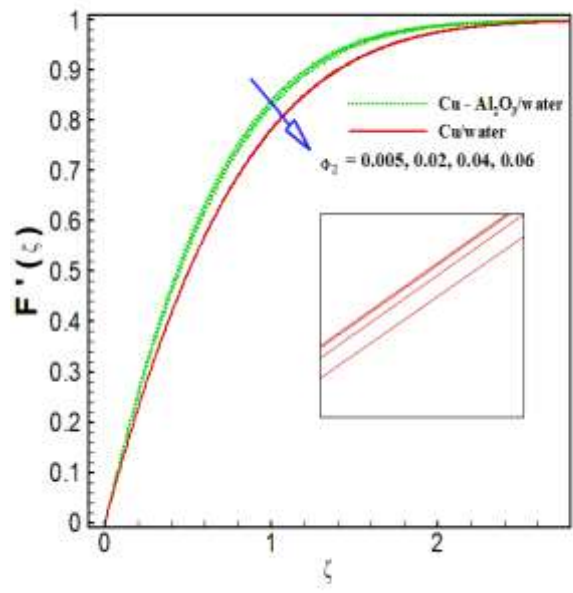


Fig. 2.2: Effect of $\Phi_2$ on both Cu/water and $Cu - Al_2O_3$/water velocity profile (along X-axis) when $\delta = 0.0$.

**Fig. 2.3**
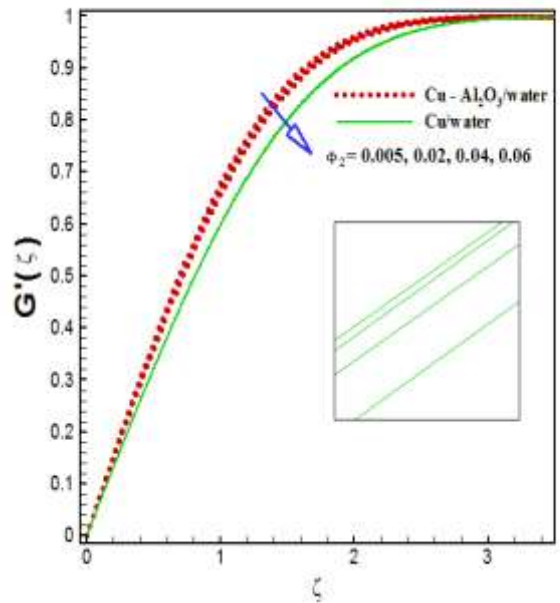


Fig. 2.3: Effect of $\Phi_2$ on both Cu/water and $Cu - Al_2O_3$/water velocity profile (along Y-axis) when $\delta = 0.0$.

**Fig. 2.4**
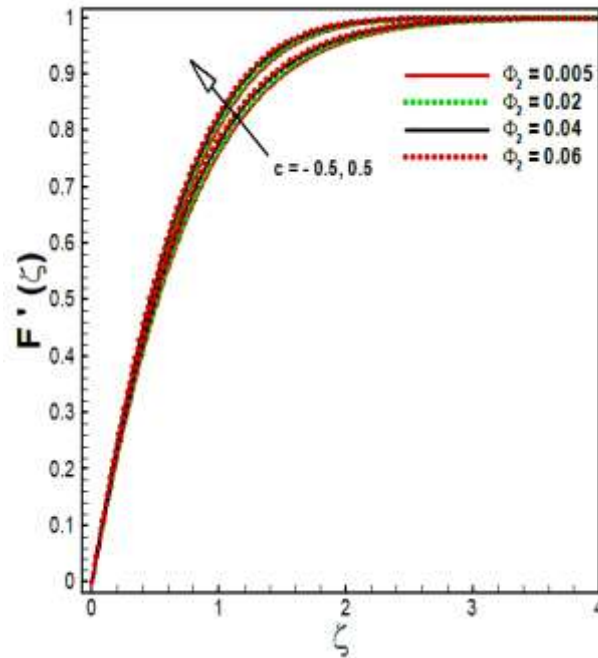


Fig. 2.4: Effect of $\Phi_2$ on Hybrid nanofluid velocity profile (along X-axis) at the both saddle and nodal points.

**Fig. 2.5**
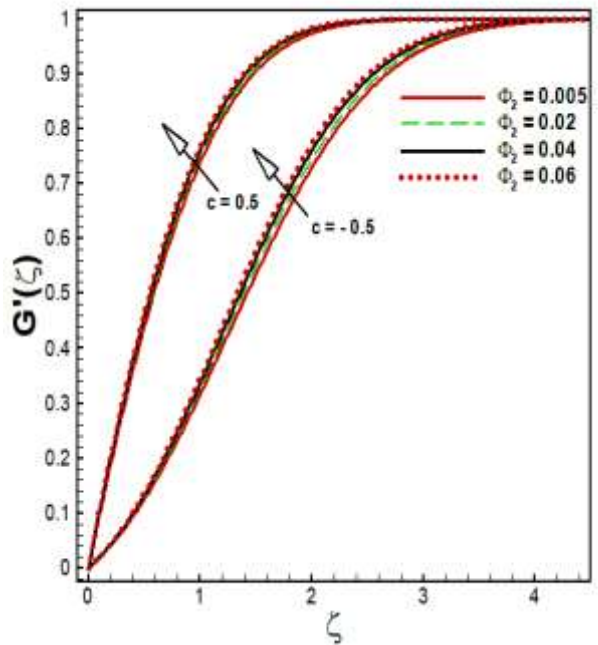


Fig. 2.5: Effect of $\Phi_2$ on Hybrid nanofluid velocity profile (along Y-axis) at the both saddle and nodal points.

**Fig. 2.6**
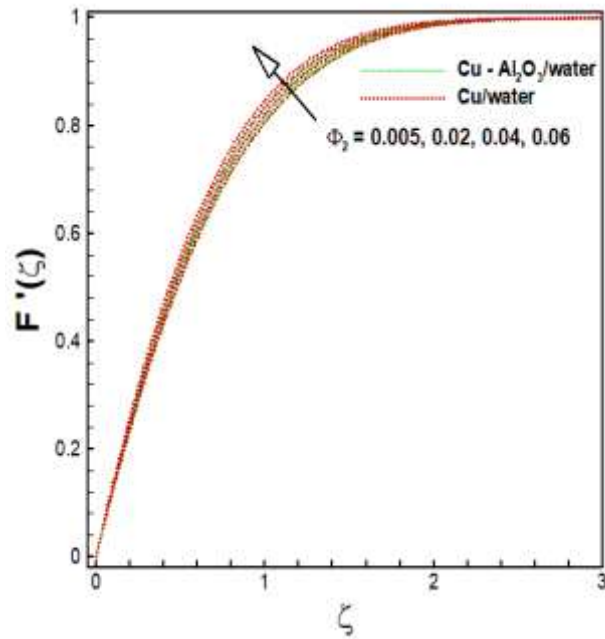


Fig. 2.6: Effect of $\Phi_2$ on both Cu/water and Cu $-$ Al$_2$O$_3$/water velocity profile (along X-axis) when $\delta = 0.6$.

**Fig. 2.7**
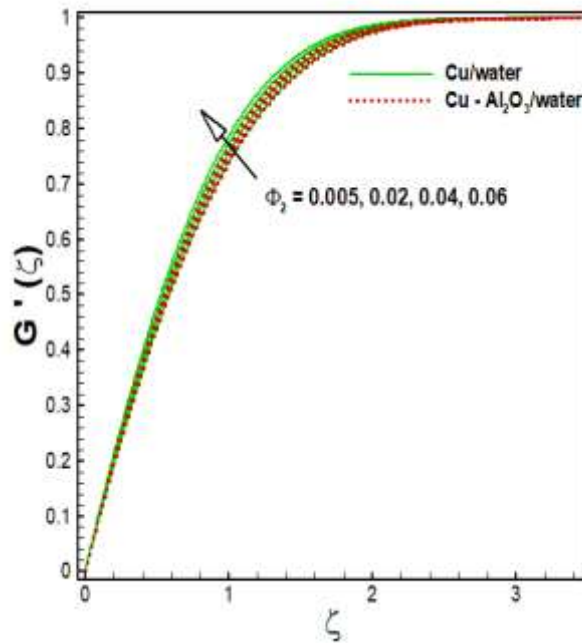


Fig. 2.7: Effect of $\Phi_2$ on both Cu/water and Cu $-$ Al$_2$O$_3$/water velocity profile (along Y-axis) when $\delta = 0.6$.

**Fig. 2.8**
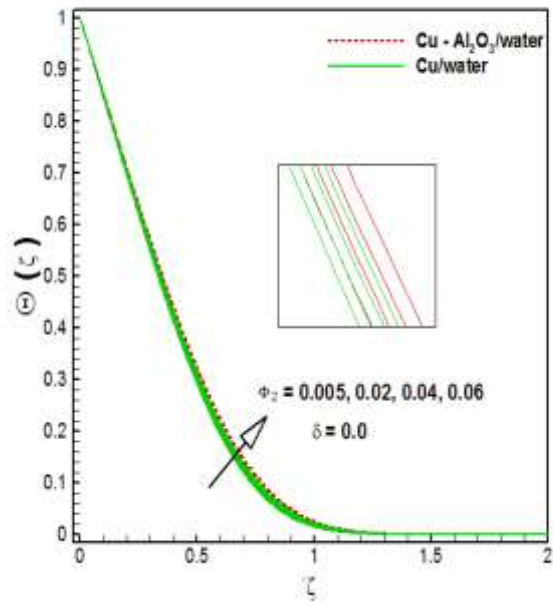


Fig. 2.8: Effect of $\Phi_2$ on both Cu/water and $Cu - Al_2O_3$/water temperature profile when $\delta = 0.0$.

**Fig. 2.9**



Fig. 2.9: Effect of $\Phi_2$ on Hybrid nanofluid temperature profile at the both saddle and nodal points.

**Fig. 2.10**



Fig. 2.10: Effect of $\Phi_2$ on both Cu/water and $Cu - Al_2O_3$/water temperature profile when $\delta = 0.6$.
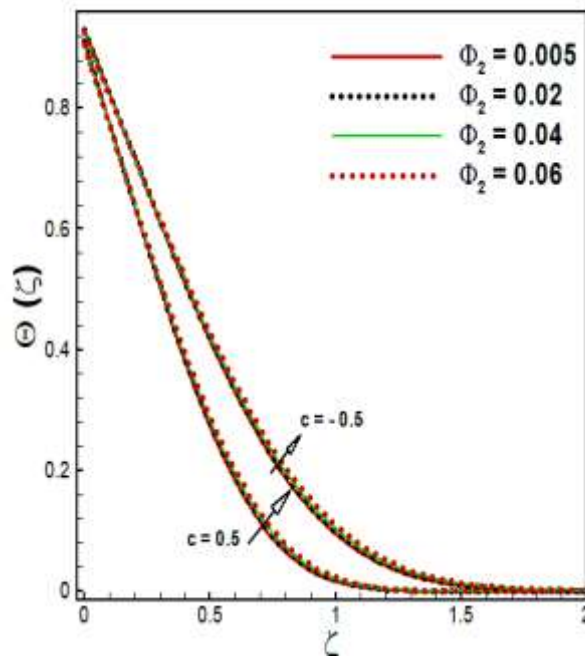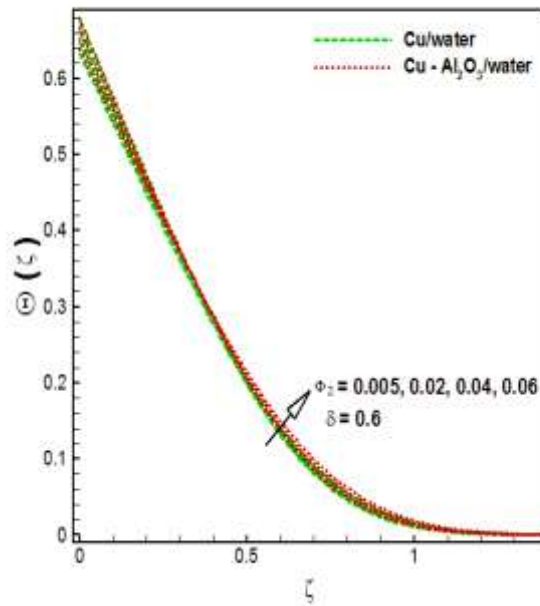
**Fig. 2.11**
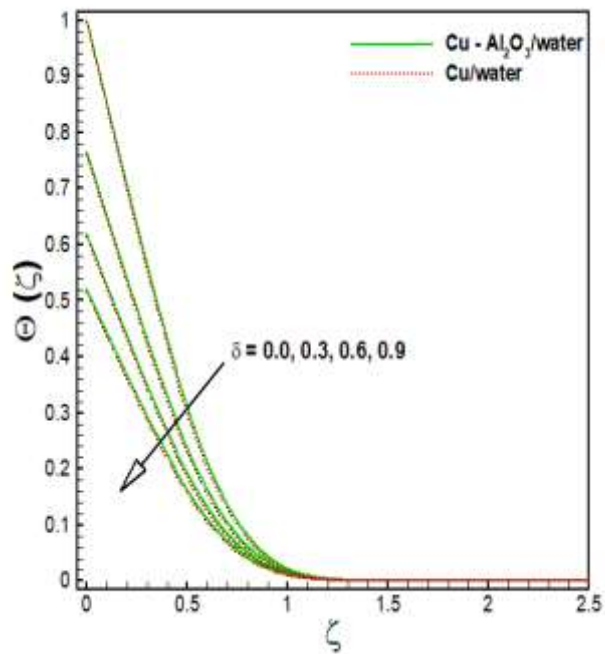


Fig. 2.11: Effect of $\delta$ on both Cu/water and $Cu - Al_2O_3$/water temperature profile.

# Chapter 03

## MHD and slip effects in micropolar Hybrid nanofluid past a circular cylinder under stagnation point region

### 3.1 Introductions

In this chapter, three dimensional flow based micropolar Hybrid nanofluid at circular cylinder with sinusoidal radius variation is analyzed. The combined slip effects is presented in the stagnation point region in this chapter. Velocity slip and thermal slip effects at the surface are analyzed. Effects of $Cu$ copper and $Al_2O_3$ aluminium with ordinary fluid is analyzed. The governing equations of the motion of micropolar Hybrid nanofluid flow are simplified under the boundary layer theory. The differential model in term of partial differential equations is dimensionlized through the suitable similarity transformations. The dimensionalized system in term of ordinary differential equations is solved through a numerical procedure. The results of Nusselt number, skin frictions, magnetic field, thermal slip, velocity slip, rotation parameter and solid nanoparticle concentration under the flow assumptions are revealed in graphs and tables. The magnetic field effect on temperature distribution and velocity distributions are itemized the same behavior of increasing.

### 3.2 Mathematical formulations

Three dimensional time independent flow of micropolar Hybrid nanofluid towards circular cylinder with sinusoidal radius variation is considered. The radius of the cylinder varies sinusoidally. At the points $M$, $N$ and $O$ (maximum and minimum radii), there exists a stagnation point. The attachment lines divide the flow, which passes through the side or at of the cylinder at points $M$ to $N$ and $O$ to $N$. The uniform ambient temperature of the micropolar Hybrid nanofluid is $T_\infty$, the constant wall temperature at the surface is $T_w$. We initially investigate the boundary layer flow in the area of the nodal stagnation point $M$. With $M$ taken as the inception, we present a facilitate framework with $X$-axis the upward way, $Y$ in the longitudinal direction and $Z$ normal to the surface. The velocities along $X-$direction, $Y-$direction and $Z-$direction are represented as $U, V$ and $W$ respectively.
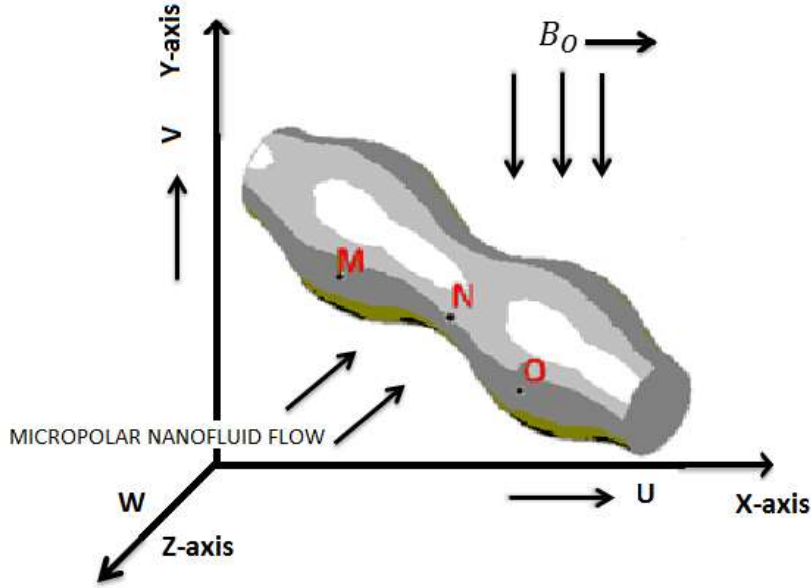
**Fig. 3.1:** Flow pattern of the physical model.

Such as

$$u_e^* = a^* X, \qquad v_e^* = b^* Y,$$

where, $b^*$ and $a^*$ are free stream dependent constants. The detailed geometry is discussed in chapter 2. The attachment lines of the nodal stagnation point range is $0 < c < 1$ while the attachment lines of the saddle stagnation point range is $-1 < c < 0$. If $c = 0$ then flow is plane. Flow equations for three dimensional micropolar Hybrid nanofluid are characterized as

$$\frac{\partial U}{\partial X} + \frac{\partial V}{\partial Y} + \frac{\partial W}{\partial Z} = 0, \tag{3.1}$$

$$U\frac{\partial U}{\partial X} + V\frac{\partial U}{\partial Y} + W\frac{\partial U}{\partial Z} = a^{*2}X + \frac{k}{\rho_{hnf}}\frac{\partial N_2}{\partial Z} - \frac{\sigma B_\circ^2}{\rho_{hnf}}(U - a^*X) + \left(\frac{\mu_{hnf} + k}{\rho_{hnf}}\right)\frac{\partial^2 U}{\partial Z^2}, \tag{3.2}$$

$$U\frac{\partial V}{\partial X} + V\frac{\partial V}{\partial Y} + W\frac{\partial V}{\partial Z} = b^{*2}Y - \frac{k}{\rho_{hnf}}\frac{\partial N_1}{\partial Z} - \frac{\sigma B_\circ^2}{\rho_{hnf}}(V - b^*Y) + \left(\frac{\mu_{hnf} + k}{\rho_{hnf}}\right)\frac{\partial^2 V}{\partial Z^2}, \tag{3.3}$$

$$U\frac{\partial T}{\partial X} + V\frac{\partial T}{\partial Y} + W\frac{\partial T}{\partial Z} = \alpha_{hnf}\frac{\partial^2 T}{\partial Z^2}, \tag{3.4}$$

$$U\frac{\partial N_1}{\partial X} + V\frac{\partial N_1}{\partial Y} + W\frac{\partial N_1}{\partial Z} = \frac{\gamma_{hnf}}{j\rho_{hnf}}\frac{\partial^2 N_1}{\partial Z^2} - \frac{k}{j\rho_{hnf}}\frac{\partial V}{\partial Z} - \frac{2k}{j\rho_{hnf}}N_1, \tag{3.5}$$

$$U\frac{\partial N_2}{\partial X} + V\frac{\partial N_2}{\partial Y} + W\frac{\partial N_2}{\partial Z} = \frac{\gamma_{hnf}}{j\rho_{hnf}}\frac{\partial^2 N_2}{\partial Z^2} + \frac{k}{j\rho_{hnf}}\frac{\partial U}{\partial Z} - \frac{2k}{j\rho_{hnf}}N_2. \tag{3.6}$$

The boundary conditions are

$$\begin{cases} U = l_1\frac{\mu_{hnf}}{\mu_f}\frac{\partial U}{\partial Z}, \ \ V = l_1\frac{\mu_{hnf}}{\mu_f}\frac{\partial V}{\partial Z}, \ \ W = 0, \ N_1 = n\frac{\partial V}{\partial Z}, \\ \qquad N_2 = -n\frac{\partial U}{\partial Z}, T = T_\infty + \gamma\kappa_{hnf}\frac{\partial T}{\partial Z}, \ \ at \ Z \to 0, \\ U \to u_e, \ V \to v_e, \ T \to T_\infty, \ N_1 \to 0, \ N_2 \to 0, \ at \ Z \to \infty, \end{cases} \tag{3.7}$$

where 'U', 'V' and 'W' are the velocities apparatuses along X, Y and Z direction respectively. The physical quantities see in Table [2.1-2.3]. Thermal jump slip parameter is γ.

$$\begin{cases} T = T_\infty + (T_w - T_\infty)\Theta(\zeta), \ \ \zeta = Z\sqrt{\left(\frac{\nu_f}{a^*}\right)}, \\ N_1 = b^*Y\sqrt{\frac{a^*}{\nu_f}}H(\zeta), \ \ N_2 = a^*X\sqrt{\frac{a^*}{\nu_f}}\ Q(\zeta), \ \ V = b^*YG'(\zeta), \\ U = a^*XF'(\zeta), \ \ W = -\sqrt{a^*\nu_f}\ (F + cG), \end{cases} \tag{3.8}$$

the non-dimensional Eqs. (3.1)-(3.7) are reduced to dimensionless non-linear ordinary equations

$$\begin{cases} \left(\frac{\mu_{hnf} + k}{\rho_{hnf}}\right)F''' + (F + cG)F'' - F'^2 + \frac{K}{\rho_{hnf}}Q' - M^2\frac{\rho_f}{\rho_{hnf}}(F' - 1) + 1 = 0, \\ \left(\frac{\mu_{hnf} + k}{\rho_{hnf}}\right)G''' + (F + cG)G'' - c\,G'^2 - \frac{K}{\rho_{hnf}}H' - M^2\frac{\rho_f}{\rho_{hnf}}(G' - 1) + c = 0, \\ \qquad \frac{\frac{K_{hnf}}{\kappa_f}}{\Pr\rho_{hnf}}\Theta'' + (F + cG)\Theta' = 0, \\ \frac{\gamma_{hnf}}{j\rho_{hnf}}H'' + (F + cG)H' - \frac{2k}{j\rho_{hnf}}H - \frac{k}{j\rho_{hnf}}G'' - cG'H = 0, \\ \frac{\gamma_{hnf}}{j\rho_{hnf}}Q'' + (F + cG)Q' - \frac{2k}{j\rho_{hnf}}Q + \frac{k}{j\rho_{hnf}}F'' - F'Q = 0. \end{cases} \tag{3.9}$$

The boundary conditions are

$$\begin{cases} F(0) = 0, \quad F'(0) = \gamma \dfrac{\mu_{hnf}}{\mu_f} F''(0), \quad F'(\infty) = 1, \\[2mm] G(0) = 0, \quad G'(0) = \gamma \dfrac{\mu_{hnf}}{\mu_f} G''(0), \quad G'(\infty) = 1, \\[2mm] \Theta(0) = 1 + \delta \dfrac{\kappa_{hnf}}{\kappa_f} \Theta'(0), \quad \Theta(\infty) = 0, \\[2mm] H(0) = nG''(0), \quad H(\infty) = 0, \\[2mm] Q(0) = -nF''(0), \quad Q(\infty) = 0, \end{cases} \qquad (3.10)$$

where, H and Q, Θ, F and G are function related to the microrotation, temperature and velocity profiles while primes indicate differentiation w. r. t. $\zeta$. The quantities of interest are presented below

$$C_{fX} = \frac{\tau_{wx}}{\rho_f u_w^2}, C_{fY} = \frac{\tau_{WY}}{\rho_f u_w^2}, \quad Nu_x = \frac{Xq_w}{k_f(T_w - T_\infty)}, \qquad (3.11)$$

$\tau_{wX}$ and $\tau_{wY}$ '' are shear stresses'' in the X- and Y- axis individually and $q_w$ is heat flux defined as

$$\left.\begin{aligned} \tau_{wX} &= [(\mu_{hnf} + K)\frac{\partial U}{\partial Z} + KN_2]_{Z=0}, \\[2mm] \tau_{wY} &= [(\mu_{hnf} + K)\frac{\partial V}{\partial Z} + KN_1]_{Z=0}, \\[2mm] q_w &= -k_{hnf}\left(\frac{\partial T}{\partial Z}\right)_{Z=0}. \end{aligned}\right\} \qquad (3.12)$$

By using equations (3.11) and (3.12), we get

$$\left.\begin{aligned} Re_X^{\frac{1}{2}} C_{fX} &= \left(\left(\frac{1}{(1-\Phi_1)^{2.5}(1-\Phi_2)^{2.5}} + K\right) - nK\right)F''(0), \\[2mm] \left(\frac{X}{Y}\right) Re_X^{-\frac{1}{2}} C_{fY} &= \left(c\left(\frac{1}{(1-\Phi_1)^{2.5}(1-\Phi_2)^{2.5}} + K\right) + nK\right)G''(0), \\[2mm] Re_X^{-1/2} Nu_X &= -\frac{k_{hnf}}{k_f}\Theta'(0). \end{aligned}\right\} \qquad (3.13)$$

## 3.3    Results and discussion

For a specific physical comprehension of the problem, we have explained the significant impressions of parameters via MHD parameter $M$, micropolar parameter $K$, velocity slip parameter $\gamma$, thermal slip parameter $\delta$ and nanoparticle volume fraction $\Phi_2$ on the temperature profile, velocity profiles and micropolar profiles. The values of Pr is chosen as 6.2 at $20^{\circ}$C temperature and 1 atmospheric pressure. Figs. 3.2-3.6 show the variation of several physical parameters. These results are illustrated by using the Maple software.

### 3.4.1  Influence of magnetic field

Figs. 3.3(a) and 3.4(a) show the behavior of M on velocity distributions towards X and Y- axis respectively. It is prominent that velocity distribution surges with rise in magnetic field parameter. Magnetic field which stabilizes the viscous impacts, provides a force to the fluid which is decelerating by the viscous force. Table-3.1 exhibits the mutual influence of $M$ for the skin friction and Nusselt number. It is noted that for both Hybrid nanofluid and nanofluid, the skin friction and Nusselt number raise with growing in $M$. The increment in the strength of physical parameter M is due to the Lorentz force related with $M$. Hence, the velocity of the fluid enhances while enhanced in magnetic field. The applications of the magnetic field produce Lorentz forces.

**Table 3.1: Comparative results of M of the skin fraction and Nusselt number.**

| M | Hybrid nanofluid ($Ni - SiC/EG$) | | | Nanofluid ($Ni/EG$) | | |
|---|---|---|---|---|---|---|
| | $\sqrt{Re_X}\, C_{fX}$ | $(X/Y)\sqrt{Re_X}\, C_{fY}$ | $\dfrac{Nu_X}{\sqrt{Re_X}}$ | $\sqrt{Re_X}\, C_{fX}$ | $(X/Y)\sqrt{Re_X}\, C_{fY}$ | $\dfrac{Nu_X}{\sqrt{Re_X}}$ |
| 0.0 | 1.46140 | 0.87815 | 0.98022 | 1.23920 | 0.79164 | 0.90520 |
| 0.5 | 1.51081 | 0.92538 | 0.99055 | 1.29202 | 0.84484 | 0.91673 |
| 1.0 | 1.64168 | 1.04642 | 1.01626 | 1.43059 | 0.97958 | 0.94478 |
| 1.5 | 1.81917 | 1.20319 | 1.04790 | 1.61655 | 1.15216 | 0.97837 |

### 3.4.2  Effect of solid nanoparticle

Figs. 3.2(b), 3.3(b), 3.4(b) and 3.5(b) present the behavior of Hybrid nanofluid flow on velocity profiles, micropolar profiles and temperature distribution respectively on the surface of the circular cylinder. It is distinguished that the velocity profile enhance with positive values of nanoparticle volume friction as seen in Figs. 3.3(b)-3.4(b). Because, in a Hybrid nanofluid model used in our inquiry, the effective viscosity of Hybrid nanofluid enhances for the positive values of the nanoparticle volume fraction which provides high resistance to the liquid movement. Fig. 3.6(b) shows the behavior of $\Phi_2$ on the micropolar profile that fluid velocity decayed for the increment of $\Phi_2$ while the opposite behavior of the solid nanoparticle is seen in Fig. 3.5(b). This behavior can be clarified within the macroscopic perspective. Fig. 3.2(a) shows the variation of $\Phi_2$ affect on the temperature profile in the Hybrid nanofluid flow over the surface of the circular cylinder. The $\Phi_2$ increases with decreasing in the temperature profile. It is famous that the Hybrid nanofluid flow of thermal conductivity expression appears the positive behavior of the heat transfer execution. From Table-3.2, for $Ni - SiC/EG$ and $Ni/EG$,

it is noted that the skin friction and Nusselt number are enhancing for the increment of solid nanoparticle.

**Table 3.2: Comparative results of $\Phi_2$ of the skin fraction and Nusselt number.**

| $\Phi_2$ | Hybrid nanofluid (Ni − SiC/EG) | | | Nanofluid (Ni/EG) | | |
|---|---|---|---|---|---|---|
| | $\sqrt{Re_X}\, C_{fX}$ | $(X/Y)\sqrt{Re_X}\, C_{fY}$ | $\dfrac{Nu_X}{\sqrt{Re_X}}$ | $\sqrt{Re_X}\, C_{fX}$ | $(X/Y)\sqrt{Re_X}\, C_{fY}$ | $\dfrac{Nu_X}{\sqrt{Re_X}}$ |
| 0.005 | 1.36046 | 1.14933 | 0.90582 | 1.14175 | 0.76647 | 0.80771 |
| 0.02 | 1.42550 | 0.88368 | 0.94215 | 1.20686 | 0.80083 | 0.84153 |
| 0.04 | 1.51081 | 0.92538 | 0.99055 | 1.29202 | 0.84484 | 0.88635 |
| 0.06 | 1.59482 | 0.96562 | 1.03895 | 1.37575 | 0.88707 | 0.93096 |

### 3.4.3 Effect of thermal and velocity slip

Effects the velocity slip parameter on fluid velocities depicted in Figs. 3.3(c) and 3.4(c). It is noted that the fluid velocity profile shows the decay curves for the positive values of velocity slip parameter. Composite effects of nanoparticle and thermal slip parameter are plotted through Fig. 3.2(b). It is noted that thermal slip parameter gives the opposite effects on temperature distribution. The temperature distribution behavior shows the decline curve for the positive values of thermal slip parameter that are shown in Fig. 3.2(b). The mutual effects of thermal slip and velocity slip of the skin fraction coefficient and Nusselt numbers which are depicted in Table-3.3. Thermal slip parameter increases for the increment of skin friction coefficients. While the Nusselt number decreases for the positive values of thermal slip parameter for $Ni - SiC/EG$ and $Ni/EG$.

**Table 3.3: Comparative results of γ and δ of the skin fraction and Nusselt number.**

| $\delta$ | $\Gamma$ | Hybrid nanofluid (Ni − SiC/EG) | | | Nanofluid (Ni/EG) | | |
|---|---|---|---|---|---|---|---|
| | | $\sqrt{Re_X}\, C_{fX}$ | $(X/Y)\sqrt{Re_X}\, C_{fY}$ | $\dfrac{Nu_X}{\sqrt{Re_X}}$ | $\sqrt{Re_X}\, C_{fX}$ | $(X/Y)\sqrt{Re_X}\, C_{fY}$ | $\dfrac{Nu_X}{\sqrt{Re_X}}$ |
| 0.0 | 0.2 | 1.46140 | 0.87815 | 0.98022 | 1.23920 | 0.79164 | 0.90520 |
| 0.2 | - | 1.51081 | 0.92538 | 0.99055 | 1.29202 | 0.84484 | 0.91672 |
| 0.4 | - | 1.64168 | 1.04642 | 1.01626 | 1.43059 | 0.97958 | 0.94478 |
| 0.6 | - | 1.81917 | 1.20319 | 1.04790 | 1.61655 | 1.15216 | 0.97837 |
| 0.2 | 0.0 | 1.87847 | 1.09140 | 0.83653 | 1.53425 | 0.96205 | 0.79219 |
| - | 0.2 | 1.68460 | 1.00742 | 0.92538 | 1.40828 | 0.90307 | 0.86220 |
| - | 0.4 | 1.51081 | 0.92538 | 0.99055 | 1.29202 | 0.84484 | 0.91672 |
| - | 0.6 | 1.36098 | 0.85001 | 1.03931 | 1.18783 | 0.78977 | 0.95971 |

### 3.4.4 Effect of vortex viscosity parameter

Figs. 3.3(d) and 3.4(d) describe the effects of vortex viscosity parameter on fluid velocities distribution. It is noted that the fluid velocity distribution reveals the decline curve behavior for

increasing values of the vortex viscosity parameter which is shown in Fig. 3.4(d). The velocity distribution increases for the increment of the vortex viscosity parameter which is revealed in Fig. 3.3(d), while the thickness of the momentum boundary layer reveals the curve beyond from the surface of the circular cylinder with an increment of the vortex viscosity parameter. Micro-rotation profile behavior is depicted in Figs. 3.5(b) and 3.6(b). It is clear from Fig. 3.5(b) that micropolar parameter $K$ increases with increasing micro-rotation profile. The flow of Hybrid nanofluid at micropolar momentum boundary layer thickness shows curve away from the surface of the circular cylinder. But the opposite behavior is shown in Fig. 3.6(b). The influence of K of the skin friction coefficients and Nusselt numbers are presented in Table-3.4. It is noted that the skin friction coefficient along X-axis minimize for the positive values of K while the opposite behavior of the skin friction coefficient along Y-axis account to our study for the Hybrid nanofluid and nanofluid. It is also appreciated that by augmenting the vortex viscosity parameter K, the rate of heat transfer declines for the $Ni - SiC/EG$ and $Ni/EG$.

**Table 3.4: Comparative results of $K$ of the skin fraction and Nusselt number.**

| K | Hybrid nanofluid ($Ni - SiC/EG$) | | | Nanofluid ($Ni/EG$) | | |
|---|---|---|---|---|---|---|
| | $\sqrt{Re_X}\, C_{fX}$ | $(X/Y)\sqrt{Re_X}\, C_{fY}$ | $\dfrac{Nu_X}{\sqrt{Re_X}}$ | $\sqrt{Re_X}\, C_{fX}$ | $(X/Y)\sqrt{Re_X}\, C_{fY}$ | $\dfrac{Nu_X}{\sqrt{Re_X}}$ |
| 0.0 | 1.51140 | 0.64911 | 1.03925 | 1.29829 | 0.55386 | 0.97369 |
| 0.5 | 1.51081 | 0.92538 | 0.99055 | 1.29202 | 0.84484 | 0.91672 |
| 1.0 | 1.54815 | 1.15908 | 0.95638 | 1.33553 | 1.08388 | 0.87987 |
| 1.5 | 1.60398 | 1.37136 | 0.93064 | 1.39916 | 1.29943 | 0.85335 |

## 3.5 Closing remarks

The flow of micropolar Hybrid nanofluid with thermal slip and magnetic hydrodynamics affects is considered over a circular cylinder. The physical parameter affects are presented, though tables the graphs. These results are obtained through Maple software. The summary of the present effort is noted as follows:

- The magnetic field affect on temperature distribution and velocity distributions itemized the same behavior of increasing.
- The nanoparticle $\Phi_2$ effects on velocity distributions are noted increasing behavior same, but opposite with the temperature distribution behavior.
- Slip parameters increased which declined the temperature and velocity profiles curves.
- Micropolar parameter enhances with declining the velocity profile.

- Our significant results itemized that micropoar Hybrid nanofluid gain finest heat transfer rate as compared to nanofluid.

**Figs. 3.2:** Impression of δ and $\Phi_2$ on the temperature profiles

$\Phi_2 = 0.005, 0.03,$

**Fig. 3.2(a)**

$\delta = 0.0, 0.2, 0.4$
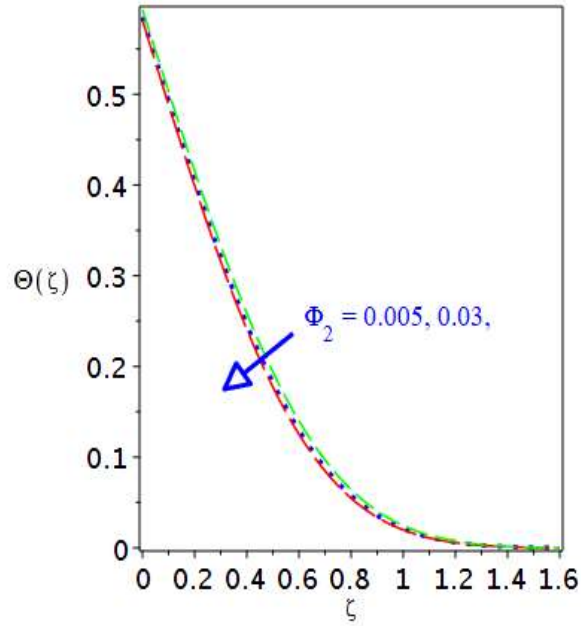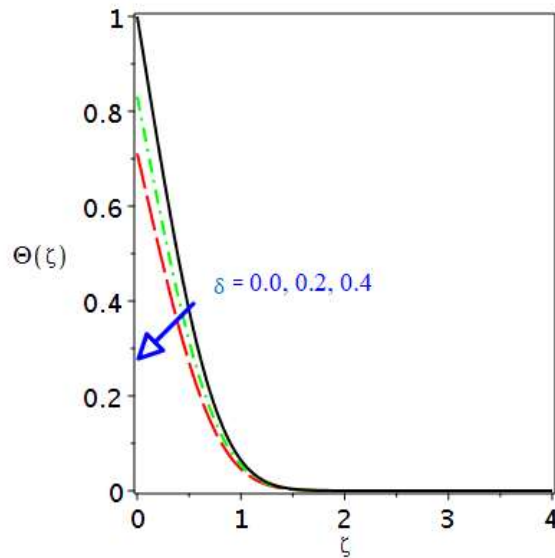
Fig. 3.2(b)

**Figs. 3.3:** Effects of K, M, γ and $\varphi_2$ on the velocity profile

Fig. 3.3(a)



$M = 0.0, 0.5, 1.5$

Fig. 3.3(b)



$\Upsilon = 0.0, 0.2, 0.4, 0.6$
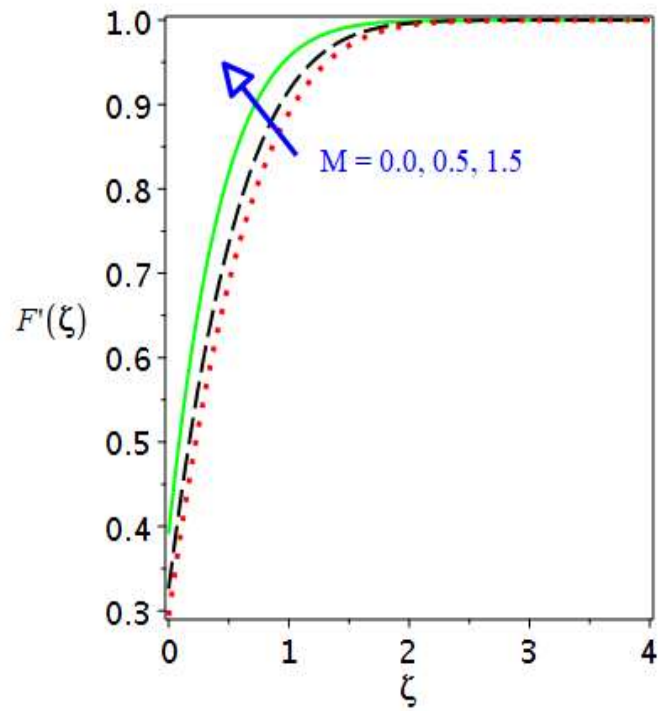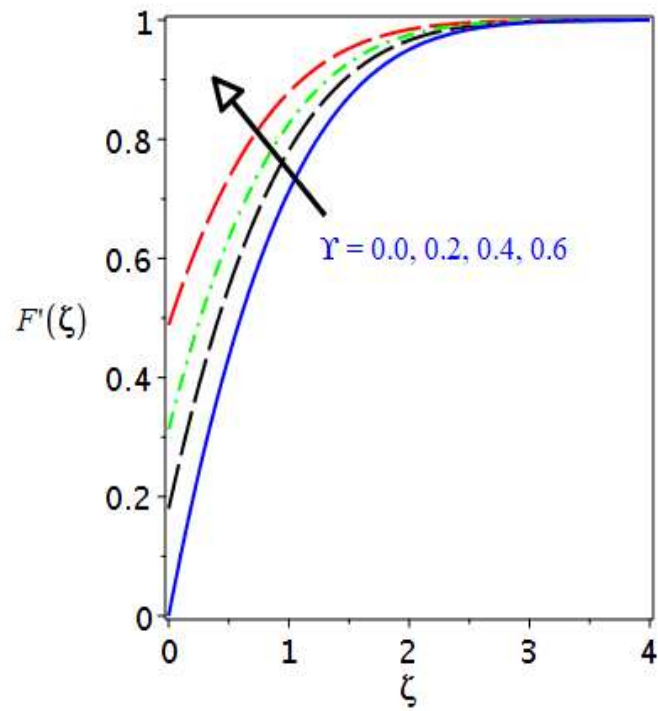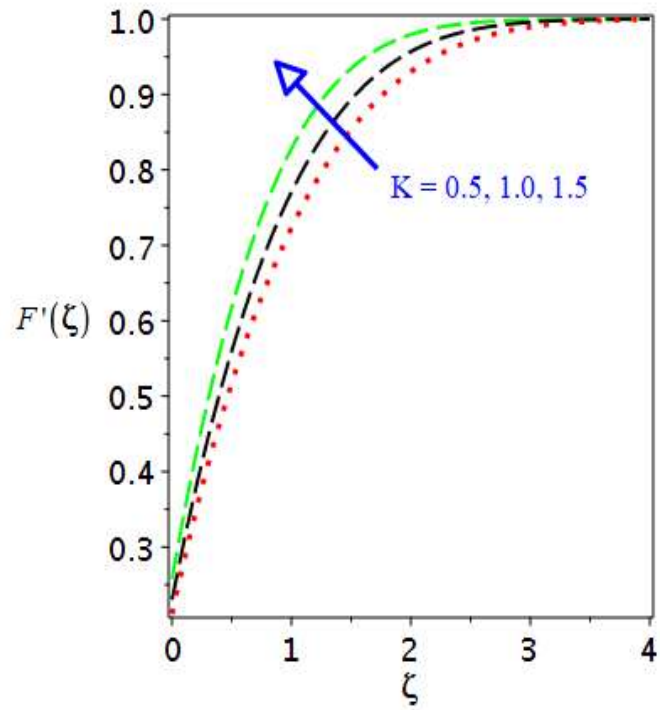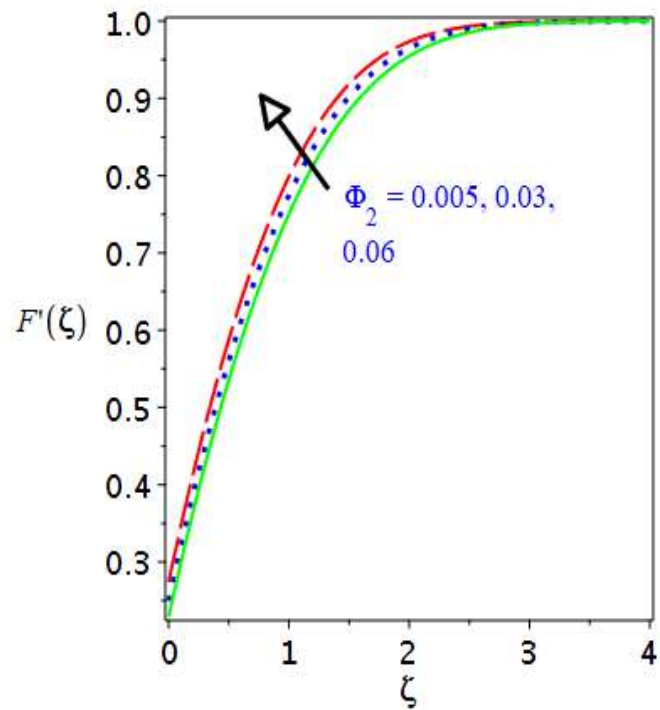
**Fig. 3.3(c)**



Fig. 3.3(d)

**Figs. 3.4:** Effects of K, M, γ and $\Phi_2$ on the velocity profile

$G'(\zeta)$

$M = 0.0, 0.5, 1.0$

$\zeta$

**Fig. 3.4(a)**

$G'(\zeta)$

$\Upsilon = 0.0, 0.2, 0.4$

$\zeta$
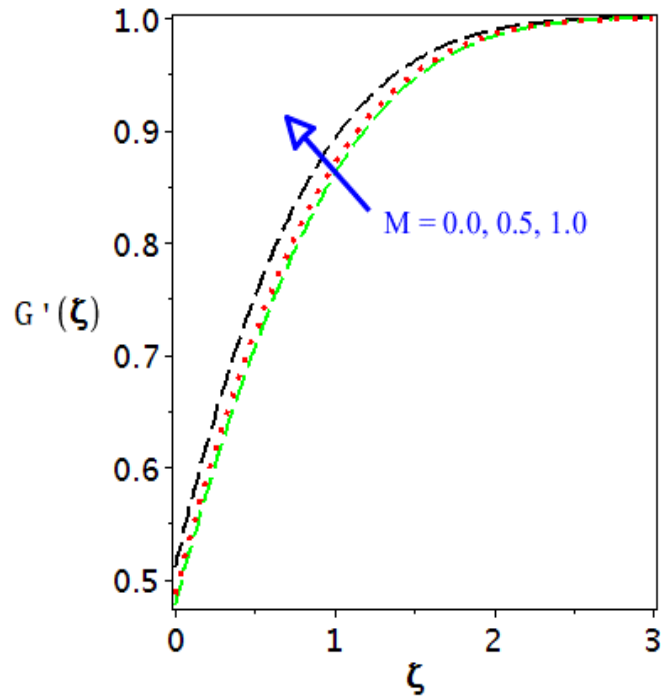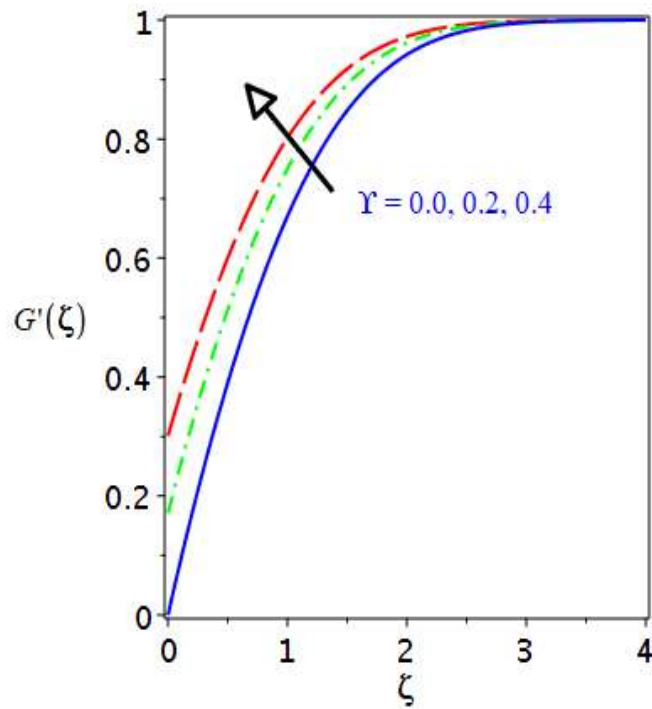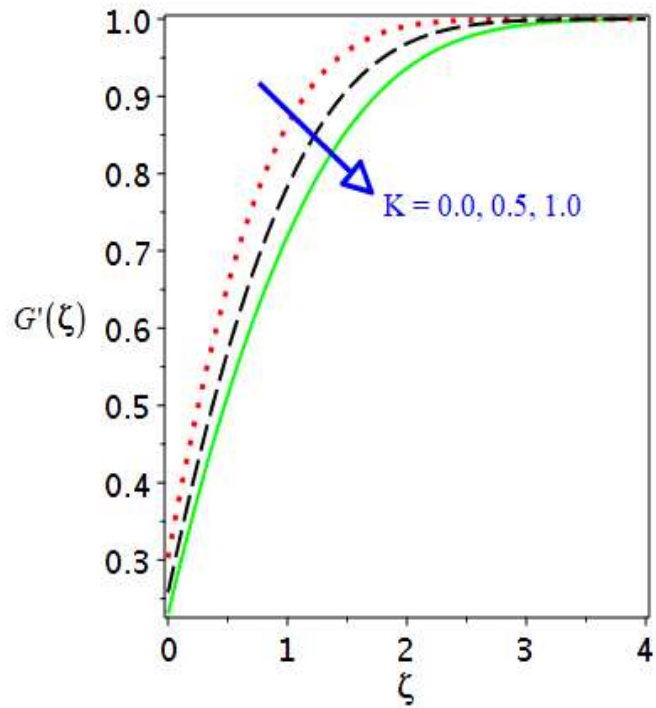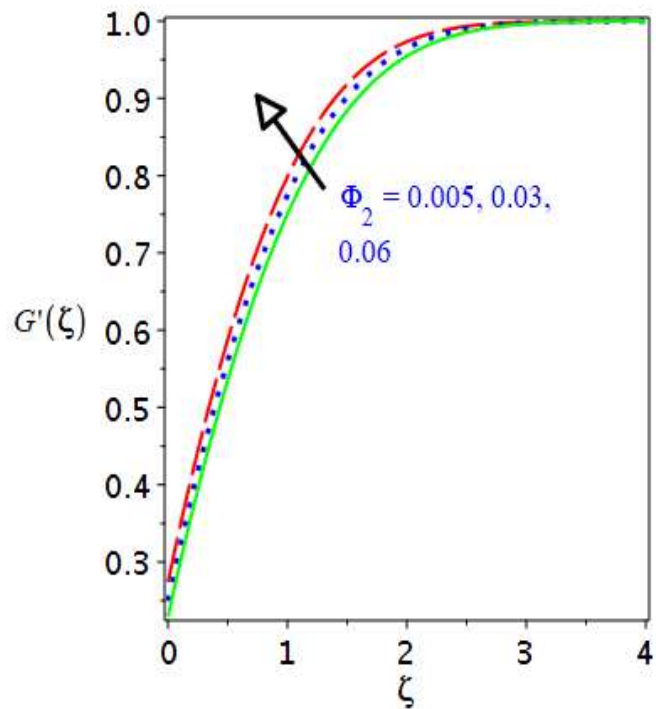
Fig. 3.4(b)

**Fig. 3.4(c)**



Fig. 3.4(d)

**Figs. 3.5:** Effects of K and $\Phi_2$ on the micro-rotation profiles.



$K = 0.0, 0.5, 1.0$

**Fig. 3.5(a)**



$\Phi_2 = 0.005, 0.03,$
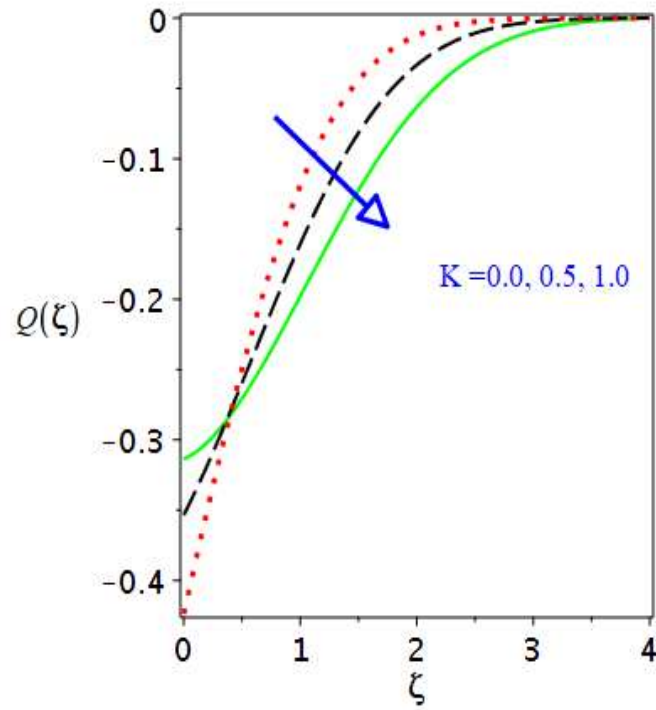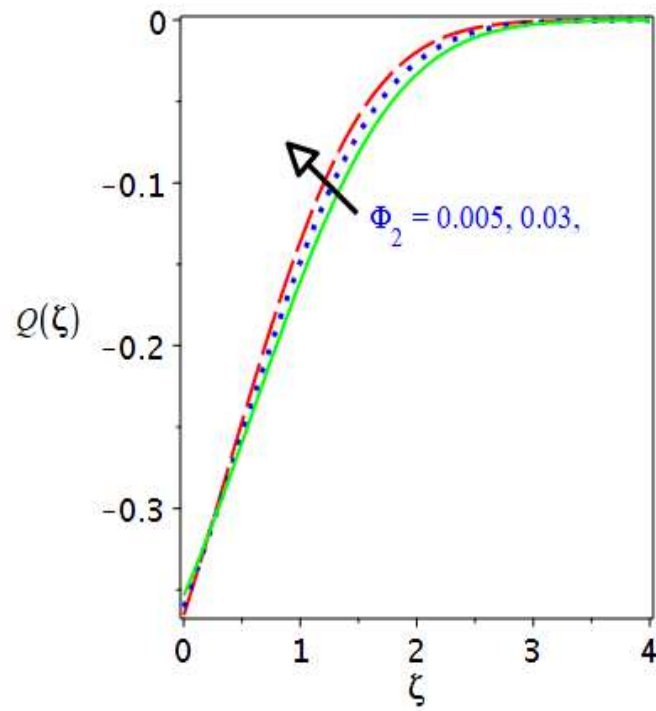
Fig. 3.5(b)

**Figs. 3.5:** Effects of K and $\Phi_2$ on the micro-rotation profiles
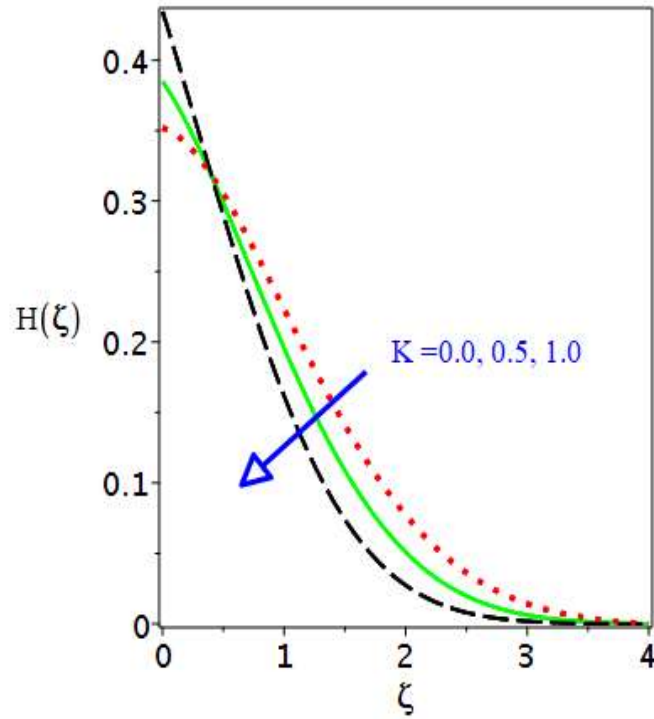


**Fig. 3.5(c)**
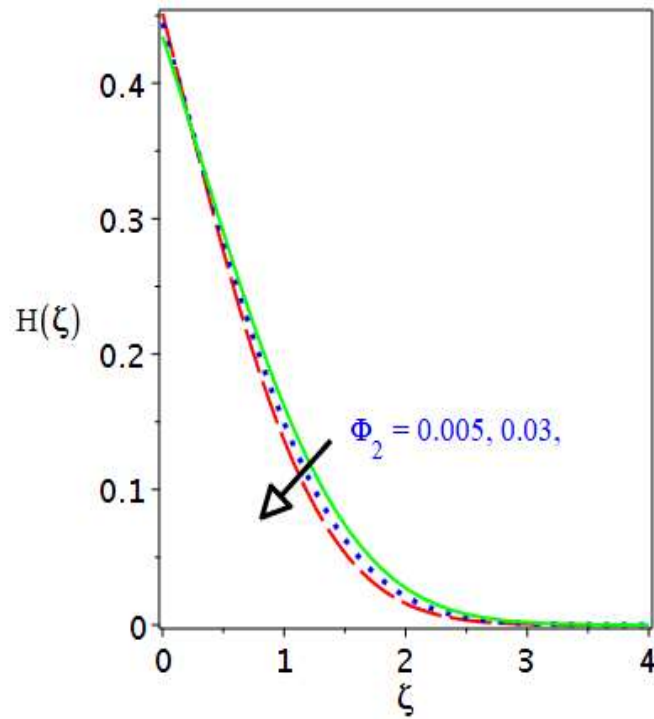


Fig. 3.5(d)

# Chapter 04

## Steady 3D stagnation point flow of Hybrid nanofluid over moving plate with anisotropic slip

## 4.1  Introduction

This chapter explains the three dimensional axisymmetric Hybrid nanofluid flow of stagnation point at moving plate under slip coefficients in two orthogonal directions. No slip condition is replaced through the partial slip condition. Such anisotropic slip happens in geometrically striated surface and super hydrophobic stripes. Using the experimental values, we have discussed the Hybrid nanofluid theoretically for boundary layer flow due to stagnation point flow. The boundary layer approximation and similarity transformations are applied on mathematical model for simplification. The dimensionless model further solved through numerical scheme. Effects of physical parameters are also discussed in detail. $H^*(0)$ and $K^*(0)$ are unity for no slip condition and decreases to zero as slip is augmented. Slip factors increases with the increase in normalized slip velocities $F'(0)$ and $G'(0)$. Anisotropic behavior is reflected in the various slip velocities $F'(0)$ and $G'(0)$. It is found that relative velocities are higher at small slip. Slip velocities upsurges with growth in slip parameter in both cases Hybrid nanofluid and nanofluid.
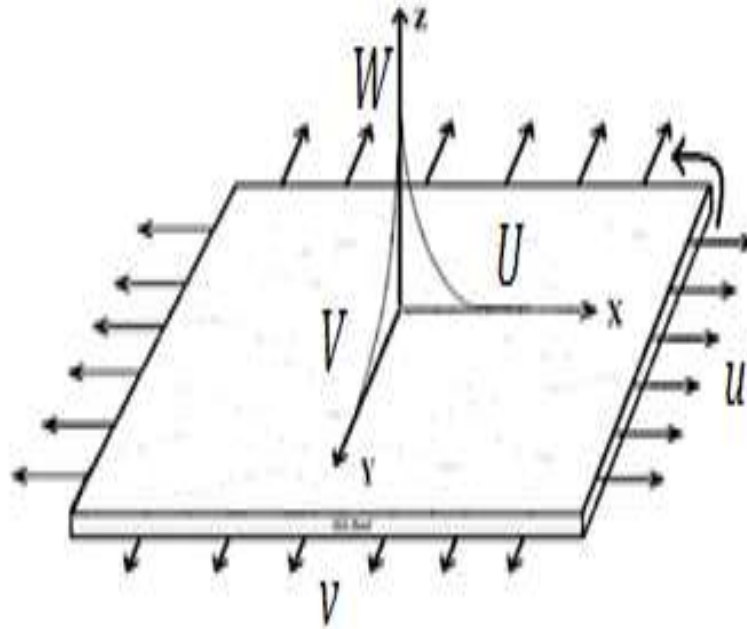


**Fig. 4.1:** Stagnation flow of Hybrid nanofluid towards a moving plate.

## 4.2 Mathematical formulation

The stagnation point flow of Hybrid nanofluid for fixed Cartesian coordinates on the moving plate is considered. Align the $X-$direction having the striations of the plate, $Y-$direction normal to the striations and along the $Z-$direction have the axis of the stagnation flow (see Fig. 4.1). $U$, $V$ and $W$ are the velocity components in $X-$, $Y-$ and $Z-$ directions respectively of the moving plate. Navier [47] studied about the partial slip

$$U = N\sigma, \tag{4.1}$$

where, $U$, $\sigma$ and $N$ are the tangential velocity, the tangential shear stress and the slip coefficient while the Navier's partial conditions are satisfied on the plate. If the potential flow is far away from the plate

$$U = a^*X, \quad V = a^*Y, \quad W = -2a^*Z, \quad p = -\frac{\rho_{hnf}a^{*2}}{2}(X^2 + Y^2) + p_0, \tag{4.2}$$

here, $U$, $V$ and $W$ are the velocity components aligns the Cartesian coordinates $(X, Y, Z)$ respectively. The strength of stagnation flow is $a^*$, the pressure is $p$, the density of Hybrid nanofluid is $\rho_{hnf}$, the kinematic viscosity of Hybrid nanofluid is $v_{hnf}$ and the stagnation pressure is $p_0$. In the Newtonian fluid flow, the constant characteristics of the Navier-Stokes equations are defined as follows

$$U_X + V_Y + W_Z = 0, \tag{4.3}$$

$$UU_X + VU_Y + WU_Z = -\frac{P_X}{\rho_{hnf}} + v_{hnf}(U_{XX} + U_{YY} + U_{ZZ}), \tag{4.4}$$

$$UV_X + VV_Y + WV_Z = -\frac{P_Y}{\rho_{hnf}} + v_{hnf}(V_{XX} + V_{YY} + V_{ZZ}), \tag{4.5}$$

$$UW_X + VW_Y + WW_Z = -\frac{P_Z}{\rho_{hnf}} + v_{hnf}(W_{XX} + W_{YY} + W_{ZZ}). \tag{4.6}$$

By utilizing Eq. (4.2), the following similarity transforms

$$\begin{cases} U = a^*XF'(\zeta) + uH^*(\zeta), \\ V = a^*YG'(\zeta) + vK^*(\zeta), \\ W = -\sqrt{a^*v_f}\big(F(\zeta) + G(\zeta)\big), \\ \qquad \zeta = \sqrt{\dfrac{a^*}{v_f}}Z. \end{cases} \tag{4.7}$$

With these transformations, the continuity equation is identically fulfilled. After using the above equations, we obtained

34

$$\frac{1}{(1-\Phi_1)^{2.5}(1-\Phi_2)^{2.5}\left[\left\{(1-\Phi_2)\left(1-\Phi_1+\Phi_1\frac{(\rho)_{s_1}}{(\rho)_f}\right)\right\}+\Phi_2\frac{(\rho)_{s_2}}{(\rho)_f}\right]}\cdot F''' + G\,F''$$

$$-\,F'^2 + F\,F'' + 1 = 0, \tag{4.8}$$

$$\frac{1}{(1-\Phi_1)^{2.5}(1-\Phi_2)^{2.5}\left[\left\{(1-\Phi_2)\left(1-\Phi_1+\Phi_1\frac{(\rho)_{s_1}}{(\rho)_f}\right)\right\}+\Phi_2\frac{(\rho)_{s_2}}{(\rho)_f}\right]}\cdot G''' + FG''$$

$$+\,GG'' - G'^2 + 1 = 0, \tag{4.9}$$

$$\frac{1}{(1-\Phi_1)^{2.5}(1-\Phi_2)^{2.5}\left[\left\{(1-\Phi_2)\left(1-\Phi_1+\Phi_1\frac{(\rho)_{s_1}}{(\rho)_f}\right)\right\}+\Phi_2\frac{(\rho)_{s_2}}{(\rho)_f}\right]}\cdot H^{*\,''}$$

$$+\,FH^{*\,'} + GH^{*\,'} - H^*F' = 0, \tag{4.10}$$

$$\frac{1}{(1-\Phi_1)^{2.5}(1-\Phi_2)^{2.5}\left[\left\{(1-\Phi_2)\left(1-\Phi_1+\Phi_1\frac{(\rho)_{s_1}}{(\rho)_f}\right)\right\}+\Phi_2\frac{(\rho)_{s_2}}{(\rho)_f}\right]}\cdot K^{*\,''}$$

$$+\,FK^{*\,'} + GK^{*\,'} - K^*F' = 0 \tag{4.11}$$

subject to the potential flow boundary conditions

$$U = a^*X,\; V = a^*Y,\; W = -2a^*Z,\; p = -\frac{\rho_{hnf}a^{*2}}{2}(X^2+Y^2)+p_0,\text{ as }\zeta \to \infty$$

$$\begin{cases} F'(\zeta) \to 1 \text{ as } \zeta \to \infty, \\ G'(\zeta) \to 1 \text{ as } \zeta \to \infty, \\ H^*(\zeta) \to 0 \text{ as } \zeta \to \infty, \\ K^*(\zeta) \to 0 \text{ as } \zeta \to \infty, \end{cases} \tag{4.12}$$

$$U - u_o = N_1\frac{\mu_{hnf}}{\mu_f}\frac{\partial U}{\partial Z}, \qquad V - v_o = N_2\frac{\mu_{hnf}}{\mu_f}\frac{\partial V}{\partial Z}, \qquad \text{as } Z \to 0. \tag{4.13}$$

Here, the dynamic viscosity of hybrid nanofluid is $\mu_{hnf} = \rho_{hnf}v_{hnf}$. $N_1$ and $N_2$ are the slip coefficients along the $X-$, and $Y-$ directions respectively. By applying the similarity variables, the above equations are reduced into the following form

$$F'(0) = \gamma_1\frac{\mu_{hnf}}{\mu_f}F''(0),\; G'(0) = \gamma_2\frac{\mu_{hnf}}{\mu_f}G''(0),\; H^*(0) - 1 = \gamma_1\frac{\mu_{hnf}}{\mu_f}H^{*'}(0),$$

$$K^*(0) - 1 = \gamma_2\frac{\mu_{hnf}}{\mu_f}K^{*'}(0), \tag{4.14}$$

$\gamma_i = N_i\sqrt{\frac{a^*}{v_{hnf}}}$ is the dimensionless slip factors while it is also noted that normal velocity on plate is zero which is defined as $F(0) + G(0) = 0$ without loss of the generality to the velocity, which can set as

$$F(0) = 0, \qquad G(0) = 0. \tag{4.15}$$

The no slip effects ($\gamma = 0$) on stagnation point flow on the plate was explored by Heimenz (1911). The numerical integration is performed of the Eqs. [4.8-4.9] by applying the bvp4c algorithms to execute the initial values of $F''(0) = 1.31033$ and $G''(0) = 1.31033$. For the

full slip $\gamma \to \infty$ mean that result is the potential flow $F = G = \zeta$, $H = K = 0$. Suppose $\epsilon \equiv \frac{1}{\gamma} \ll$

1 and expand

$$F = \zeta + \epsilon F_0 + \epsilon^2 F_1 + \cdots, \tag{4.16}$$
$$G = \zeta + \epsilon G_0 + \epsilon^2 G_1 + \cdots, \tag{4.17}$$
$$H^* = \epsilon H^*_0 + \epsilon^2 H^*_1 + \cdots, \tag{4.18}$$
$$K^* = \epsilon K^*_0 + \epsilon^2 K^*_1 + \cdots, \tag{4.19}$$

Eqs $(4.8 - 4.11)$ are the set of nonlinear coupled ordinary differential equations having boundary conditions $(4.12), (4.14)$, and $(4.15)$ for the case of isotropic slip surface.

## 4.3  Asymptotic behavior for large slip

Consider that $\gamma_1$ and $\gamma_2$ are the slip factors which are very large when compared to unity. Eq. (4.12) then suggest the expansions of the following form

$$F = \zeta + A_1 + \frac{\chi(\zeta)}{\gamma_1} + \cdots, \quad G = \zeta + A_2 + \frac{\psi(\zeta)}{\gamma_2} + \cdots, \tag{4.20}$$

here, the $A_i (i = 1, 2, 3, \dots)$ are constants and $\chi, \psi \ll 1$. Eqs. (4.8-4.9) linearize to

$$\frac{1}{(1-\Phi_1)^{2.5}(1-\Phi_2)^{2.5}\left[\left\{(1-\Phi_2)\left(1-\Phi_1+\Phi_1\frac{(\rho)_{s_1}}{(\rho)_f}\right)\right\}+\Phi_2\frac{(\rho)_{s_2}}{(\rho)_f}\right]} \cdot \chi'''(\zeta) + 2\zeta\chi''(\zeta) - 2\chi'(\zeta) = 0, \tag{4.21}$$

$$\frac{1}{(1-\Phi_1)^{2.5}(1-\Phi_2)^{2.5}\left[\left\{(1-\Phi_2)\left(1-\Phi_1+\Phi_1\frac{(\rho)_{s_1}}{(\rho)_f}\right)\right\}+\Phi_2\frac{(\rho)_{s_2}}{(\rho)_f}\right]} \psi'''(\zeta) + 2\zeta\psi''(\zeta) - 2\psi'(\zeta) = 0. \tag{4.22}$$

The corresponding boundary conditions Eqs. (4.12, 4.14) become

$$\begin{aligned} \chi(0) = 0, \quad &\chi''(0) = 1, \quad \chi'(\zeta) \to 0 \ as \ \zeta \to \infty, \\ \psi(0) = 0, \quad &\psi''(0) = 1, \quad \psi'(\zeta) \to 0 \ as \ \zeta \to \infty, \end{aligned} \tag{4.23}$$

and Eqs. $(4.16 - 4.19)$ have been integrated with the results of $\chi'(0) = -0.526126$ and $\psi'(0) = -0.526126$. Subsequently, Eqs. $(4.16 - 4.19)$ are identical. Therefore, for large slip

$$F'(0) = 1 - \frac{0.526126}{\gamma_1} + \cdots, \quad G'(0) = 1 - \frac{0.526126}{\gamma_2} + \cdots \tag{4.24}$$

The decline rate for large $\zeta$ will be

$$\chi'(\zeta) = c \, \zeta. \tag{4.25}$$

Applying the variation parameters, the solutions that decline at infinity are

$$\chi'(\zeta) = \zeta \int_{\zeta}^{\infty} \frac{e^{-\zeta^2/A_0}}{\zeta^2} d\zeta, \tag{4.26}$$

$$\text{where} \quad A_0 = \frac{1}{(1-\Phi_1)^{2.5}(1-\Phi_2)^{2.5}\left[\left\{(1-\Phi_2)\left(1-\Phi_1+\Phi_1\frac{(\rho)_{s_1}}{(\rho)_f}\right)\right\}+\Phi_2\frac{(\rho)_{s_2}}{(\rho)_f}\right]}.$$

The asymptotic behavior for large $\zeta$, applying the integration by parts, we have

$$\chi \sim \sqrt{A_0} \frac{e^{-\zeta^2/A_0}}{\zeta^3}. \tag{4.27}$$

This quick decrease permits numerical integration to be exceptionally effective. For sidelong development at huge slip, we consider

$$H^* = \frac{\phi(\zeta)}{\gamma_1} + \cdots, \qquad K^* = \frac{\kappa(\zeta)}{\gamma_2} + \cdots, \tag{4.28}$$

Eqs. $(4.11 - 4.12)$ are reduced by using the Eqs $(4.18 - 4.19)$, and are defined as follow

$$\frac{1}{(1-\Phi_1)^{2.5}(1-\Phi_2)^{2.5}\left[\left\{(1-\Phi_2)\left(1-\Phi_1+\Phi_1\frac{(\rho)_{s_1}}{(\rho)_f}\right)\right\}+\Phi_2\frac{(\rho)_{s_2}}{(\rho)_f}\right]}\phi''(\zeta) \tag{4.29}$$
$$+ 2\zeta\phi'(\zeta) - \phi(\zeta) = 0,$$

$$\frac{1}{(1-\Phi_1)^{2.5}(1-\Phi_2)^{2.5}\left[\left\{(1-\Phi_2)\left(1-\Phi_1+\Phi_1\frac{(\rho)_{s_1}}{(\rho)_f}\right)\right\}+\Phi_2\frac{(\rho)_{s_2}}{(\rho)_f}\right]}\kappa''(\zeta) \tag{4.30}$$
$$+ 2\zeta\kappa'(\zeta) - \kappa(\zeta) = 0,$$

the corresponding conditions are

$$\phi'(0) = -1, \qquad \kappa'(0) = -1, \qquad \kappa(\zeta) \to 0, \qquad \kappa(\zeta) \to 0, \, as \, \zeta \to \infty. \tag{4.31}$$

Eqs $(4.29 - 4.30)$ with Eq. $(4.31)$ are cracked numerically by applying the bvp4c technique, and obtain the values of $\phi(0) = 0.630343$ and $\kappa(0) = 0.630343$ with these values we can write

$$H^*(0) = \frac{0.630343}{\gamma_1} + \cdots, \qquad K^*(0) = \frac{0.630343}{\gamma_2} + \cdots \tag{4.32}$$

For the general $\gamma$ the original equations can be solved easily. Eqs $(4.8, 4.9, 4.12, 4.14$ and $4.15)$ are integrated numerically. More accurate results of the initial values are given in Tables [4.1-4.2].

**Table-4.1: The initial and final values of $\gamma$ for different values of slip factor $\gamma_1$ and $\gamma = \frac{\gamma_2}{\gamma_1}$ for the hybrid nanofluid. The values in the each cell from top: $F'(0)$, $G'(0)$, $K^*(0)$ and $H^*(0)$. The outcomes from approximate formulas Eq. (4.24) and Eq. (4.32) are given in parenthesis.**

| $\gamma = \frac{\gamma_2}{\gamma_1}$ | $\gamma_1 = 0$ | $\gamma_1 = 0.1$ | $\gamma_1 = 0.2$ | $\gamma_1 = 0.5$ | $\gamma_1 = 1$ | $\gamma_1 = 2$ | $\gamma_1 = 5$ | $\gamma_1 = 10$ |
|---|---|---|---|---|---|---|---|---|
| **0** | 0 | 0.179677 | 0.311965 | 0.545037 | 0.713014 | 0.835916 | 0.928402 (0.8948) | 0.963106 (0.9474) |
| **0** | 0 | 0 | 0 | 0 | 0 | 0 | 0 | 0 |
| **0** | 1 | 0.860584 | 0.745032 | 0.517791 | 0.337205 | 0.19700 | 0.0872909 (0.1261) | 0.0452321 (0.06301) |
| **0** | 1 | 1 | 1 | 1 | 1 | 1 | 1 | 1 |
| **0.25** | 0 | 0.180515 | 0.314201 | 0.55019 | 0.719429 | 0.841726 | 0.931973 (0.8948) | 0.965201 (0.9474) |
| **0.25** | 0 | 0.0511468 | 0.099742 | 0.22626 | 0.380542 | 0.562789 | 0.770963 | 0.872895 |
| **0.25** | 1 | 0.859442 | 0.74182 | 0.509764 | 0.32671 | 0.187206 | 0.0811592 (0.1261) | 0.0416155 (0.06301) |
| **0.25** | 1 | 0.96197 | 0.923622 | 0.816185 | 0.673372 | 0.490662 | 0.265617 | 0.149621 |
| **0.5** | 0 | 0.181281 | 0.316061 | 0.553456 | 0.722243 | 0.843261 | 0.932395 (0.8948) | 0.965328 (0.9474) |
| **0.5** | 0 | 0.0984738 | 0.184695 | 0.377134 | 0.560483 | 0.726423 | 0.872654 (0.7895) | 0.93277 (0.8948) |
| **0.5** | 1 | 0.858401 | 0.739163 | 0.504744 | 0.322204 | 0.18469 | 0.0804606 (0.1261) | 0.0414033 (0.06301) |
| **0.5** | 1 | 0.92527 | 0.853791 | 0.678204 | 0.494107 | 0.315608 | 0.15001 | 0.0798425 |

| | | | | | | | (0.2521) | (0.1261) |
|---|---|---|---|---|---|---|---|---|
| 0.75 | 0 | 0.181981 | 0.317614 | 0.555644 | 0.723762 | 0.843945 | 0.932555 (0.8948) | 0.965374 (0.9474) |
| 0.75 | 0 | 0.142213 | 0.257054 | 0.481598 | 0.661105 | 0.801479 | 0.911877 (0.8597) | 0.954309 (0.9298) |
| 0.75 | 1 | 0.857452 | 0.736954 | 0.501407 | 0.319793 | 0.183578 | 0.0801968 (0.1261) | 0.0413282 (0.06301) |
| 0.75 | 1 | 0.890105 | 0.791038 | 0.576098 | 0.387707 | 0.231774 | 0.104415 (0.1681) | 0.0544332 (0.0840) |
| 1.0 | 0 | 0.182621 | 0.318921 | 0.557194 | 0.724704 | 0.844331 | 0.932639 (0.8948) | 0.965397 (0.9474) |
| 1.0 | 0 | 0.182621 | 0.318921 | 0.557194 | 0.724704 | 0.844331 | 0.932639 (0.8948) | 0.965397 (0.9474) |
| 1.0 | 1 | 0.856585 | 0.735103 | 0.499058 | 0.318307 | 0.182954 | 0.0800584 (0.1261) | 0.0412894 (0.06301) |
| 1.0 | 1 | 0.856585 | 0.735103 | 0.499058 | 0.318307 | 0.182954 | 0.0800584 (0.1261) | 0.0412894 (0.0630) |

Eqs. (4.16 − 4.19) have been integrated with the results of $\chi'(0) = -0.564871$ and $\psi'(0) = -0.564871$. Subsequently, Es. (4.19 − 4.20) are identical, therefore, for large slip

$$F'(0) = 1 - \frac{0.564871}{\gamma_1} + \cdots, \qquad G'(0) = 1 - \frac{0.564871}{\gamma_2} + \cdots \qquad (4.33)$$

Eqs (4.29 − 4.30) with (4.33) are cracked numerically by applying the bvp4c technique, which gives $\phi(0) = 0.676772$ and $\kappa(0) = 0.676772$. Thus

$$H^*(0) = \frac{0.676772}{\gamma_1} + \cdots, \qquad K^*(0) = \frac{0.676772}{\gamma_2} + \cdots \qquad (4.34)$$

**Table-4.2: The initial and final values for different slip factor $\gamma_1$ and $\gamma = \frac{\gamma_2}{\gamma_1}$ for the Nanofluid. The values in the each cell from top: $F'(0)$, $G'(0)$, $K^*(0)$ and $H^*(0)$. The outcomes from approximate formulas Eq. (4.33) and Eq. (4.34) are given in parenthesis.**

| $\gamma = \frac{\gamma_2}{\gamma_1}$ | $\gamma_1 = 0$ | $\gamma_1 = 0.1$ | $\gamma_1 = 0.2$ | $\gamma_1 = 0.5$ | $\gamma_1 = 1$ | $\gamma_1 = 2$ | $\gamma_1 = 5$ | $\gamma_1 = 10$ |
|---|---|---|---|---|---|---|---|---|
| **0** | 0 | 0.151154 | 0.2687 | 0.492349 | 0.668505 | 0.805788 | 0.913751 (0.8870) | 0.95527 (0.9435) |
| **0** | 0 | 0 | 0 | 0 | 0 | 0 | 0 | 0 |
| **0** | 1 | 0.884114 | 0.783957 | 0.571635 | 0.386335 | 0.231972 | 0.104903 (0.1354) | 0.0547702 (0.0677) |
| **0** | 1 | 1 | 1 | 1 | 1 | 1 | 1 | 1 |
| **0.25** | 0 | 0.151761 | 0.27043 | 0.496878 | 0.674746 | 0.811938 | 0.917825 (0.8870) | 0.957736 (0.9435) |
| **0.25** | 0 | 0.0420657 | 0.082527 | 0.191217 | 0.331629 | 0.510154 | 0.732357 | 0.848496 |
| **0.25** | 1 | 0.883296 | 0.781512 | 0.564699 | 0.376249 | 0.221675 | 0.0979268 (0.1354) | 0.0505178 (0.0677) |
| **0.25** | 1 | 0.968914 | 0.937421 | 0.846909 | 0.719907 | 0.544876 | 0.308583 | 0.177719 |
| **0.5** | 0 | 0.152326 | 0.271919 | 0.499981 | 0.677835 | 0.813841 | 0.918402 (0.8870) | 0.957918 (0.9435) |
| **0.5** | 0 | 0.0815616 | 0.154975 | 0.328153 | 0.507446 | 0.682912 | 0.848158 (0.7741) | 0.918935 (0.8870) |
| **0.5** | 1 | 0.882537 | 0.779418 | 0.56000 | 0.371348 | 0.218573 | 0.0969707 | 0.0502149 |

| | | | | | | | | |
|---|---|---|---|---|---|---|---|---|
| | | | | | | | (0.1354) | (0.0677) |
| **0.5** | 1 | 0.93867 | 0.878998 | 0.724764 | 0.548862 | 0.363421 | 0.178262 (0.2707) | 0.0960951 (0.1354) |
| **0.75** | 0 | 0.15285 | 0.273203 | 0.502184 | 0.679611 | 0.814732 | 0.918627 (0.8870) | 0.957984 (0.9435) |
| **0.75** | 0 | 0.118608 | 0.21851 | 0.428328 | 0.612125 | 0.766385 | 0.894124 (0.8494) | 0.944681 (0.9247) |
| **0.75** | 1 | 0.881834 | 0.777619 | 0.55669 | 0.368558 | 0.217133 | 0.0966009 (0.1354) | 0.0501058 (0.0677) |
| **0.75** | 1 | 0.909398 | 0.825205 | 0.629345 | 0.440404 | 0.271412 | 0.125161 (0.1805) | 0.0658224 (0.0902) |
| **1.0** | 0 | 0.153338 | 0.274315 | 0.503808 | 0.680752 | 0.815246 | 0.918747 (0.8870) | 0.958018 (0.9435) |
| **1.0** | 0 | 0.153338 | 0.274315 | 0.503808 | 0.680752 | 0.815246 | 0.918747 (0.8870) | 0.958018 (0.9435) |
| **1.0** | 1 | 0.881181 | 0.776066 | 0.554261 | 0.366777 | 0.216306 | 0.0964046 (0.1354) | 0.0500496 (0.0677) |
| 1.0 | 1 | 0.881181 | 0.776066 | 0.554261 | 0.366777 | 0.216306 | 0.0964046 (0.1354) | 0.0500496 (0.0677) |

## 4.4 Thermal axisymmetric stagnation flow

As discussed in Ref. [48], the temperature far away from the plate is considered to be $T_\infty$ and temperature on the surface is $T_w$. The energy equation takes the form

$$UT_X + VT_Y + WT_Z = \alpha_{hnf}(T_{XX} + T_{YY} + T_{ZZ}). \tag{4.35}$$

Introducing

$$\Theta(\zeta) = \frac{T - T_\infty}{T_w - T_\infty}. \tag{4.36}$$

After applying the above transformation, the dimensionless energy equation is

$$\frac{\frac{\kappa_{hnf}}{\kappa_f}\Theta''}{\Pr\left(\left\{(1-\Phi_2)\left(1-\Phi_1+\Phi_1\frac{(\rho C_p)_{s_1}}{(\rho C_p)_f}\right)\right\} + \Phi_2\frac{(\rho C_p)_{s_2}}{(\rho C_p)_f}\right)} + (G + F)\Theta' = 0, \tag{4.37}$$

with Pr is Prandtl number. The temperature slip may exist on the plate surface. The temperature slip condition similar to Navier-Stokes condition is

$$-k_f\frac{\partial T}{\partial z} = h_w(T_w - T), \qquad as \ Z \to 0. \tag{4.38}$$

The dimensionless form of the above equation is

$$\Theta(0) = \delta\left(\frac{k_{hnf}}{k_f}\right)\Theta'(0) + 1. \tag{4.39}$$

For away from the surface of plate, the boundary condition is written as

$$T \to T_\infty \ , as \ Z \to \infty, \tag{4.40}$$

and the dimensionless form is written as

$$\Theta(\infty) = 0. \tag{4.41}$$

The velocity slip factor $\gamma$ that enter in the function $F$ and $G$ while the thermal slip effect

introduce the two extra parameters $\gamma(\frac{k_{hnf}}{k_f})$ and $\alpha_{hnf}$. For the large parameter $\epsilon \equiv \frac{1}{\gamma} \ll 1$ yield the dominant equation

$$\Theta = \epsilon\Theta_0 + \epsilon^2\Theta_1 + \cdots \tag{4.42}$$

Such that $\gamma$ is very large, after using the Eqs. (4.16, 4.17, 4.42) in Eqs. (4.37, 4.39, 4.41), we obtain the following equations

$$\frac{\frac{\kappa_{hnf}}{\kappa_f}\theta_0''}{Pr\left(\left\{(1-\Phi_2)\left(1-\Phi_1+\Phi_1\frac{(\rho C_p)_{S_1}}{(\rho C_p)_f}\right)\right\}+\Phi_2\frac{(\rho C_p)_{S_2}}{(\rho C_p)_f}\right)} + 2\zeta\Theta_0' = 0, \tag{4.43}$$

$$\Theta_0(0) = \delta(\frac{k_{hnf}}{k_f})\Theta_0'(0) + 1. \tag{4.44}$$

The solution of above initial values problem is

$$\Theta_0 = Cerfc\left(\sqrt{\frac{P_0}{\zeta}}\right), \tag{4.45}$$

where, $P_0 = \dfrac{Pr\left(\left\{(1-\Phi_2)\left(1-\Phi_1+\Phi_1\frac{(\rho C_p)_{S_1}}{(\rho C_p)_f}\right)\right\}+\Phi_2\frac{(\rho C_p)_{S_2}}{(\rho C_p)_f}\right)}{\frac{\kappa_{hnf}}{\kappa_f}}$ and $C$ is found from conditions at zero

$$C = \frac{1}{1+\beta_0\sqrt{\frac{2P_0}{\pi}}}, \tag{4.46}$$

where, $\beta_0 = \gamma\left(\frac{k_{hnf}}{k_f}\right)$. For large $\gamma$, temperature is defined as

$$\Theta'(0) = -\frac{\sqrt{\frac{2P_0}{\pi}}}{1+\delta_0\sqrt{\frac{2P_0}{\pi}}} + O(\gamma^{-1}). \tag{4.47}$$

We noted from (see Ref. [48]) that $\Theta$ is proportional to $F''$ and $G''$. Eq. (4.43) is indistinguishable to the differential Eqs. (4.8 − 4.9). Thus for $P = 1$,

$$\Theta(\zeta) = \frac{F''(\zeta) + G''(\zeta)}{\{F''(0) + G''(0) - \beta_0[\gamma_1{}^2(F''(0)^2 + \gamma_2{}^2G''(0)^2) - 1]\}}, \tag{4.48}$$

and

$$\Theta'(0) = \left\{\frac{F''(0) + G''(0)}{[\gamma_1{}^2(F''(0)^2 + \gamma_2{}^2G''(0)^2) - 1]} - \beta_0\right\}^{-1}, \tag{4.49}$$

for the arbitrary $P_0$ and large values of $\gamma = \gamma_1 = \gamma_2$, $F$ and $G \sim \zeta$ and solution of Eq. (4.43) is proportional to $erfc(\sqrt{P_0\zeta})$. the initial values found to be

$$\Theta'(0) = -\frac{2\sqrt{P_0/\pi}}{1+2\beta_0\sqrt{P_0/\pi}} + o(\gamma^{-1}), \tag{4.50}$$

for the general $\gamma$, Eqs. (4.41, 4.43, 4.44) are integrated numerically. The numerical values are calculated in the Tables [4.3-4.4] for both Hybrid nanofluid and nanofluid.

**Table-3: Thermal initial values of Hybrid nanofluid for axisymmetric flow. The values in the bracket are calculated from Eq. (4.50).**

| Pr | $\gamma_1$ | $\gamma = 0.0$ | $\gamma = 0.2$ | $\gamma = 0.5$ | $\gamma = 1$ | $\gamma = 2$ | $\gamma = 5$ | $\gamma = 10$ |
|---|---|---|---|---|---|---|---|---|
| 6.2 | 1 | -2.51242 | -1.42303 | -0.862236 | -0.520419 | -0.290273 | -0.124758 (-0.1240) | -0.0639669 (-0.0638) |
| 6.2 | 2 | -2.64461 | -1.4645 | -0.877286 | -0.525864 | -0.291959 | -0.125068 | -0.0640485 |
| 6.2 | 3 | -2.69537 | -1.47993 | -0.882800 | -0.52784 | -0.292567 | -0.125179 | -0.0640777 |
| 6.2 | 4 | -2.72215 | -1.48797 | -0.885654 | -0.528859 | -0.292880 | -0.125237 | -0.0640927 |

**Table-4: Thermal initial valued of Nanofluid for axisymmetric flow. The values in the bracket are calculated from Eq (4.50).**

| Pr | $\gamma_1$ | $\gamma = 0.0$ | $\gamma = 0.2$ | $\gamma = 0.5$ | $\gamma = 1$ | $\gamma = 2$ | $\gamma = 5$ | $\gamma = 10$ |
|---|---|---|---|---|---|---|---|---|
| 6.2 | 1 | -2.63778 | -1.55646 | -0.963806 | -0.589623 | -0.331907 (-0.3281) | -0.143604 (-0.1429) | -0.0738114 (-0.0736) |
| 6.2 | 2 | -2.80721 | -1.61393 | -0.98554 | -0.597686 | -0.334447 | -0.144078 | -0.0739363 |
| 6.2 | 3 | -2.87409 | -1.63582 | -0.993658 | -0.600662 | -0.335377 | -0.14425 | -0.0739816 |
| 6.2 | 4 | -2.90983 | -1.64733 | -0.997895 | -0.602208 | -0.335858 | -0.144339 | -0.074005 |

## 4.5  Results and discussion

The flow equations presented in the previous section are solved numerically and the obtained results are discussed in this section. First of all, it is noted that the functions $\psi$ and $\chi$ are partially non-coupled from $F$ and $G$ respectively. The initial value problem is started fom  Eq. (4.16) for the given slip factors $\gamma_1$ and $\gamma_2$ respectively. Further, it is checked that the values of $[F'(\zeta) - 1]^2 + [G'(\zeta) - 1]^2 \to 0$ for large values of $\xi$. The quantity of $F'(0)$ and $G'(0)$ denoted as stretching velocities owing to the stagnation point flow. The quantities $K^*(0)$ and $H^*(0)$ are the fluid slip velocities owing to moving plate. Suppose that $\gamma = \frac{\gamma_2}{\gamma_1}$ is ratio of slip factors. The range of $\gamma$ is taken to be $0.1 \leq \gamma \leq 1$ and having ''1'' being the case of isotropic. In the case of isotropic, we noted that $F = G$ and $K^* = H^*$. The large slip asymptotic solution concurs well with the numerical outcomes when $\gamma \geq 10$. It is noted that as the slip factor increases from zero, the slip velocities $F'(0)$ and $G'(0)$ are increased in both cases nanofluid and Hybrid nanofluid as shown in Tables [4.1-4.2]. It is also distinguished that velocity profiles $F'(\zeta)$ and $G'(\zeta)$ growth for large values of slip parameter of Hybrid nanofluid and nanofluid respectively as shown in Figs. (4.3) and (4.4). The universal functions $F(\xi)$ and $G(\xi)$ are coordinated by the stagnation flow and are not impacted by the horizontal movement of the plate. A few ordinary similarity velocities as appeared in Tables [4.1-4.2]. The slip velocities owing to lateral are described by the $H^*(0) - 1$ aligns the striations and $K^*(0) - 1$ through the striations. For no slip, $H^*(0)$, $K^*(0)$ are unity and decline to zero as slip parameter is

augmented. Note that the velocities owing to the sidelong development depend on the stagnation flow. Typically, universal profiles are revealed in Tables [4.1-4.2] for Nanofluid and Hybrid nanofluid.

The current study is focused on heat transfer of Hybrid nanofluid and nanofluid for stagnation slip flow on moving plate. The exact similarity solution in closed form is achieved for energy equation. The flow owing to the literal motion of the plate depends heavily upon the velocity slip parameter $\gamma = \gamma_1 = \gamma_2$ of Hybrid nanofluid and nanofluid both on the boundary and in governing equations over the stagnation flow. The following concludes that asymptotic formulas resulting from Eqs (4.47) and (4.50) agrees for large $\gamma$ and $\delta$ as revealed in Tables [4.3-4.4] for both hybrid nanofluid and simple nanofluid respectively. The heat transfer upsurges with rise in $\gamma_1$, declines with rise in $\gamma$ and increases for Prandtl number (Pr). It is seen that $\Theta'(0)$ is high for axisymmetric stagnation flow of Hybrid nanofluid and nanofluid. But the heat transfer rate for the axisymmetric case is actually less. Due to the fact, the normal velocities at infinity are equal and one should divide Eq. (4.50) through $\sqrt{2}$. However, the denominator is larger for $\gamma > 0$. Temperature profile increases for the increment of $\Phi_2$ and $\delta$ as revealed in Figs. (4.7-4.8) both for Hybrid nanofluid and nanofluid.

## 4.6 Final results

Three dimensional Hybrid nanofluid stagnation flow and heat transfer on the moving plate is considered in this study. The stagnation flow with an isotropic slip and asymptotic behavior for large slip in Hybrid nanofluid is also discussed here. The following key factors are concluded:

- The asymptotic formulas and the exact solution are accurate for large slip $\gamma$ and $\delta$.
- With the increment of physical parameters $\delta$ and $Pr$, temperature profile for both cases hybrid nanofluid and nanofluid increases.
- $H^*(0)$ and $K^*(0)$ are unity for no slip condition and are decreased to zero as slip is increased.
- Slip factors increases with the increase in normalized slip velocities $F'(0)$ and $G'(0)$.
- Anisotropic is reflected in the various slip velocities $F'(0)$ and $G'(0)$. It is found that relative velocities are higher at small slip.
- Velocity slip increases with increase in slip parameter in both cases Hybrid nanofluid and nanofluid.
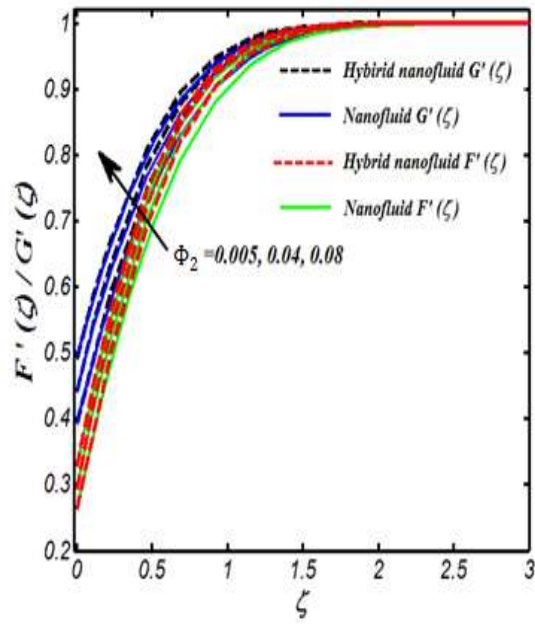
**Fig. 4.2:** Impact of $\Phi_2$ on the $F'(\zeta)$ and $G'(\zeta)$.
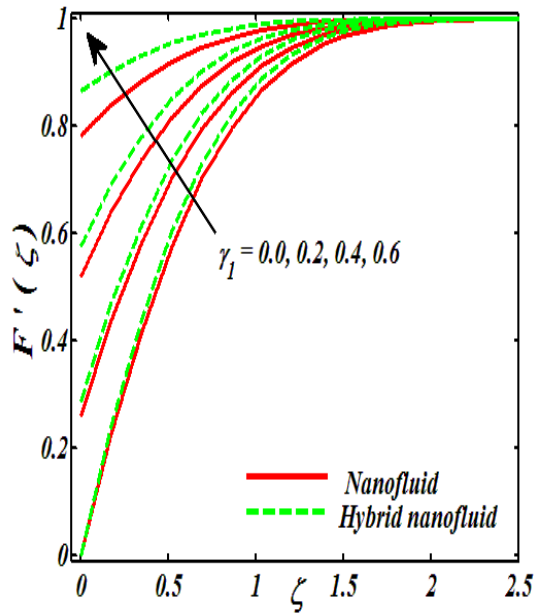


**Fig. 4.3:** Impact of $\gamma_1$ on the $F'(\zeta)$.
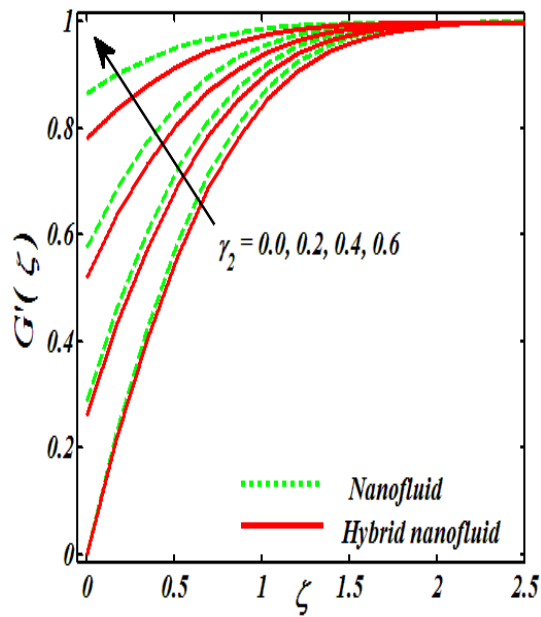
**Fig. 4.4:** Impact of $\gamma_2$ on the $G'(\zeta)$.
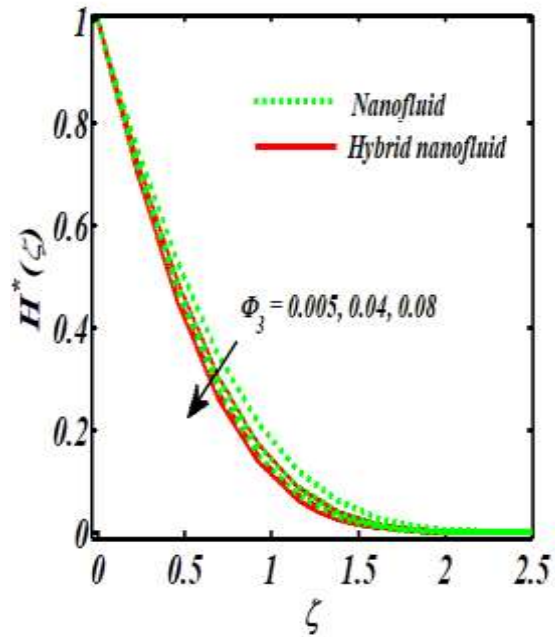


**Fig. 4.5:** Impact of $\Phi_2$ on the $H^*(\zeta)$.
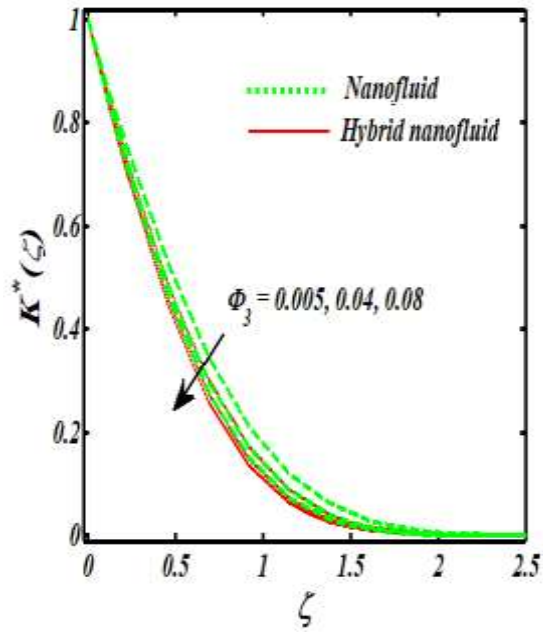
**Fig. 4.6:** Impact of $\Phi_2$ on the $K^*(\zeta)$.
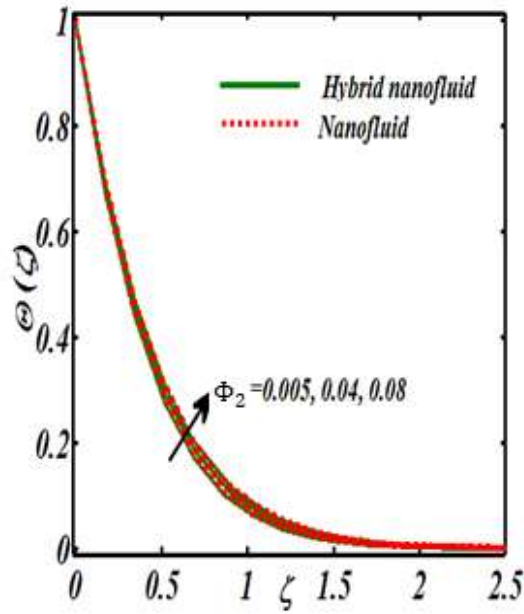


**Fig. 4.7:** Impact of $\Phi_2$ on the $\theta(\zeta)$.
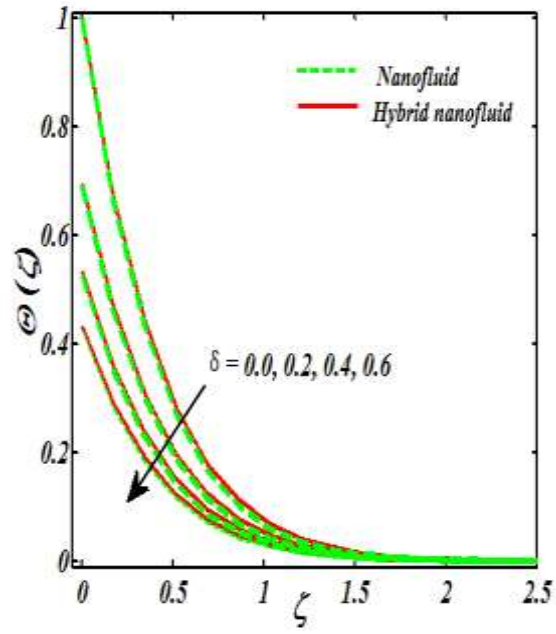
**Fig. 4.8:** Impact of $\delta$ on the $\Theta(\zeta)$.

# Chapter 05

## Computational analysis of water based $Cu - Al_2O_3/H_2O$ flow over a vertical wedge

### 5.1 Introduction

Hybrid nanomaterial fluid fluctuating flow at vertical Riga wedge is studied in this chapter. Different nanoparticles (two kinds) with base water fluid at vertical Riga wedge effects are discussed. The steady and unsteady cases also analyzed. The water has low thermal conductivity, thus we added the nanoparticle $Cu$ and $Al_2O_3$ which increases the thermal conductivity of the base fluid. This phenomena increase the heat transfer rate at the surface Riga plate. Partial differential equations are reduced into an ordinary differential equation by means of dimensionless similarity variables. The resulting ordinary differential equation is further solved through numerical and perturbation methods. Thickness of momentum boundary layer is declined because of the solid nanoparticle rises in all cases of $\xi = 0$, $(2i\xi)^0$, $(2i\xi)^1$ and $(2i\xi)^n$.
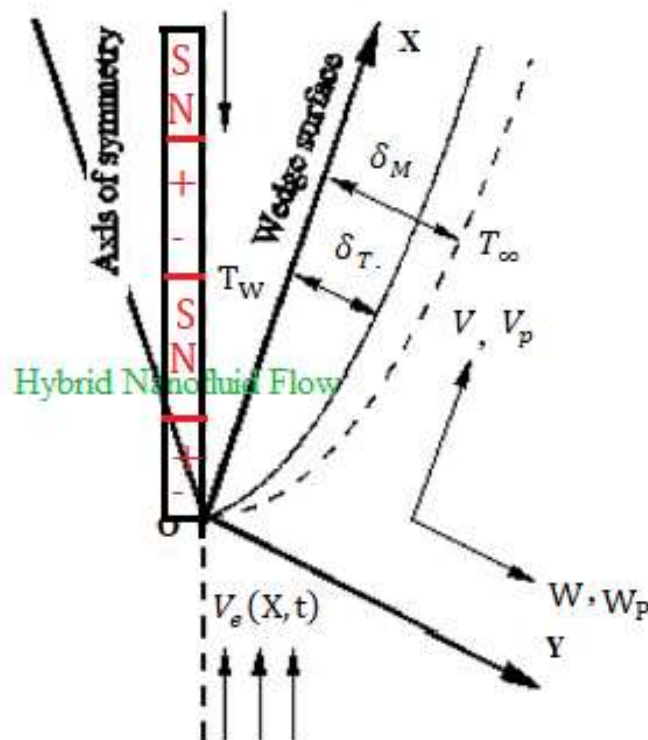


**Fig. 5.1:** Unsteady flow of Hybrid nanofluid over wedge.

## 5.2 Mathematical formulation

Consider the mixed convection fluctuating flow of Hybrid nanofluid over a vertical Riga wedge in the presence of solid nanoparticle see Fig. 5.1. The thermal and momentum boundary layer thickness is represented by $\delta_M$ and $\delta_T$. It is considered that both the free stream and surface temperature present small amplitude oscillations in time about steady, non-zero free stream velocity and mean temperature. The electro-magneto-hydrodynamic applied on the vertical wedge. Under the assumption and usual boundary layer approximation, the following mathematical system is

$$\frac{\partial V}{\partial X} + \frac{\partial W}{\partial Y} = 0,\tag{5.1}$$

$$\frac{\partial V}{\partial t} + V\frac{\partial V}{\partial X} + W\frac{\partial V}{\partial Y}$$
$$= -\frac{\partial P}{\partial X} + \left(\frac{\mu_{hnf}}{\rho_{hnf}}\right)\frac{\partial^2 V}{\partial Y^2} + \frac{\rho_f g\beta \cos(\pi/4)\,\bar{\bar{T}}}{\rho_{hnf}} + \frac{\pi J_0 M_0}{8\rho_{hnf}}exp(-\frac{\pi}{a}Y),\tag{5.2}$$

$$\left(\frac{\partial T}{\partial t} + V\frac{\partial T}{\partial X} + W\frac{\partial T}{\partial Y}\right) = \alpha_{hnf}\frac{\partial^2 T}{\partial Y^2},\tag{5.3}$$

where, $\bar{T} = T - T_\infty$ and the boundary conditions are

$$V = \lambda\frac{\partial V}{\partial Y},\;\; W = 0,\;\; \bar{T} = T_W + \lambda_1\kappa_{hnf}\frac{\partial T}{\partial Y},\;\; at\; Y \to 0,$$
$$V \to v_e(X,t),\;\; \bar{T} = T_\infty = 0,\;\; at\;\; Y \to \infty.\tag{5.4}$$

The coefficient of the volumetric expression for temperature expresses as $\beta$, $v_e(X,t)$ be the fre stream velocity, $V$ and $W$ be the local velocity components of the fluid, $\rho_{hnf}$, $\mu_{hnf}$, $\alpha_{hnf}$ and $\rho C_{p_{hnf}}$ is the density, viscosity, thermal conductivity and heat capacity of hybrid nanofluid. The above equations are simplified as

$$\frac{\partial V}{\partial X} + \frac{\partial W}{\partial Y} = 0,\tag{5.5}$$

$$\frac{\partial V}{\partial t} + V \frac{\partial V}{\partial X} + W \frac{\partial V}{\partial Y}$$

$$= \frac{\partial V_0}{\partial t} + V_0 \frac{\partial V_0}{\partial X} + v_{hnf} \frac{\partial^2 V}{\partial Y^2} + \frac{g\beta \cos(\pi/4)\bar{T}}{\rho_{hnf}} \tag{5.6}$$

$$+ \left(\frac{1}{\rho_{hnf}}\right) \frac{\pi J_0 M_0}{8} exp(-\frac{\pi}{a}Y),$$

$$\left(\frac{\partial \bar{T}}{\partial t} + V \frac{\partial \bar{T}}{\partial X} + W \frac{\partial \bar{T}}{\partial Y}\right) = \alpha_{hnf} \frac{\partial^2 \bar{T}}{\partial Y^2}, \tag{5.7}$$

and the corresponding boundary conditions are

$$V = \lambda \frac{\partial V}{\partial Y}, \quad W = 0, \bar{T} = T_W + \lambda_1 \kappa_{hnf} \frac{\partial \bar{T}}{\partial Y}, \quad at \ Y \to 0$$

$$V \to V_\infty(X,t), \quad \bar{T} = 0, \quad at \ Y \to \infty, \tag{5.8}$$

where,

$$V_w(X,t) = V_w(X)[1 + \epsilon \cos(\omega t)] \ and \ T_W(X,t) = \bar{T}_w(X)[1 + \epsilon \cos(\omega t)]. \tag{5.9}$$

The mean surface temperature and mean velocity represent as $\bar{T}_0(X)$ and $V_0(X)$, $\epsilon$ is the amplitude of oscillation which is $\epsilon \ll 1$ while the frequency of oscillation is $\omega$.

## 5.3 Solution procedure

On the behalf of the boundary conditions given in Eq. (5.8), we deliberate solutions of the system (5.5)-(5.8) in the following form

$$V(X,Y,t) = V_1(X,Y) + \epsilon V_2(X,Y) \ exp(i\omega t), \tag{5.10}$$

$$W(X,Y,t) = W_1(X,Y) + \epsilon W_2(X,Y) \ exp(i\omega t), \tag{5.11}$$

$$\bar{T}(X,Y,t) = T_1(X,Y) + \epsilon T_2(X,Y) \ exp(i\omega t), \tag{5.12}$$

where, $V_1$, $V_2$ are the fluctuating parts and $W_1$, $W_2$ are the velocity components, $V$, $W$ and $T_1$, $T_2$ are the real and fluctuating part of the temperature function $T$. The predictable solution functions are the real parts of the functions known in Eq. (5.9). The thermophysical properties are presented in Tables [5.3-5.4]. After applying the Eqs. (5.10)-(5.12) in Eqs. (5.6)-(5.8) and getting the terms and conditions to $0(\epsilon)$, we obtained succeeding equations

$$\frac{\partial V_1}{\partial X} + \frac{\partial W_1}{\partial Y} = 0, \tag{5.13}$$

$$V_1 \frac{\partial V_1}{\partial X} + W_1 \frac{\partial V_1}{\partial Y}$$

$$= V_w \frac{\partial V_w}{\partial X} + v_{hnf} \frac{\partial^2 V_1}{\partial Y^2} + \frac{g\beta \cos\left(\pi/4\right) T_1}{\rho_{hnf}} \tag{5.14}$$

$$+ \left(\frac{1}{\rho_{hnf}}\right) \frac{\pi J_0 M_0}{8} exp(-\frac{\pi}{a} Y),$$

$$\frac{\partial \Psi_1}{\partial Y} \frac{\partial T_1}{\partial X} - \frac{\partial \Psi_1}{\partial X} \frac{\partial T_1}{\partial Y} = \alpha_{hnf} \frac{\partial^2 T_1}{\partial Y^2}, \tag{5.15}$$

with the boundary conditions

$$V_1 = \lambda \frac{\partial V_1}{\partial Y}, \quad W = 0, T_1 = \bar{T}_0(X) + \lambda_1 \kappa_{hnf} \frac{\partial T_1}{\partial Y}, \quad at \ Y \to 0$$

$$V_1 \to V_0(X, t), \quad T_1 = 0, \quad at \ Y \to \infty, \tag{5.16}$$

and

$$\frac{\partial V_2}{\partial X} + \frac{\partial W_2}{\partial Y} = 0, \tag{5.17}$$

$$i\omega t V_2 + V_1 \frac{\partial V_2}{\partial X} + V_2 \frac{\partial V_1}{\partial X} + W_1 \frac{\partial V_2}{\partial Y} + W_2 \frac{\partial V_1}{\partial Y}$$

$$= i\omega t V_w(X) + V_0 \frac{\partial V_0}{\partial X} + v_{hnf} \frac{\partial^2 V_2}{\partial Y^2} + \frac{g\beta \cos\left(\pi/4\right) T_2}{\rho_{hnf}}, \tag{5.18}$$

$$i\omega t T_2 + V_1 \frac{\partial T_2}{\partial X} + V_2 \frac{\partial T_1}{\partial X} + W_1 \frac{\partial T_2}{\partial Y} + W_2 \frac{\partial T_1}{\partial Y} = \alpha_{hnf} \frac{\partial^2 T_2}{\partial Y^2}, \tag{5.19}$$

and relevant boundary conditions are

$$V_2 = \lambda \frac{\partial V_2}{\partial Y}, \quad W = 0, T_2 = \bar{T}_0(X) + \lambda_1 \kappa_{hnf} \frac{\partial T_2}{\partial Y}, \quad at \ Y \to 0,$$

$$V_2 \to V_0(X), \quad T_2 = 0, \quad at \ Y \to \infty. \tag{5.20}$$

Now, considering the functions $V_0(X)$ and $\bar{T}_0(X)$ like as $V_0(X) = V_c X^{1/2}$ and $\bar{T}_0(X) = T_c$ while $V_c$ and $T_c$ are the constants, we introduce the following similarity transformations for simplification

$$\Psi_1 = v_f X \sqrt{Re_X}(1 + Pr)^{-3/4} F(\zeta), \qquad T_1 = T_w \Theta(\zeta),$$

$$\Psi_2 = v_f X \sqrt{Re_X}(1 + Pr)^{-3/4} G(\zeta, \xi), \qquad T_2 = T_w H(\zeta, \xi), \tag{5.21}$$

$$\zeta = Y \sqrt{Re_X}(1 + Pr)^{1/4}, \xi = \frac{\omega}{V_c} \sqrt{X},$$

where, $\Psi_1$ and $\Psi_2$ are the stream function which satisfy the Eqs. (5.14) and (5.18)

correspondingly. The similarity and local frequency variables are $\zeta$ and $\xi$. By applying the similarity transformation Eq. (5.23) on Eqs. (5.20-5.22), we get the dimensionless form

$$(1 + Pr)\nu_{hnf}F''' + {}^{3}/_{4}\, FF'' - \frac{1}{2}(F'F' - 1 - Pr) + \frac{\rho_f Ri}{(1 + Pr)\rho_{hnf}}\theta + (1 \tag{5.22}$$

$$+ Pr)\frac{\rho_f M}{\rho_{hnf}}exp(-\sigma\zeta(1 + Pr)^{-1/4}),$$

$$\frac{1 + Pr}{Pr}\alpha_{hnf}\theta'' + {}^{3}/_{4}\, F\theta', \tag{5.23}$$

$$F(\zeta) = 0, \qquad F'(\zeta) = \gamma\frac{\mu_{hnf}}{\mu_f}(1 + Pr)^{\frac{1}{2}}F''(\zeta),$$

$$\theta(\zeta) = 1 + \delta\frac{\kappa_{hnf}}{\kappa_f}(1 + Pr)^{1/4}\theta'(\zeta), \quad \zeta \to 0, \tag{5.24}$$

$$F'(\zeta) \to (1 + Pr)^{1/2}, \quad \theta(\zeta) \to 0, as\ \zeta \to \infty.$$

The steady part of the flow is presented as

$$(1 + Pr)\nu_{hnf}G''' + {}^{3}/_{4}\, (FG'' + F''G) - F'G' + i\xi\left\{1 + Pr - (1 + Pr)^{\frac{1}{2}}G'\right\} + 1$$

$$+ Pr + (1 + Pr)\frac{\rho_f Ri}{\rho_{hnf}}H + (1 + Pr)\frac{\rho_f M}{\rho_{hnf}}exp\left(-\sigma\zeta(1 + Pr)^{-1/4}\right) \tag{5.25}$$

$$= \frac{1}{2}\xi\left(F'\frac{\partial G'}{\partial\xi} - F''\frac{\partial G}{\partial\xi}\right),$$

$$\frac{1 + Pr}{Pr}\alpha_{hnf}H'' + {}^{3}/_{4}\, (FH' + \theta'G) - i\xi(1 + Pr)^{\frac{1}{2}}H = \frac{1}{2}\xi\left(F'\frac{\partial H}{\partial\xi} - \theta'\frac{\partial G}{\partial\xi}\right), \tag{5.26}$$

and the boundary conditions are

$$G(\zeta) = 0, \qquad G'(\zeta) = \gamma\frac{\mu_{hnf}}{\mu_f}(1 + Pr)^{\frac{1}{2}}G''(\zeta),$$

$$H(\zeta) = 1 + \delta\frac{\kappa_{hnf}}{\kappa_f}(1 + Pr)^{1/4}H'(\zeta), \quad \zeta \to 0, \tag{5.27}$$

$$G'(\zeta) \to (1 + Pr)^{1/2}, \quad H(\zeta) \to 0, as\ \zeta \to \infty.$$

## 5.4 Pertur b a t i o n    s o l u t i o n s    f o r    s m a l l

To gain the impacts of mixed convection near the leading edge, the results based on the series ' finite numbers of terms are only valid for the small frequency range. The physical properties are discussed in Tables [5.2-5.3]. So,

$$G(\zeta, \xi) = \sum_{n=0}^{\infty} (2i\xi)^n G_n(\zeta), \quad H(\zeta, \xi) = \sum_{n=0}^{\infty} (2i\xi)^n H_n(\zeta). \tag{5.28}$$

Putting these values in Eqs. (5.25)-(5.27), then equating the coefficients of $(2i\xi)^0$

$$(1 + Pr)\nu_{hnf}G_0''' + \frac{3}{4}(FG_0'' + F''G_0) - F'G_0' + 1 + Pr + (1 + Pr)\frac{\rho_f Ri}{\rho_{hnf}}H_0$$

$$+ (1 + Pr)\frac{\rho_f M}{\rho_{hnf}}exp(-\sigma\zeta(1 + Pr)^{-1/4}) = 0, \tag{5.29}$$

$$\frac{1 + Pr}{Pr}\alpha_{hnf}H_0'' + \frac{3}{4}(FH_0' + \Theta'G_0) = 0, \tag{5.30}$$

and the boundary conditions are

$$G_0(\zeta) = 0, \quad G_0'(\zeta) = \gamma\frac{\mu_{hnf}}{\mu_f}(1 + Pr)^{\frac{1}{2}}G_0''(\zeta),$$

$$H_0(\zeta) = 1 + \delta\frac{\kappa_{hnf}}{\kappa_f}(1 + Pr)^{1/4}H_0'(\zeta), \quad \zeta \to 0, \tag{5.31}$$

$$G_0'(\zeta) \to (1 + Pr)^{1/2}, \quad H_0(\zeta) \to 0, as \; \zeta \to \infty.$$

Equating the coefficients of $(2i\xi)^1$

$$(1 + Pr)\nu_{hnf}G_1''' + \frac{3}{4}FG_1'' + \frac{5}{4}F''G_1 - \frac{3}{2}F'G_1' + \frac{\rho_f Ri}{\rho_{hnf}}(1 + Pr)H_1$$

$$+ \frac{1}{2}(1 + Pr) - \frac{1}{2}(1 + Pr)^{\frac{1}{2}}G_0' = 0, \tag{5.32}$$

$$\frac{1 + Pr}{Pr}\alpha_{hnf}H_1'' + \frac{3}{4}FH_1' + \frac{5}{4}\Theta'G_1 - \frac{1}{2}F'H_1 - \frac{1}{2}(1 + Pr)^{\frac{1}{2}}H_0 = 0, \tag{5.33}$$

and the relevant boundary conditions are

$$G_1(\zeta) = 0, \quad G_1'(\zeta) = \gamma\frac{\mu_{hnf}}{\mu_f}(1 + Pr)^{\frac{1}{2}}G_1''(\zeta),$$

$$H_1(\zeta) = \delta\frac{\kappa_{hnf}}{\kappa_f}(1 + Pr)^{1/4}H_1'(\zeta), \quad \zeta \to 0, \tag{5.34}$$

$$G_1'(\eta) \to 0, \quad H_1(\zeta) \to 0, as \; \zeta \to \infty.$$

Equating the coefficients of $(2i\xi)^n$

$$(1 + Pr)\nu_{hnf}G_n''' + \frac{3}{4}FG_n'' + \left\{\frac{3}{4} + \frac{n}{2}\right\}F''G_n - \left\{1 + \frac{n}{2}\right\}F'G_n' + \frac{\rho_f Ri}{\rho_{hnf}}(1$$

$$+ Pr)H_n - \frac{1}{2}(1 + Pr)^{\frac{1}{2}}G_{n-1}' = 0, \tag{5.35}$$

$$\frac{1 + Pr}{Pr} \alpha_{hnf} H_n'' + \frac{3}{4} F H_n' + \{\frac{3}{4} + \frac{n}{2}\} \Theta' G_n - \frac{1}{2} F' H_n - \frac{1}{2} (1 + Pr)^{\frac{1}{2}} H_{n-1} \quad (5.36)$$
$$= 0,$$

with the relevant boundary conditions are

$$G_n(\zeta) = 0, \qquad G_n'(\zeta) = \gamma \frac{\mu_{hnf}}{\mu_f} (1 + Pr)^{\frac{1}{2}} G_n''(\zeta),$$

$$H_n(\zeta) = \delta \frac{\kappa_{hnf}}{\kappa_f} (1 + Pr)^{1/4} H_n'(\zeta), \quad \zeta \to 0, \quad (5.37)$$

$$G_n'(\zeta) \to 0, \quad H_n(\zeta) \to 0, as \ \zeta \to \infty.$$

## 5.5  Results and discussion

The inspiration of the physical parameters on the heat transfer and skin fraction is presented in Table 5.1. The skin friction improved because of improving the solid nanoparticle. Heat transfer rate declines as well as solid nanoparticle enhances which is revealed in Table 5.1. The heat transfer rate $(2i\xi)^n$ (Unsteady flow) achieve much higher than that of the $\xi = 0$ (Steady flow) in case of the $Re_X^{1/2} C_f$ and $Re_X^{1/2} N_{ux}$. Skin friction reduces when the slip parameter rises. The thickness of momentum is reduced by cause of the enhancing $\gamma$. While, the heat transfer improved with improving the $\gamma$ because thickness of thermal boundary rises by cause of velocity slip enhances. In the case of $\xi = 0$, variation of the modified Hartman number on the skin friction and heat transfer is revealed in Table 5.1. Skin friction reduces when the modified Hartman number rises. The thickness of momentum is reduced because of the enhancing modified Hartman number, but opposite results are achieved for the $(2i\xi)^n$, while the heat transfer reduced with improving the modified Hartman number because thickness of thermal boundary declines because of velocity slip enhances, but opposite results are achieved for the $(2i\xi)^n$. In case of $\xi = 0$, variation of the Richardson number on the skin friction and heat transfer is revealed in Table 5.1. Skin friction improves when the Richardson number rises. The thickness of momentum is improved because of enhancing Richardson number, but opposite results are achieved for the $(2i\xi)^n$. In case of $\xi = 0$, the heat transfer is improved by improving the Richardson number because thickness of thermal boundary improves because velocity slip enhances but opposite results are achieved for the $(2i\xi)^n$. In case of $\xi = 0$, variation of the dimensionless number on the skin friction and heat transfer is revealed in Table 5.1. Skin friction improves when the dimensionless number rises. The thickness of momentum improves

because of enhancing dimensionless number, but opposite results are achieved for the $(2i\xi)^n$. In case of $\xi = 0$, the heat transfer improved with improving the dimensionless number because thickness of thermal boundary improves because velocity slip enhances but opposite results are achieved for the $(2i\xi)^n$. Impressions of the parameters on the modified Hartman number, thermal slip, velocity slip and solid nanoparticle on the temperature gradient are highlighted in Figs. 5.2-5.5 for the various cases $\xi = 0$, $(2i\xi)^0$, $(2i\xi)^1$and $(2i\xi)^n$. Fig. 5.2 reveals the variation of thermal thickness and thermal slip. It is achieved that thermal thickness is reduced because of improving the thermal slip parameter for all cases: $\xi = 0$, $(2i\xi)^0$, $(2i\xi)^1$and $(2i\xi)^n$. But, the thermal thickness reduces $(2i\xi)^0$, $(2i\xi)^1$and $(2i\xi)^n$ respecticly, as the values of $n$ are enhanced at the surface of the Riga vertical wedge.

Fig. 5.3 reveals the variation of thermal thickness and solid nanoparticle concentration $\Phi_2$. It is achieved that thermal thickness rises because of improving the solid nanoparticle for all cases of $\xi = 0$, $(2i\xi)^0$, $(2i\xi)^1$and $(2i\xi)^n$. The thermal thickness growths owing to enhancing the $\delta$ increases. When the solid nanoparticles added in the base fluid which improves the $\delta$ but in case of the thermal thickness improved $(2i\xi)^0$, $(2i\xi)^1$and $(2i\xi)^n$ respecticly, as the values of $n$ are enhanced at the surface of the Riga vertical wedge. Fig. 5.4 reveals the variation of thermal thickness and modified Hartman number. It is achieved that thermal thickness rises because of improving the modified Hartman number for all cases $\xi = 0$, $(2i\xi)^0$, $(2i\xi)^1$and $(2i\xi)^n$ but in case of the thermal thickness improved $(2i\xi)^0$, $(2i\xi)^1$and $(2i\xi)^n$ respecticly, as the values of $n$ are enhanced at the surface of the Riga vertical wedge. This phenomena exists due to Lorentz forces $F_m = (-F_m, 0, 0)$ which are explained physically. The electromagnetic forces $F_m = \left(\frac{1}{\rho_{hnf}}\right)\frac{\pi J_0 M_0}{8} exp(-\frac{\pi}{a}Y)$ work as opposite along to the motion of fluid as drag-like forces which successful extents are rotting exponentially along the y axis. Fig. 5.5 reveals the variation of thermal thickness and velocity slip. It is achieved that thermal thickness is reduced because of improving the velocity slip parameter for all cases $\xi = 0$, $(2i\xi)^0$, $(2i\xi)^1$and $(2i\xi)^n$, but in case of the thermal thickness reduced $(2i\xi)^0$, $(2i\xi)^1$and $(2i\xi)^n$ respecticly, as the values of $n$ are enhanced at the surface of the Riga vertical wedge. Impacts of the physical parameters on the modified Hartman number, $\delta$, $\gamma$ and solid nanoparticle on the velocity distribution are highlighted in Figs. 5.6-5.9 for the various cases $\xi = 0$, $(2i\xi)^0$, $(2i\xi)^1$and $(2i\xi)^n$. Variation of the thermal slip and velocity profile are presented in Fig. 5.6. Thickness of momentum is reduced because of the thermal slip rises in all cases $\xi = 0$, $(2i\xi)^0$, $(2i\xi)^1$and $(2i\xi)^n$.

Momentum thickness decreases because of enhancing the values of $n$. Variation of the velocity slip and velocity profile are presented in Fig. 5.7. Momentum thickness enhanced due to velocity slip upsurges in all cases of $\xi = 0$, $(2i\xi)^0$, $(2i\xi)^1$and $(2i\xi)^n$. Momentum thickness decreases because of enhancing the values of $n$. Variation of the solid nanoparticle and velocity profile is presented in Fig. 5.8. Momentum thickness is reduced because of the solid nanoparticle rises in all cases of $\xi = 0$, $(2i\xi)^0$, $(2i\xi)^1$and $(2i\xi)^n$ and thermal thickness upsurges owing to enhancing the thermal conductivity of the fluid increases. Momentum thickness decreases because of enhancing the values of $n$. Variation of the modified Hartman number and velocity profile is presented in Fig. 5.9. Thickness of momentum improved because the modified Hartman number rises in all cases $\xi = 0$, $(2i\xi)^0$, $(2i\xi)^1$and $(2i\xi)^n$. Momentum thickness decreases because of enhancing the values of $n$.

**Table 5.1: Numerical results of heat transfer and skin friction.**

| Physical parameters | | | | | | Steady case | | Unsteady case | |
|---|---|---|---|---|---|---|---|---|---|
| $\Phi_2$ | $\gamma$ | $\delta$ | $M$ | $Ri$ | $\sigma$ | $Re_X^{1/2}C_f$ | $Re_X^{1/2}Nu_X$ | $Re_X^{1/2}C_f$ | $Re_X^{1/2}Nu_X$ |
| 0.005 | 0.3 | 0.4 | 0.5 | 0.4 | 0.4 | 1.3863 | 0.6330 | 17.8755 | 1.3177 |
| 0.02 | | | | | | 1.4122 | 0.5991 | 18.1203 | 1.2363 |
| 0.04 | | | | | | 1.4489 | 0.5572 | 18.4219 | 1.1373 |
| 0.06 | | | | | | 1.4880 | 0.5185 | 18.6809 | 1.0481 |
| 0.04 | 0.0 | | | | | 3.0803 | 0.4734 | 53.3095 | 1.0877 |
| | 0.3 | | | | | 1.4489 | 0.5572 | 18.1219 | 1.1373 |
| | 0.6 | | | | | 0.8782 | 0.5690 | 10.5880 | 1.1343 |
| | 0.3 | 0.0 | | | | 1.5126 | 1.2494 | 18.2691 | 7.6309 |
| | | 0.2 | | | | 1.4689 | 0.7694 | 18.1219 | 2.3232 |
| | | 0.4 | | | | 1.4489 | 0.5572 | 17.8755 | 1.1373 |
| | | 0.6 | | | | 1.4373 | 0.4370 | 17.4383 | 0.6821 |
| | | 0.4 | 0.0 | | | 1.7618 | 0.4498 | 1.4169 | 0.1913 |
| | | | 0.5 | | | 1.4373 | 0.4370 | 18.2691 | 0.6821 |
| | | | 1.0 | | | 1.0372 | 0.4172 | 40.1539 | 1.5455 |
| | | | 0.5 | 0.0 | | 1.3938 | 0.4354 | 18.7622 | 0.7086 |
| | | | | 0.4 | | 1.4373 | 0.4370 | 18.2691 | 0.6821 |
| | | | | 0.8 | | 1.4789 | 0.4385 | 17.8242 | 0.6584 |
| | | | | 0.4 | 0.0 | 1.2104 | 0.4244 | 25.2105 | 1.0087 |
| | | | | | 0.2 | 1.3646 | 0.4333 | 20.7774 | 0.7881 |
| | | | | | 0.4 | 1.4373 | 0.4370 | 18.2691 | 0.6821 |
| | | | | | 0.6 | 1.4817 | 0.4392 | 16.5176 | 0.6145 |

## Table 5.2. Thermo-physical properties.

| Properties | Nanofluid | Hybrid nanofluid |
|---|---|---|
| Heat capacity | $(\rho C_p)_{nf} = (1 - \Phi)(\rho C_p)_f + \Phi(\rho C_p)_s$ | $(\rho C_p)_{hnf} = [\{(1 - \Phi_2)(1 - \Phi_1)(\rho C_p)_f\} + \Phi_1(\rho C_p)_{s_1}] + \Phi_2 \rho(\rho C_p)_{s_2}$ |
| Density | $\rho_{nf} = (1 - \Phi)\rho_f + \Phi\rho_s$ | $\rho_{hnf} = \{[(1 - \Phi_2)(1 - \Phi_1)\rho_f\} + \Phi_1\rho_{s_1}] + \Phi_2\rho_{s_2}$ |
| Thermal conductivity | $\dfrac{\kappa_{nf}}{\kappa_f} = \dfrac{\kappa_s + (n-1)\kappa_f - (n-1)\Phi(\kappa_f - \kappa_s)}{\kappa_s + (n-1)\kappa_f + \Phi(\kappa_f - \kappa_s)}$ | $\dfrac{\kappa_{hnf}}{\kappa_{bf}} = \dfrac{\kappa_{s_2} + (n-1)\kappa_{bf} - (n-1)\Phi_2(\kappa_{bf} - \kappa_{s_2})}{\kappa_{s_2} + (n-1)\kappa_{bf} + \Phi_2(\kappa_{bf} - \kappa_{s_2})}$ where $\dfrac{\kappa_{bf}}{\kappa_f} = \dfrac{\kappa_{s_1} + (n-1)\kappa_f - (n-1)\Phi_1(\kappa_f - \kappa_{s_1})}{\kappa_{s_1} + (n-1)\kappa_f + \Phi_1(\kappa_f - \kappa_{s_1})}$ |
| Viscosity | $\mu_{nf} = \dfrac{\mu_f}{(1 - \Phi)^{2.5}}$ | $\mu_{hnf} = \dfrac{\mu_f}{(1 - \Phi_1)^{2.5}(1 - \Phi_2)^{2.5}}$ |

## Table 5.3: Properties of the thermo-physical.

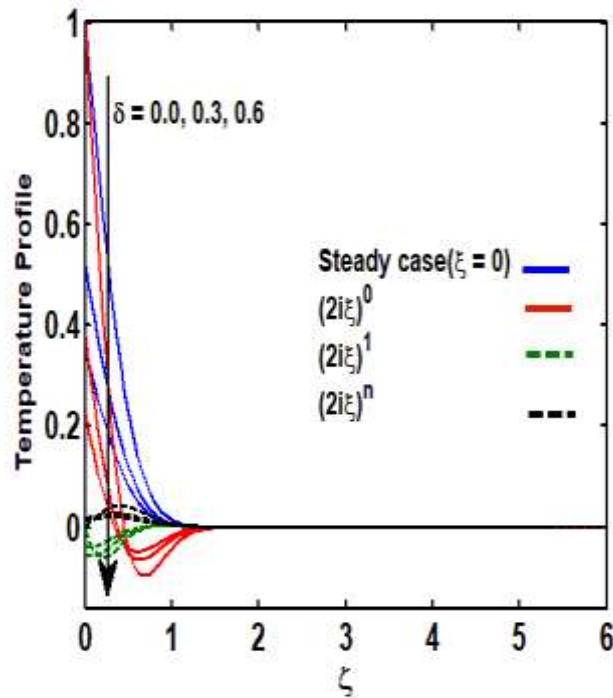| Thermo-physical properties | Fluid phase (water) | $Al_2O_3$ | Cu |
|---|---|---|---|
| $C_p(j/kg)K$ | 4179 | 765 | 385 |
| $\rho(kg/m^3)$ | 997.1 | 3970 | 8933 |
| $k(W/mK)$ | 0.613 | 40 | 400 |
| $\alpha \times 10^7 (m^2/s)$ | 1.47 | 131.7 | 1163.1 |

**Fig. 5.2**

**Fig. 5. 3**
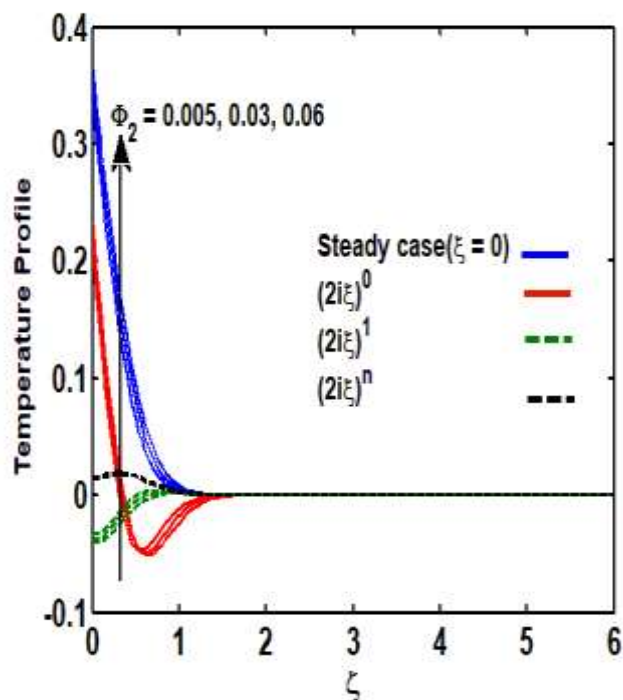


Variation of thermal slip and solid nanoparticle on temperature profile.

**Fig. 5. 4**
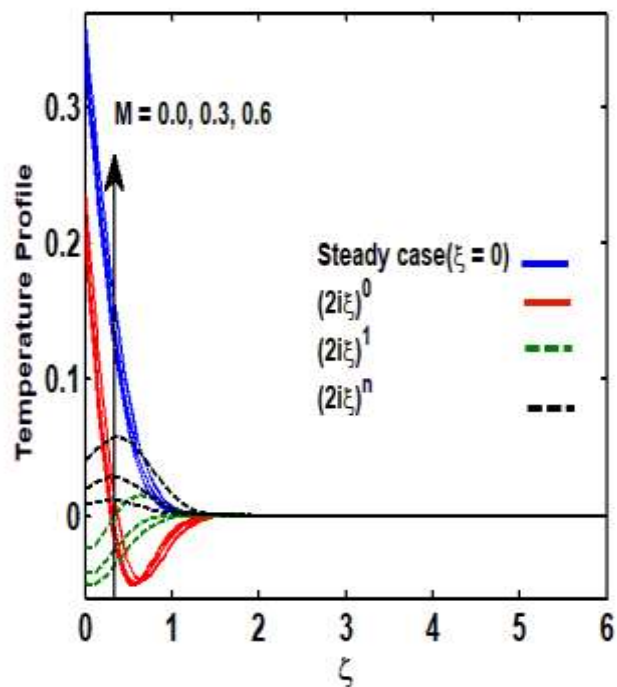
**Fig. 5. 5**
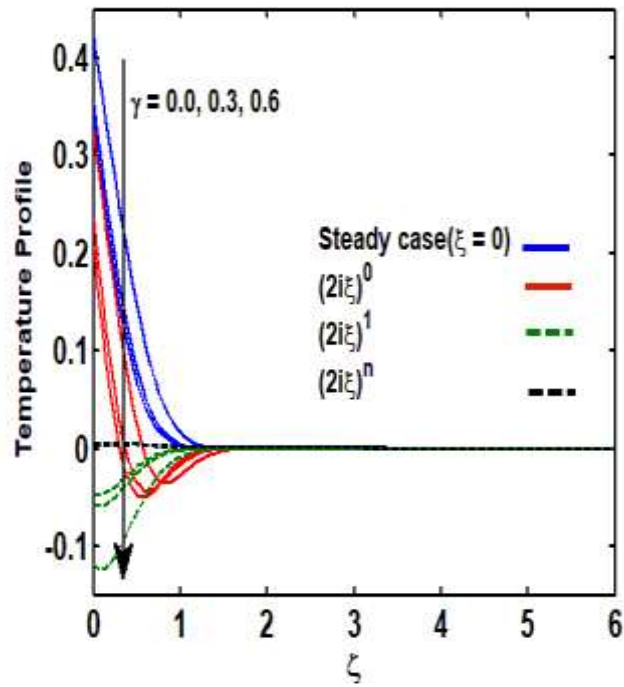


Variation of modified Hartman number and velocity slip on temperature profile.

**Fig. 5. 6**
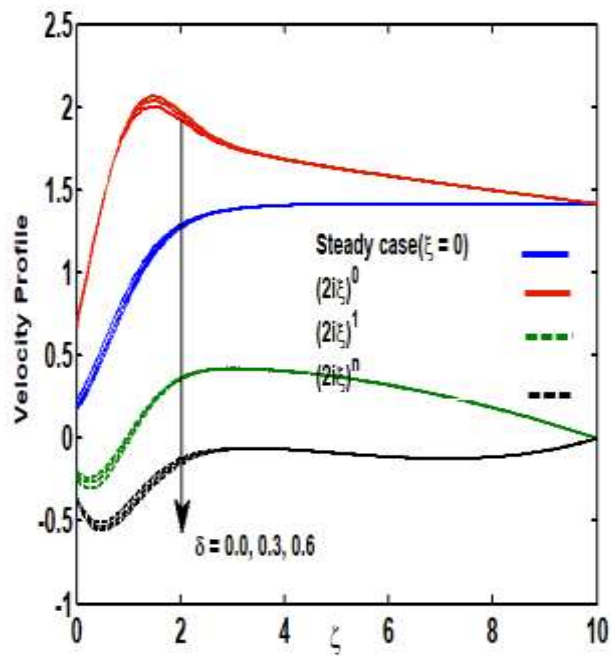
**Fig. 5. 7**
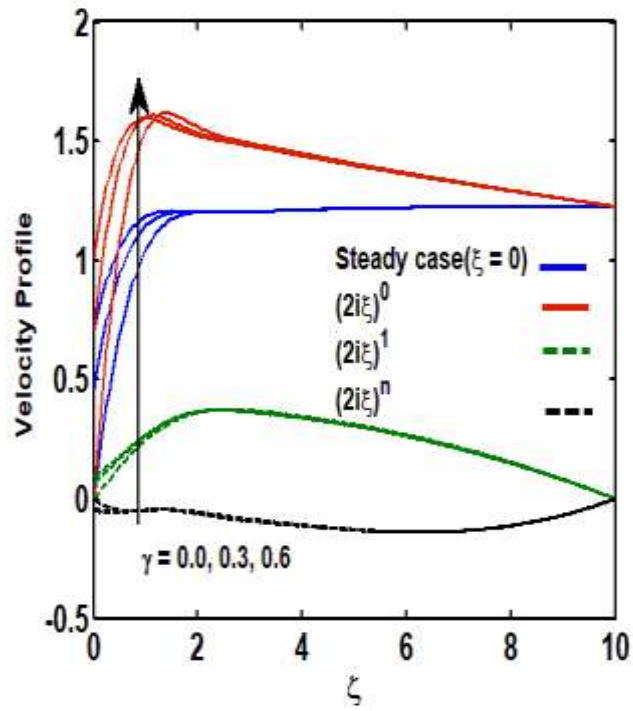


Variation of thermal slip and velocity slip on velocity profile.

**Fig. 5. 8**
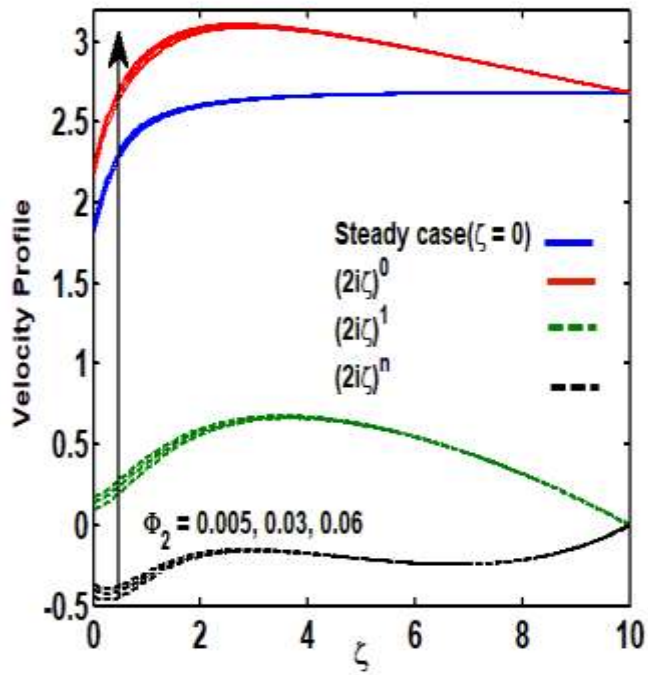
**Fig. 5. 9**
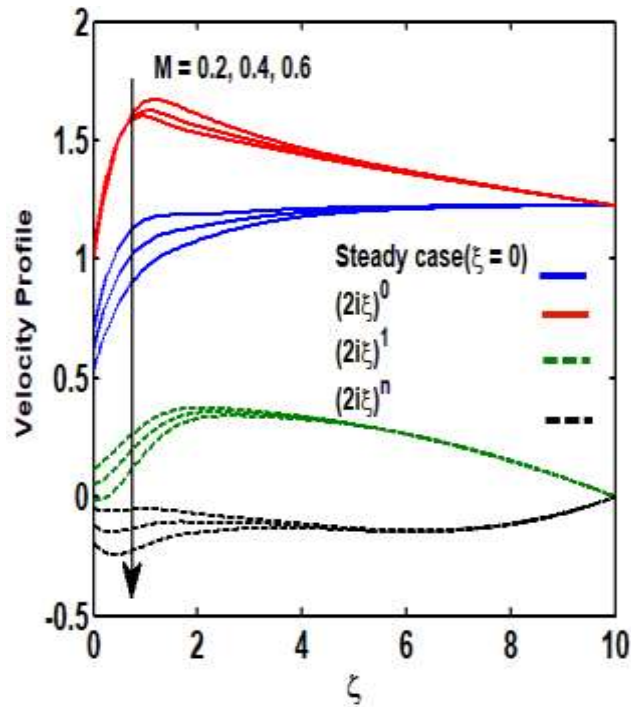


Variation of modified Hartman number and solid nanoparticle on velocity profile.

## 5.6 Final remarks

The mixed convection fluctuating flow of Hybrid nanoparticle fluid at a vertical Riga wedge is studied. Major expression of involving parameters on the temperature, velocity, heat transfer and skin friction on the Riga vertical wedge are highlighted as

- The momentum thickness is reduced because of enhancing $\gamma$ while the heat transfer improved with improving $\gamma$.

- In case of $\xi = 0$, the heat transfer improved with improving the Richardson number because thickness of thermal boundary improves due to velocity slip enhances but opposite results are achieved for the $(2i\xi)^n$.

- Momentum thickness decreases by cause of enhancing the values of $n$ $((2i\xi)^0$, $(2i\xi)^1$ and $(2i\xi)^n)$.

- Thickness of momentum reduced due to solid nanoparticle growths in all cases of $\xi = 0$, $(2i\xi)^0$, $(2i\xi)^1$ and $(2i\xi)^n$.

## Chapter 06

## Theoretical analysis of slip effects based micropolar Hybrid nanofluid over a Riga curved surface

### 6.1  Introduction

In this chapter, the steady flow of micropolar Hybrid nanomaterial fluid at a nonlinear stretching curved surface is analyzed. Two different types of the nanoparticles are studied at the curved surface. The influences of thermal and velocity slips on the curved surface are discussed. The governing equations of the motions for the micropolar Hybrid nanomaterial fluid flow are simplified under the assumptions of boundary layer theory. The system of differential equations in term of partial differential equations becomes dimensionless by means of similarity transformations. The simplified ODE's are elucidated through a numerical scheme. The results of the thermal and velocity slip, curvature parameter, microrotation parameter, and solid nanoparticle concentration at the curved surface are highlighted through graphs and tables. Surprisingly, the numerical values of $SWCNT - MWCNT/H_2$ gains higher values than that of $MWCNT/H_2O$ in all the cases for weak concentration $(n = 0.5)$ and $n = 0.0$. The values of $Re_s^{1/2}C_f$, $Re_s^{1/2}N_{u_s}$ and $Re_s^{1/2}C_m$, the weak concentration $(n = 0.5)$ achieves sophisticated values as compared to the $n = 0.0$.



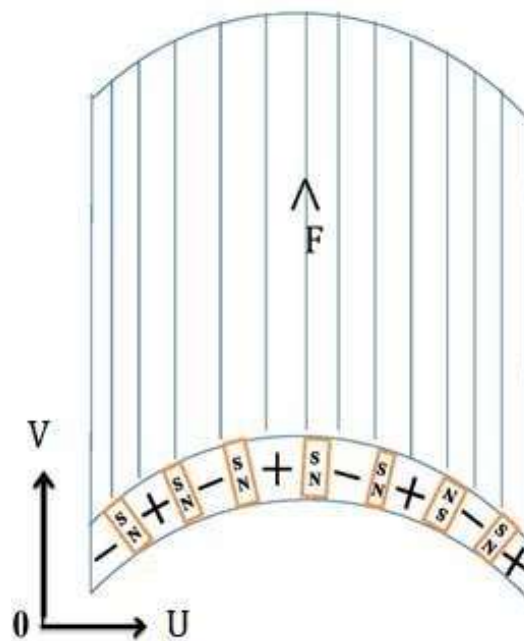**Fig. 6.1:** Flow of Hybrid nanomaterial fluid at Riga curved surface.

## 6.2 Mathematical formulation

The steady base flow of micropolar Hybrid nanofluid at a nonlinear stretching Riga curved surface is studied (see Fig. 6.1). Here, $R$ is the radius of curvature while $r$ and $s$ are the curvilinear coordinate. The mathematical model under flow assumption are defined as

$$\vec{\nabla}.\vec{V} = 0, \tag{6.1}$$

$$\rho\left(\frac{\partial\vec{V}}{\partial t}\right) + (\vec{V}.\vec{\nabla})\vec{V} = -\vec{\nabla}P + K\vec{\nabla}\times\vec{\Omega} + (\mu + K)\,\nabla^2\vec{V} + \sigma(\vec{J}\times\vec{B}) + \vec{F}, \tag{6.2}$$

$$\rho\left(\frac{\partial\vec{V}}{\partial t}\right) + (\vec{V}.\vec{\nabla})\vec{V} = -2K\vec{\Omega} + K\vec{\nabla}\times\vec{V} - \gamma(\vec{\nabla}\times\vec{\nabla}\times\vec{\Omega}) + (\alpha + \beta + \gamma)\vec{\nabla}(\vec{\nabla}\,\vec{\Omega}), \tag{6.3}$$

$$\rho c_p\left(\left(\frac{\partial\vec{T}}{\partial t}\right) + (\vec{V}.\vec{\nabla})\vec{T}\right) = \vec{\nabla}(K\vec{\nabla}.\vec{T}). \tag{6.4}$$

By introducing approximations to the physical phenomenon, the over-conditions are transformed into following forms:

$$\frac{1}{r + R_1}\frac{\partial}{\partial r}\big((r + R_1)V\big) + \frac{R_1}{r + R_1}\frac{\partial U}{\partial s} = 0, \tag{6.5}$$

$$\frac{U^2}{r + R_1} = \frac{1}{\rho_{hnf}}\frac{\partial p}{\partial r}, \tag{6.6}$$

$$\begin{aligned}
\left(V\frac{\partial U}{\partial r} + \frac{R_1 U}{r + R_1}\frac{\partial U}{\partial s} + \frac{VU}{r + R_1}\right) &+ \frac{1}{\rho_{hnf}}\frac{1}{r + R_1}\frac{\partial p}{\partial r}\\
&= \frac{\rho_f}{\rho_{hnf}}\left(\frac{1}{(1 - \Phi_2)^{5/2}(1 - \Phi_1)^{5/2}} + K\right)\left(\frac{\partial^2 U}{\partial^2 r} + \frac{1}{r + R_1}\frac{\partial U}{\partial r}\right.\\
&\left. - \frac{U}{(r + R_1)^2}\right) - \frac{K_1}{\rho_{hnf}}\frac{\partial N}{\partial r} + \frac{\pi J_0 M_0}{8\rho_f}\exp\left(-\frac{\pi}{a}r\right),
\end{aligned} \tag{6.7}$$

$$\begin{aligned}
\left(V\frac{\partial N}{\partial r} + \frac{R_1 U}{r + R_1}\frac{\partial N}{\partial s}\right) &= \frac{\rho_f}{\rho_{hnf}}\left(\frac{1}{(1 - \Phi_2)^{5/2}(1 - \Phi_1)^{5/2}} + K/2\right)\left(\frac{\partial^2 N}{\partial^2 r} + \frac{1}{r + R_1}\frac{\partial N}{\partial r}\right)\\
&- \frac{K_1}{2\rho_{hnf}}\left(\frac{\partial N}{\partial r} + 2N + \frac{u}{r + R_1}\right),
\end{aligned} \tag{6.8}$$

$$\left(V\frac{\partial T}{\partial r} + \frac{R_1 U}{r + R_1}\frac{\partial T}{\partial s}\right) = \alpha_{hnf}\left(\frac{\partial^2 T}{\partial^2 r} + \frac{1}{r + R_1}\frac{\partial T}{\partial r}\right). \tag{6.9}$$

$U - u_w\,\alpha\,\mu[\tau_{rz}]$ is the partial slip at curved surface whose expression finally takes the following form along with the boundary conditions

$$V = 0, \quad T = T_w + \lambda_1\frac{k_{hnf}}{k_f}\left(\frac{\partial T}{\partial r}\right), U = L\left[\frac{\partial U}{\partial r} + \frac{U}{r + R_1} + kN\right] + u_0 e^{s/l}, \tag{6.10}$$

$$N = -n\frac{\partial U}{\partial r}, \quad \text{at } r \to 0,$$
$$U \to 0, \quad N \to 0, \quad T \to T_\infty, \quad \text{at } r \to \infty.$$

The appropriate transformations are

$$T = T_\infty + (T_w - T_\infty)\Theta(\zeta), \quad \zeta = \sqrt{\frac{a}{\nu_f}}r, \quad U = u_0\left(e^{s/l}\right)F'(\zeta),$$

$$V = -\frac{R_1}{r + R_1}\sqrt{\frac{\nu_f}{a}}\left(e^{s/l}\right)F(\zeta),$$

$$N = \sqrt{a\nu_f}\left(e^{s/l}\right)H(\zeta), \quad P = \rho a^2\left(e^{2s/l}\right)p(\zeta).$$

(6.11)

Utilization of above expression in Eqs. (6.5) to (6.10) give the following equations

$$P' = \frac{F'^2}{\zeta + K_1},$$

(6.12)

$$\frac{2K}{\zeta + K_1}P = \frac{\rho_f}{\rho_{hnf}}\left(\frac{1}{(1 - \Phi_2)^{5/2}(1 - \Phi_1)^{5/2}} + K\right)\left[F''' + \frac{F''}{\zeta + K_1} - \frac{F'}{(\zeta + K_1)^2}\right]$$
$$- \frac{R_0 K_1}{\zeta + K_1}F'^2 + \frac{R_0 K_1}{\zeta + K_1}F'F'' + \frac{R_0 K_1}{(\zeta + K_1)^2}FF' - \frac{\rho_f}{\rho_{hnf}}R_0 KH(\zeta)$$
$$+ \emptyset \exp(-\omega\zeta) = 0,$$

(6.13)

$$\frac{\rho_f}{\rho_{hnf}}\left(\frac{1}{(1 - \Phi_2)^{5/2}(1 - \Phi_1)^{5/2}} + K/2\right)\left[H'' + \frac{H'}{\zeta + K_1}\right] - \frac{R_0 K_1}{2(\zeta + K_1)}F'H$$
$$+ \frac{R_0 K_1}{2(\zeta + K_1)}FH' - \frac{R_0 K}{2\rho_{hnf}}\left(2H + F'' + \frac{1}{\zeta + K_1}F'\right),$$

(6.14)

$$\alpha_{hnf}\left(\Theta'' + \frac{1}{\zeta + K_1}\Theta'\right) + \frac{R_0}{\zeta + K_1}F\Theta' - \frac{R_0}{\zeta + K_1}\Theta = 0.$$

(6.15)

Eliminating the pressure term, and solving Eqs. (6.12) and (6.13)

$$\frac{\rho_f}{\rho_{nf}}\left(\frac{1}{(1 - \Phi_1)^{5/2}} + K\right)\left(F'''' + \frac{2}{\zeta + K_1}F''' - \frac{1}{(\zeta + K_1)^2}F'' + \frac{1}{(\zeta + K_1)^3}F'\right)$$
$$- \frac{R_0 K_1}{\zeta + K_1}(F''F' - FF''') - \frac{R_0 K_1}{(\zeta + K_1)^2}(F'^2 - FF'') - \frac{R_0 K_1}{(\zeta + K_1)^3}FF'$$
$$- \frac{\rho_f}{\rho_{nf}}R_0 KH'(\zeta) - \omega\emptyset\exp(-\omega\zeta) = 0,$$

(6.16)

$$\frac{\rho_f}{\rho_{nf}}\left(\frac{1}{(1 - \Phi_1)^{5/2}} + K/2\right)\left(H'' + \frac{H'}{\zeta + K_1}\right) - \frac{R_0 K}{2(\zeta + K_1)}F'H + \frac{R_0 K}{2(\zeta + K_1)}FH'$$
$$- \frac{\rho_f}{\rho_{nf}}\frac{R_0 K}{2}\left(2H + F'' + \frac{1}{\zeta + K_1}F'\right),$$

(6.17)

$$\alpha_{nf}\left(\Theta'' + \frac{1}{\zeta + K_1}\Theta'\right) + \frac{K_1 R_0}{\zeta + K_1}F\Theta' - \frac{K_1 R_0}{\zeta + K_1}\Theta = 0.$$

(6.18)

Relevant conditions are

$$F(0) = 0, \quad F'(0) = 1 + \gamma[\frac{F'(0)}{K_1}(1 - n)F''(0)], \quad F'(\infty) = 0, \quad F''(\infty) = 0,$$
$$H(0) = nF''(0), \quad H(\infty) = 0,$$

(6.19)

$$\Theta(0) = 1 + \delta \frac{k_{hnf}}{k_f} \Theta'(0), \qquad \Theta(\infty) = 0.$$

The parameters $C_f$ and $N_{us}$ and $C_m$ are described as

$$C_f = \frac{\tau_{rs}}{\rho_{hnf} u_w^2}, \quad N_{us} = \frac{s q_w}{k_{hnf}(T_w - T_\infty)}, C_m = \left(e^{s/l}\right) \frac{\tau_m}{\rho_{hnf} u_w^2}, \qquad (6.24)$$

where, $\tau_{rs}$ is the wall shear stress, $q_w$ is the heat flux and $C_m$ is the couple stress which are defined as

$$\tau_{rs} = \frac{\rho_f}{\rho_{hnf}} \left( \frac{1}{(1-\Phi_2)^{\frac{5}{2}}(1-\Phi_1)^{\frac{5}{2}}} + K \right) \left( \frac{\partial u}{\partial r} + \frac{u}{r+R} + kN \right)_{r=0},$$

$$\tau_m = \frac{\rho_f}{\rho_{hnf}} \left( \frac{1}{(1-\Phi_2)^{5/2}(1-\Phi_1)^{5/2}} + K/2 \right) \left( \frac{\partial N}{\partial r} + \frac{N}{r+R} \right)_{r=0}, \qquad (6.25)$$

$$q_w = -k_{hnf} \left( \frac{\partial T}{\partial r} \right)_{r=0}.$$

Using Eq. (6.24) in Eq. (6.25), we get

$$Re_s^{1/2} C_f = \frac{\rho_f}{\rho_{hnf}} \left( \frac{1}{(1-\Phi_2)^{5/2}(1-\Phi_1)^{5/2}} + K \right) \left( F''(0) + \frac{F'(0)}{K_1} - nKF''(0) \right), \qquad (6.26)$$

$$Re_s^{1/2} C_m = \frac{\rho_f}{\rho_{hnf}} \left( \frac{1}{(1-\Phi_2)^{5/2}(1-\Phi_1)^{5/2}} + K/2 \right) \left( H'(0) - \frac{nF''(0)}{K_1} \right), \qquad (6.27)$$

$$Re_s^{1/2} N_{u_s} = -\frac{k_{hnf}}{k_f} \Theta'(0), \qquad (6.28)$$

where, $Re_s = \left( \frac{u_0 e^{2s/l}}{\nu_f} \right)$ is the local Reynold number.

**Thermo physical properties:**

| Thermophysical properties | SWCNT | MWCNT | Pure water |
|---|---|---|---|
| $C_p((j/kg)K)$ | 425 | 796 | 4179 |
| $\rho((kg/m^3))$ | 2600 | 1600 | 997:1 |
| $k((W/mK))$ | 6600 | 3000 | 0.613 |

The thermophysical charactristics are emphasized above. In this case, Pr is fixed as 6.2.

## 6.3    Results and discussion

The dimensionless system defined by Eqs. (6.16-6.18) having boundary conditions (6.19) is solved as numerically. Physical effects on the flow behavior are discussed through graphs and tables. Table 6.1 reveals the comparative outcome with existing literature. It is seen that ours rsults are matching with them when $K_1 \to 1000, \Phi_2 = \gamma = \omega = 0$ and $R_0 = 1$ for the various values of $\alpha$.

**Table 6.1: The comparative numerical values of $Re_s^{1/2}C_f$ with our outcomes when $K_1 \to 1000, \Phi_2 = S = \omega = K = 0$ and $R_0 = 1.0$.**

| α | Present | Wang [49] | Sahoo and Do [50] | Abbas et al. [51] | Nogrehabadi et al. [52] |
|---|---|---|---|---|---|
| 0.00 | 1.0000 | 1.00 | 1.00110 | 1.00000 | 1.00020 |
| 0.10 | 0.87180 | - | 0.87140 | 0.87200 | 0.87200 |
| 0.20 | 0.77620 | - | 0.77490 | 0.77630 | 0.77630 |
| 0.30 | 0.70140 | 0.7010 | 0.69970 | 0.70150 | 0.70150 |
| 0.50 | 0.59060 | - | 0.58910 | 0.59110 | 0.59110 |
| 1.00 | 0.43000 | 0.4300 | 0.42840 | 0.43010 | 0.43010 |
| 2.00 | 0.28410 | 0.2840 | 0.28280 | 0.28390 | 0.28390 |
| 3.00 | 0.21420 | - | 0.21330 | 0.21400 | 0.21400 |
| 5.00 | 0.14570 | 0.1450 | 0.14440 | 0.14480 | 0.14480 |
| 10.00 | 0.08110 | - | 0.08100 | 0.08120 | 0.08120 |
| 20.00 | 0.04290 | 0.04380 | 0.04370 | 0.04370 | 0.04370 |

Tables [6.2-6.3] show the weak concentration (n = 0.5) and strong concentration (n = 0.0) of couple stress, Nusselt numbers and skin friction for nanomaterial fluid and Hybrid nanomaterial fluid. Theses tables show the variation of the $\Phi_2$, $R_0$, K, $K_1$, ω, γ and δ on the $Re_s^{1/2}C_f$, $Re_s^{1/2}N_{u_s}$ and $Re_s^{1/2}C_m$ for $SWCNT - MWCNT/H_2O$ and $MWCNT/H_2O$. It is observed that the values of $Re_s^{1/2}C_f$, $Re_s^{1/2}N_{u_s}$ and $Re_s^{1/2}C_m$ decline for the large values of $\Phi_2$ for the both cases $SWCNT - MWCNT/H_2O$ and $MWCNT/H_2O$. In the case of $SWCNT - MWCNT/H_2O$ gains higher values than that of $MWCNT/H_2O$. The dimensionless parameter $R_0$ shows the impacts on $Re_s^{1/2}C_f$, $Re_s^{1/2}N_{u_s}$ and $Re_s^{1/2}C_m$. The numerical values of $Re_s^{1/2}C_f$ and $Re_s^{1/2}C_m$ decrease and increases the values of $Re_s^{1/2}N_{u_s}$ for the large values of $R_0$ in both cases of $SWCNT - MWCNT/H_2O$ and $MWCNT/H_2O$. The impacts of the curvature parameter $K_1$ on the $Re_s^{1/2}C_f$, $Re_s^{1/2}N_{u_s}$ and $Re_s^{1/2}C_m$. It is seen that the curvature parameter K increases which decrease in $Re_s^{1/2}C_f$, $Re_s^{1/2}N_{u_s}$ and $Re_s^{1/2}C_m$ in both cases of $SWCNT - MWCNT/H_2O$ and $MWCNT/H_2O$. The dimensionless micropolar parameter K shows the effects on $Re_s^{1/2}C_f$, $Re_s^{1/2}N_{u_s}$ and $Re_s^{1/2}C_m$. It is realized that the values of the $Re_s^{1/2}$ and $Re_s^{1/2}N_{u_s}$ enhances for large values of the K but opposite behavior to be noted for $Re_s^{1/2}C_m$ decrease. The impacts of ω on $Re_s^{1/2}C_f$, $Re_s^{1/2}N_{u_s}$ and $Re_s^{1/2}C_m$ are shown in these tables. It is detected that the values of $Re_s^{1/2}C_f$ and $Re_s^{1/2}C_m$ augments for growing in the values of ω while decline the values of $Re_s^{1/2}N_{u_s}$. The velocity slip γ shows the effects on $Re_s^{1/2}C_f$, $Re_s^{1/2}N_{u_s}$ and $Re_s^{1/2}C_m$. It is noted that velocity slip rises with growing the values of $Re_s^{1/2}C_f$, $Re_s^{1/2}N_{u_s}$ and $Re_s^{1/2}C_m$. The effects of thermal slip parameter δ are to be noted on the $Re_s^{1/2}N_{u_s}$ in these tables. As the thermal slip parameter δ increases as $Re_s^{1/2}N_{u_s}$ decreases.

**Table 6.2: Numerical values of $Re_s^{1/2}C_f$, $Re_s^{1/2}N_{u_s}$ and $Re_s^{1/2}C_m$ when $n = 0.5$.**

| Physical parameters | | | | | | | Nanofluids | | | Hybrid nanofluids | | |
|---|---|---|---|---|---|---|---|---|---|---|---|---|
| $\Phi_2$ | $R_0$ | $K_1$ | K | Ω | Γ | M | $-Re_s^{1/2}C_f$ | $Re_s^{1/2}N_u$ | $Re_s^{1/2}C_m$ | $-Re_s^{1/2}C_f$ | $Re_s^{1/2}N_{u_s}$ | $Re_s^{1/2}C_m$ |
| 0.005 | 0.5 | 0.5 | 0.5 | 0.4 | 0.2 | 0.4 | 2.6842 | 1.3904 | 1.2638 | 2.7518 | 0.9714 | 1.3675 |
| 0.02 | - | - | - | - | - | - | 2.5899 | 1.3162 | 1.2155 | 2.6495 | 0.9191 | 1.3132 |
| 0.04 | - | - | - | - | - | - | 2.4695 | 1.2245 | 1.1537 | 2.5188 | 0.8545 | 1.2437 |
| 0.06 | - | - | - | - | - | - | 2.3547 | 1.1403 | 1.0948 | 2.3944 | 0.7953 | 1.1775 |
| 0.04 | 0.1 | - | - | - | - | - | 2.5910 | 0.8554 | 1.5389 | 2.6612 | 0.5895 | 1.6534 |
| - | 0.3 | - | - | - | - | - | 2.5010 | 1.1017 | 1.2979 | 2.5577 | 0.7644 | 1.3984 |
| - | 0.5 | - | - | - | - | - | 2.4695 | 1.2245 | 1.1537 | 2.5188 | 0.8545 | 1.2437 |

| Φ₂ | R₀ | K₁ | K | Ω | Γ | M | $Re_s^{1/2}C_f$ | $Re_s^{1/2}N_{u_s}$ | $Re_s^{1/2}C_m$ | $Re_s^{1/2}C_f$ | $Re_s^{1/2}N_{u_s}$ | $Re_s^{1/2}C_m$ |
|---|---|---|---|---|---|---|---|---|---|---|---|---|
| - | 0.5 | 0.1 | - | - | - | - | 4.6703 | 1.6778 | 5.7113 | 4.7848 | 1.2182 | 5.3475 |
| - | - | 0.3 | - | - | - | - | 3.1504 | 1.3769 | 1.9745 | 3.2113 | 0.9745 | 2.0741 |
| - | - | 0.5 | - | - | - | - | 2.4695 | 1.2245 | 1.1537 | 2.5188 | 0.8545 | 1.2437 |
| - | - | 0.5 | 0.0 | - | - | - | 2.0303 | 1.2115 | 1.2675 | 2.2690 | 0.8437 | 1.4243 |
| - | - | - | 0.5 | - | - | - | 2.4695 | 1.2245 | 1.1537 | 2.5188 | 0.8545 | 1.2437 |
| - | - | - | 1.0 | - | - | - | 2.8950 | 1.2303 | 1.0889 | 2.8318 | 0.8593 | 1.1389 |
| - | - | - | 0.5 | 0.0 | - | - | 2.3772 | 1.2287 | 1.0832 | 2.4247 | 0.8578 | 1.1695 |
| - | - | - | - | 0.2 | - | - | 2.4239 | 1.2266 | 1.1188 | 2.4723 | 0.8561 | 1.2070 |
| - | - | - | - | 0.4 | - | - | 2.4695 | 1.2245 | 1.1537 | 2.5188 | 0.8545 | 1.2437 |
| - | - | - | - | 0.6 | - | - | 2.5139 | 1.2225 | 1.1880 | 2.5642 | 0.8530 | 1.2799 |
| - | - | - | - | 0.4 | 0.0 | - | 4.1409 | 1.2576 | 1.8518 | 4.2081 | 0.8781 | 1.9869 |
| - | - | - | - | - | 0.2 | - | 2.4695 | 1.2245 | 1.1537 | 2.5188 | 0.8545 | 1.2437 |
| - | - | - | - | - | 0.4 | - | 1.7666 | 1.2090 | 0.8473 | 1.8058 | 0.8435 | 0.9163 |
| - | - | - | - | - | 0.4 | 0.0 | 2.4695 | 2.7272 | 1.1537 | 2.5188 | 1.7534 | 1.2437 |
| - | - | - | - | - | - | 0.2 | 2.4695 | 1.6902 | 1.1537 | 2.5188 | 1.1491 | 1.2437 |
| - | - | - | - | - | - | 0.4 | 2.4695 | 1.2245 | 1.1537 | 2.5188 | 0.8545 | 1.2437 |

**Table 6.3: Numerical values of $Re_s^{1/2}C_f$, $Re_s^{1/2}N_{u_s}$ and $Re_s^{1/2}C_m$ when $n = 0.0$.**

| Physical parameters | | | | | | | Nanofluids | | | Hybrid nanofluids | | |
|---|---|---|---|---|---|---|---|---|---|---|---|---|
| Φ₂ | R₀ | K₁ | K | Ω | Γ | M | $Re_s^{1/2}C_f$ | $Re_s^{1/2}N_{u_s}$ | $Re_s^{1/2}C_m$ | $Re_s^{1/2}C_f$ | $Re_s^{1/2}N_{u_s}$ | $Re_s^{1/2}C_m$ |
| 0.005 | 0.5 | 0.5 | 0.5 | 0.4 | 0.4 | 0.4 | -2.3326 | 1.3625 | 0.2798 | -2.3946 | 0.9505 | 0.3179 |
| 0.02 | - | - | - | - | - | - | -2.2504 | 1.2896 | 0.2724 | -2.3051 | 0.8992 | 0.3091 |
| 0.04 | - | - | - | - | - | - | -2.1454 | 1.1994 | 0.2628 | -2.1908 | 0.8359 | 0.2977 |
| 0.06 | - | - | - | - | - | - | -2.0453 | 1.1166 | 0.2535 | -2.0820 | 0.7778 | 0.2867 |
| 0.04 | 0.1 | - | - | - | - | - | -2.1122 | 0.8421 | 0.3287 | -2.1711 | 0.5805 | 0.3552 |
| - | 0.3 | - | - | - | - | - | -2.1147 | 1.0803 | 0.3021 | -2.1663 | 0.7488 | 0.3361 |
| - | 0.5 | - | - | - | - | - | -2.1454 | 1.1994 | 0.2628 | -2.1908 | 0.8359 | 0.2977 |
| - | 0.5 | 0.1 | - | - | - | - | -3.0561 | 1.6615 | 0.0822 | -3.1471 | 1.2033 | 0.0738 |
| - | - | 0.3 | - | - | - | - | -2.5049 | 1.3515 | 0.2216 | -2.5580 | 0.9548 | 0.2642 |
| - | - | 0.5 | - | - | - | - | -2.1454 | 1.1994 | 0.2628 | -2.1908 | 0.8359 | 0.2977 |
| - | - | 0.5 | 0.0 | - | - | - | -1.4006 | 1.1975 | 0.1989 | -1.5655 | 0.8339 | 0.2299 |
| - | - | - | 0.5 | - | - | - | -2.1454 | 1.1994 | 0.2628 | -2.1908 | 0.8359 | 0.2977 |
| - | - | - | 1.0 | - | - | - | -2.9148 | 1.1993 | 0.2971 | -2.8320 | 0.8364 | 0.3304 |
| - | - | - | 0.5 | 0.0 | - | - | -1.9867 | 1.2079 | 0.3679 | -2.0235 | 0.8426 | 0.4175 |
| - | - | - | - | 0.2 | - | - | -2.0634 | 1.2039 | 0.3191 | -2.1037 | 0.8395 | 0.3625 |
| - | - | - | - | 0.4 | - | - | -2.1454 | 1.1994 | 0.2628 | -2.1908 | 0.8359 | 0.2977 |
| - | - | - | - | 0.6 | - | - | -2.2381 | 1.1942 | 0.1898 | -2.3006 | 0.8312 | 0.2011 |
| - | - | - | - | 0.4 | 0.0 | - | -5.3459 | 1.2509 | 0.7355 | -5.4412 | 0.8724 | 0.8066 |
| - | - | - | - | - | 0.2 | - | -3.0436 | 1.2154 | 0.4118 | -3.1030 | 0.8473 | 0.4599 |
| - | - | - | - | - | 0.4 | - | -2.1454 | 1.1994 | 0.2628 | -2.1908 | 0.8359 | 0.2977 |
| - | - | - | - | - | 0.4 | 0.0 | -2.1454 | 2.6057 | 0.2628 | -2.1908 | 1.6767 | 0.2977 |
| - | - | - | - | - | - | 0.2 | -2.1454 | 1.6427 | 0.2628 | -2.1908 | 1.1156 | 0.2977 |
| - | - | - | - | - | - | 0.4 | -2.1454 | 1.1994 | 0.2628 | -2.1908 | 0.8359 | 0.2977 |

## 6.4    Graphical analysis

The variation of the physical parameters namely, dimensionless stretching parameter $R_0$, solid nanoparticle $\Phi_2$, micropolar parameter $K$, modified Harman number ω, curvature parameter $K_1$, velocity slip parameter γ and thermal slip parameter M temperature, micropolar and velocity profiles. The variation of solid nanoparticle of MWCNT $\Phi_2$ with velocity profile, micropolar and temperature profile respectively is seen in Figs. (6.2-6.3). Micropolar and velocity profiles are boosted as well as solid nanoparticle growths, see in Fig. 6.2. The curves of the velocity function boosted due to enhancing the $\Phi_2$. Thermal thickness and $\Phi_2$ have the same behavior of enhancing in Fig. 6.3. Influence of velocity and micropolar functions with $K$ which reveals in

Fig. 6.4. velocity function and $K$ have the same behavior of enhancing but in case of micropolar function and $K$ have opposite behavior. Variation of the modified Harman number $\omega$ and velocity and micropolar function depicted in Fig. 6.5. The curves of the velocity declines for larger values of $\omega$. Variations of dimensionless stretching parameter $R_0$ with velocity and temperature functions depicted in Fig. 6.6. Velocity function and stretching parameter $R_0$ same behavior of enhancing but opposite in case of temperature function. Thermal slip and temperature function variation revealed in Fig. 6.7. thermal slip improve which declines the temperature function. The velocity slip parameter and velocity function variation depicted in Fig. 6.7. Velocity slip and velocity function opposite behavior seen in Fig. 6.7. The curves of the velocity function declines with enhancing the values of velocity slip. The variation of the curvature parameter and stretching parameter with micropolar function is seen in Fig. 6.8. The curves of the micropolar function declines due to rising the values of stretching and micropolar parameters.

## 6.5 Final remarks

The based micropolar fluid of $SWCNT - MWCNT/H_2O$ flow with velocity and thermal slips at Riga channel is deliberated. The nonlinear stretching is also taken in this in this chapter. For the various physical parameters, significant findings are illuminated like as dimensionless stretching parameter $R_0$, solid nanoparticle $\Phi_2$, micropolar parameter $K$, modified Harman number $\omega$, curvature parameter $K_1$, velocity slip parameter $\gamma$ and thermal slip parameter M. Some importing finding are:

- The numerical values of $SWCNT - MWCNT/H_2O$ gains higher values than that of $MWCNT/H_2O$ in all the cases for weak concentration $(n = 0.5)$ and strong concentration $(n = 0.0)$.
- For the values of $Re_s^{1/2}C_f$, $Re_s^{1/2}N_{u_s}$ and $Re_s^{1/2}C_m$, the weak concentration $(n = 0.5)$ achieves sophisticated values as compared to the $n = 0.0$.
- The modified Harman number $\omega$ increases as increasing velocity function and decreases micropolar function.
- The present investigation is in great deal with the already available results.

**Fig. 6.2**
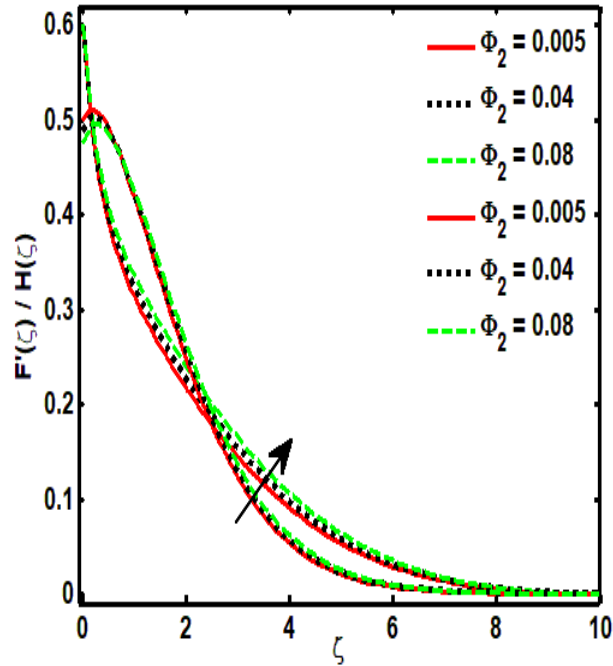


**Fig. 6.3**
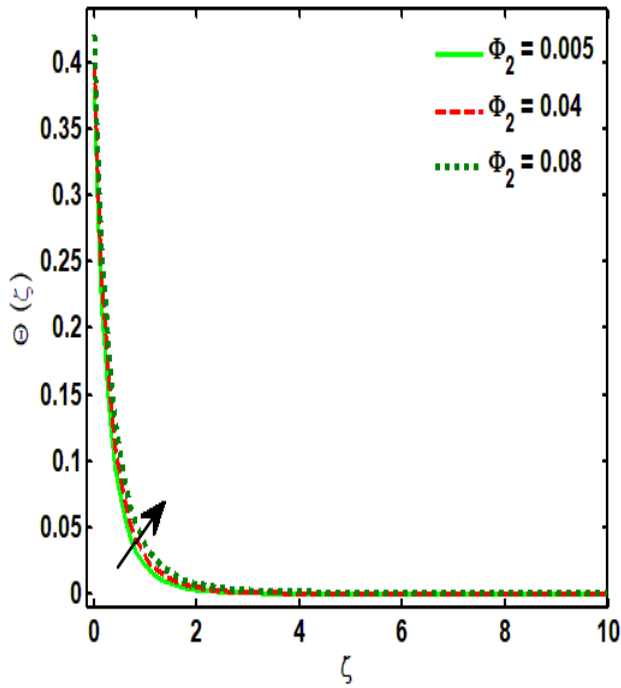


Impacts of $\Phi_2$ on the $F'(\zeta)$, $H(\zeta)$ and $\Theta(\zeta)$.

**Fig. 6.4**
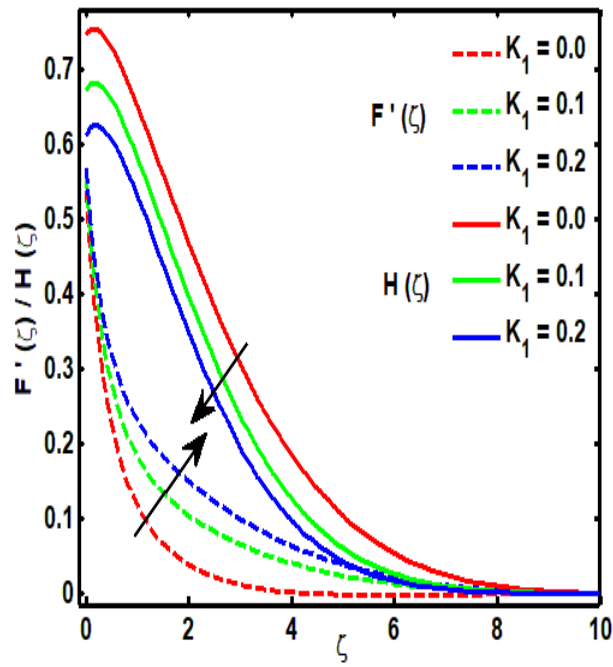


**Fig. 6.5**
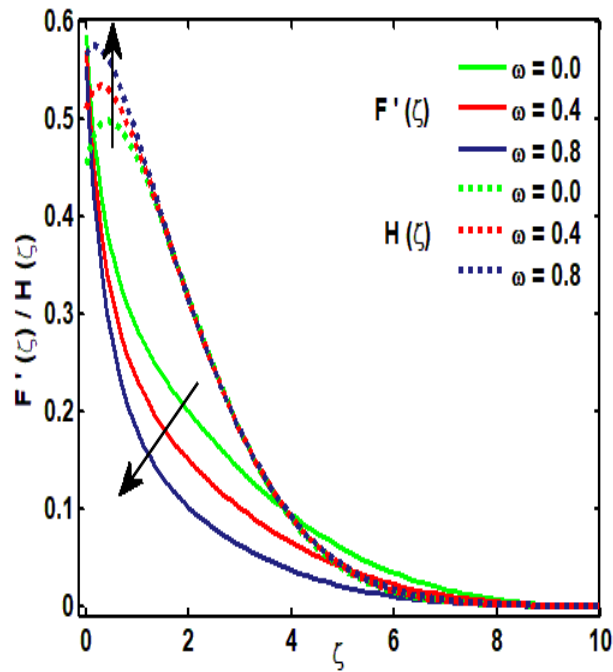


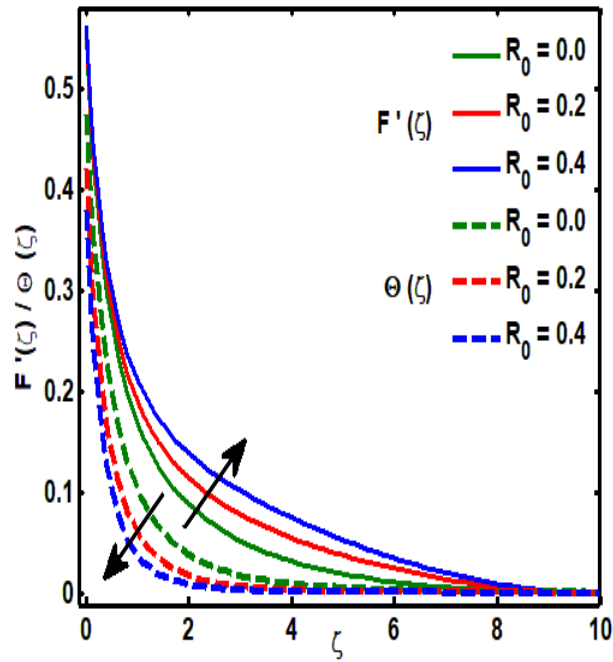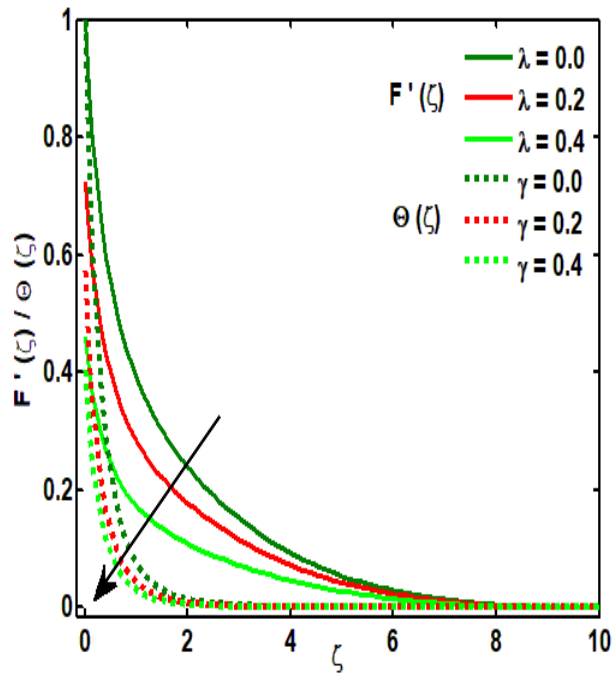Impacts of $\mathbf{K_1}$ and $\boldsymbol{\omega}$ on the $F'(\zeta)$ and $H(\zeta)$.

**Fig. 6.6**



Impacts of $R_0$ on the $F'(\zeta)$ and $\Theta(\zeta)$.
**Fig. 6.7**



Impacts of $\gamma$ on the $\Theta(\zeta)$ and $\lambda$ on $F'(\zeta)$.

**Fig. 6.8**
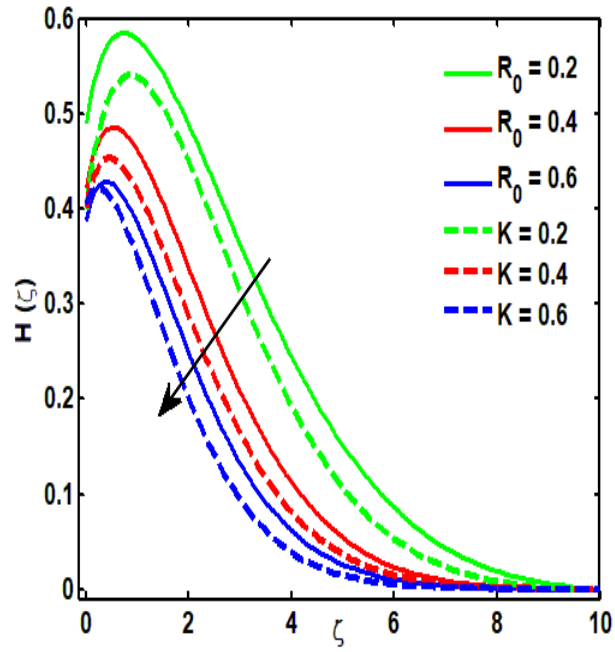


Impacts of $R_0$ and K on the H($\zeta$).

# Chapter 07

## Model based analysis of Yamada and Ota model and Xue of micropolar Hybrid nanofluid at curved surface

### 7.1 Introduction

In this chapter, the flow of based analysis of Yamada-Ota and Xue models of micropolar Hybrid nanomaterial fluid at curved surface is analyzed. The nonlinear stretching curved surface is considered. The system under the flow suppositions is established and dimensionlized through similarity transformations. Furthermore, the results of the dimensionless system built through a numerical procedure. The phenomena of physical parameters on the curved surface are revealed through graphs and tables.

### 7.2 Mathematical formulation

The micropolar Hybrid nanomaterial fluid at a curved stretching surface is deliberated. The curvilinear coordinates are taken in which flow path is shown along the arc length which is normal to tangent vector as shown in Fig. 7.1.
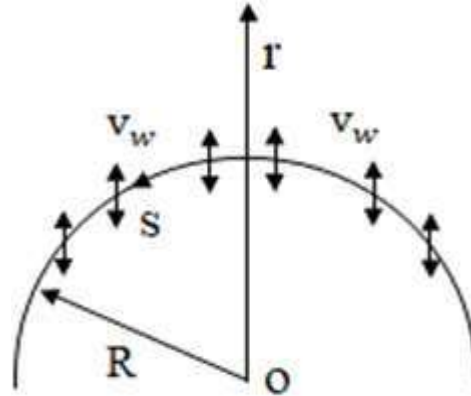


**Fig. 7.1:** Hybrid nanomaterial flow pattern of micropolar fluid.

It is considered that the surface is stretched along the velocity $v_w$ in the $s$ direction. It is noted that $v_w < 0$ or $v_w > 0$ resemble to injection or suction correspondingly. Under these deliberations, the flow equations

$$\vec{\nabla}.\vec{V} = 0, \tag{7.1}$$

$$\rho\left(\frac{\partial \vec{V}}{\partial t}\right) + \vec{\nabla}P + (\vec{V}.\vec{\nabla})\vec{V} = K\vec{\nabla} \times \vec{\Omega} + (\mu + K)\,\nabla^2\vec{V} + \sigma(\vec{J} \times \vec{B}) + \vec{F}, \tag{7.2}$$

$$\rho\left(\frac{\partial \vec{V}}{\partial t}\right) + (\vec{V}.\vec{\nabla})\vec{V} = -2K\vec{\Omega} + K\vec{\nabla} \times \vec{V} - \gamma(\vec{\nabla} \times \vec{\nabla} \times \vec{\Omega}) + (\alpha + \beta + \gamma)\vec{\nabla}(\vec{\nabla}\,\vec{\Omega}), \tag{7.3}$$

$$\rho c_p \left( \left( \frac{\partial \vec{T}}{\partial t} \right) + (\vec{V}.\vec{\nabla})\vec{T} \right) = \vec{\nabla}(K\vec{\nabla}.\vec{T}). \tag{7.4}$$

By introducing approximations to the physical phenomenon, the above equations are transformed into subsequent form:

$$\frac{R_1}{r+R_1}\frac{\partial U}{\partial s} = \frac{-1}{r+R_1}\frac{\partial}{\partial r}((r+R_1)V), \tag{7.5}$$

$$\frac{U^2}{r+R_1} = \frac{1}{\rho_{hnf}}\frac{\partial p}{\partial r}, \tag{7.6}$$

$$\left( V\frac{\partial u}{\partial r} + \frac{RU}{r+R_1}\frac{\partial U}{\partial s} + \frac{VU}{r+R_1} \right) + \frac{1}{\rho_{hnf}}\frac{1}{r+R_1}\frac{\partial p}{\partial r}$$

$$= \frac{\rho_f}{\rho_{hnf}} \left( \frac{1}{(1-\Phi_2)^{5/2}(1-\Phi_1)^{5/2}} + K_1 \right) \left( \frac{\partial^2 U}{\partial r^2} - \frac{U}{(r+R_1)^2} \right) \tag{7.7}$$

$$+ \frac{1}{r+R_1}\frac{\partial u}{\partial r} \right) - \frac{K_1}{\rho_{hnf}}\frac{\partial N}{\partial r},$$

$$\left( \frac{R_1 U}{r+R_1}\frac{\partial N}{\partial s} + V\frac{\partial N}{\partial r} \right)$$

$$= \frac{\rho_f}{\rho_{hnf}} \left( \frac{1}{(1-\Phi_2)^{5/2}(1-\Phi_1)^{5/2}} + K_1/2 \right) \left( \frac{\partial^2 N}{\partial r^2} + \frac{1}{r+R_1}\frac{\partial N}{\partial r} \right) \tag{7.8}$$

$$- \frac{K_1}{2\rho_{hnf}} \left( \frac{\partial N}{\partial r} + 2N + \frac{U}{r+R_1} \right),$$

$$\left( V\frac{\partial T}{\partial r} + \frac{RU}{r+R_1}\frac{\partial T}{\partial s} \right) = \alpha_{hnf} \left( \frac{\partial^2 T}{\partial r^2} + \frac{1}{r+R_1}\frac{\partial T}{\partial r} \right), \tag{7.9}$$

with the boundary conditions

$$U = ae^{\frac{s}{a}}, \ V = v_w, \ T = T_w + \lambda_1\frac{k_{hnf}}{k_f}\left( \frac{\partial T}{\partial r} \right), \ -n\frac{\partial u}{\partial r} = N, \ \text{at } r \to 0,$$

$$U \to u_w, \ N \to 0, \ T \to T_\infty, \ \text{at } r \to \infty. \tag{7.10}$$

Suitable transformations are

$$T = T_\infty + (T_w - T_\infty)\Theta(\zeta), \ \zeta = \sqrt{\frac{a}{\nu_f}}r, \ U = u_0\left(e^{s/l}\right)F'(\zeta),$$

$$V = -\frac{R_1}{r+R_1}\sqrt{\frac{\nu_f}{a}}\left(e^{s/l}\right)F(\zeta), \tag{7.11}$$

$$N = \sqrt{a\nu_f}\left(e^{s/l}\right)G(\zeta), \ P = \rho a^2 \left(e^{2s/l}\right)p(\zeta),$$

where, the curvature radius is $R$, $u$ and $v$ are the velocity along the axis of $r$ and $s$. The dimensionless system is obtained as

$$P' = \frac{F'^2}{\zeta + K_1}, \tag{7.12}$$

$$\frac{2K}{\zeta + K}P = \frac{\rho_f}{\rho_{hnf}}\left(\frac{1}{(1-\Phi_2)^{5/2}(1-\Phi_1)^{5/2}} + K\right)\left[F''' + \frac{F''}{\zeta + K_1} - \frac{F'}{(\zeta + K_1)^2}\right]$$
$$- \frac{R_0 K_1}{\zeta + K_1}F'^2 + \frac{R_0 K_1}{\zeta + K_1}F'F'' + \frac{R_0 K_1}{(\zeta + K_1)^2}FF' - \frac{\rho_f}{\rho_{hnf}}R_0 KG(\zeta), \quad (7.13)$$

$$\frac{\rho_f}{\rho_{hnf}}\left(\frac{1}{(1-\Phi_2)^{5/2}(1-\Phi_1)^{5/2}} + K/2\right)\left[\frac{F'}{\zeta + K_1} + F''\right] - \frac{R_0 K_1}{2(\zeta + K_1)}F'G$$
$$+ \frac{R_0 K_1}{2(\zeta + K_1)}FG' - \frac{R_0 K}{2\rho_{hnf}}\left(2G + F'' + \frac{1}{\zeta + K_1}F'\right) = 0, \quad (7.14)$$

$$\alpha_{hnf}\left(\Theta'' + \frac{1}{\zeta + K_1}\Theta'\right) + \frac{R_0}{\zeta + K_1}F\Theta' - \frac{R_0}{\zeta + K_1}\Theta = 0. \quad (7.15)$$

Eliminating the pressure term, we have

$$\frac{\rho_f}{\rho_{hnf}}\left(\frac{1}{(1-\Phi_2)^{5/2}(1-\Phi_1)^{5/2}} + K\right)\left(F'''' + \frac{2}{\zeta + K_1}F''' - \frac{1}{(\zeta + K_1)^2}F''\right.$$
$$\left. + \frac{1}{(\zeta + K_1)^3}F'\right) - \frac{R_0 K_1}{\zeta + K_1}(F''F' - FF''') - \frac{R_0 K_1}{(\zeta + K_1)^2}(F'^2 - FF'') \quad (7.16)$$
$$- \frac{R_0 K_1}{(\zeta + K_1)^3}FF' - \frac{\rho_f}{\rho_{hnf}}R_0 KH'(\zeta) = 0,$$

$$\frac{\rho_f}{\rho_{hnf}}\left(\frac{1}{(1-\Phi_2)^{5/2}(1-\Phi_1)^{5/2}} + K/2\right)\left(H'' + \frac{H'}{\zeta + K_1}\right) - \frac{R_0 K}{2(\zeta + K_1)}F'H$$
$$+ \frac{R_0 K}{2(\zeta + K_1)}FH' - \frac{\rho_f}{\rho_{hnf}}\frac{R_0 K}{2}\left(2H + F'' + \frac{1}{\zeta + K_1}F'\right) = 0, \quad (7.17)$$

$$\alpha_{hnf}\left(\Theta'' + \frac{1}{\zeta + K_1}\Theta'\right) + \frac{K_1 R_0}{\zeta + K_1}F\Theta' - \frac{K_1 R_0}{\zeta + K_1}\Theta = 0. \quad (7.18)$$

Non dimensional boundary conditions take the form

$$F(0) = S, \quad F'(0) = \alpha, \quad F'(\infty) = 1, \quad F''(\infty) = 0,$$
$$H(0) = nG''(0), \quad H(\infty) = 0,$$
$$\theta(0) = 1 + \delta\frac{k_{hnf}}{k_f}\Theta'(0), \qquad \Theta(\infty) = 0. \quad (7.19)$$

In above expressions, $S < 0$ correspond to suction and $S > 0$ is for injection. The physical interpretation of thermodynamics are

$$\frac{k_{hnf}}{k_{bf}} = \frac{1 + \frac{k_{bf}}{k_{s_2}}\frac{L}{R}\Phi_2^{0.2} + \left(1 - \frac{k_{bf}}{k_{s_2}}\right)\Phi_2\frac{L}{R}\Phi_2^{0.2} + 2\Phi_2\left(\frac{k_{s_2}}{k_{s_2} - k_{bf}}\right)\ln\left(\frac{k_{s_2} + k_{bf}}{2k_{s_2}}\right)}{1 - \Phi_2 + 2\Phi_2\left(\frac{k_{bf}}{k_{s_2} - k_{bf}}\right)\ln\left(\frac{k_{s_2} + k_{bf}}{2k_{bf}}\right)}, \quad (7.20)$$

$$\frac{k_{bf}}{k_f} = \frac{1 + \frac{k_f}{k_{s_1}}\frac{L}{R}\Phi_1^{0.2} + \left(1 - \frac{k_f}{k_{s_1}}\right)\Phi_1\frac{L}{R}\Phi_1^{0.2} + 2\Phi_1\left(\frac{k_{s_1}}{k_{s_1} - k_f}\right)\ln\left(\frac{k_{s_1} + k_f}{2k_{s_1}}\right)}{1 - \Phi_1 + 2\Phi_1\left(\frac{k_f}{k_{s_1} - k_f}\right)\ln\left(\frac{k_{s_1} + k_f}{2k_f}\right)}, \quad (7.21)$$

here $L$ and $R$ are be the length and radius of nanotube. Eq. (7.21) is the Yamada and Ota model of nanofluid [53]. We extended the Yamada and Ota model of nanofluid into the Hybrid nanofluid which is executed in Eq. (7.20). We analyzed the significant results through the

74

following expression

$$\frac{k_{hnf}}{k_{bf}} = \frac{1 - \Phi_2 + 2\Phi_2 \left(\frac{k_{s_2}}{k_{s_2} - k_{bf}}\right) \ln\left(\frac{k_{s_2} + k_{bf}}{2k_{bf}}\right)}{1 - \Phi_2 + 2\Phi_2 \left(\frac{k_{bf}}{k_{s_2} - k_{bf}}\right) \ln\left(\frac{k_{s_2} + k_{bf}}{2k_{bf}}\right)}, \tag{7.22}$$

$$\frac{k_{bf}}{k_f} = \frac{1 - \Phi_1 + 2\Phi_1 \left(\frac{k_{s_1}}{k_{s_1} - k_f}\right) \ln\left(\frac{k_{s_1} + k_f}{2k_f}\right)}{1 - \Phi_1 + 2\Phi_1 \left(\frac{k_f}{k_{s_1} - k_f}\right) \ln\left(\frac{k_{s_1} + k_f}{2k_f}\right)}. \tag{7.23}$$

Eq. (7.23) is the Xue model nanofluid [54]. We extended the Xue model nanofluid into the Hybrid nanofluid which is executed in Eq. (7.22). We analyzed the significant results for different physical parameter. The physical quantities namely Nusselt number, skin friction and couple stress are defined as

$$C_f = \frac{\tau_{rs}}{\rho_{hnf} u_w^2}, \quad N_{us} = \frac{s q_w}{k_{hnf}(T_w - T_\infty)}, C_m = \left(e^{s/l}\right)\frac{\tau_m}{\rho_{hnf} u_w^2}, \tag{7.24}$$

where $\tau_{rs}$, $q_w$ and $C_m$ are wall shear stress, heat flux and couple stress respectively. These are defined as

$$\tau_{rs} = \frac{\rho_f}{\rho_{hnf}} \left(\frac{1}{(1 - \Phi_2)^{\frac{5}{2}}(1 - \Phi_1)^{\frac{5}{2}}} + K\right)\left(\frac{\partial u}{\partial r} + \frac{u}{r + R} + kN\right)_{r=0},$$

$$\tau_m = \frac{\rho_f}{\rho_{hnf}} \left(\frac{1}{(1 - \Phi_2)^{5/2}(1 - \Phi_1)^{5/2}} + K/2\right)\left(\frac{\partial N}{\partial r} + \frac{N}{r + R}\right)_{r=0}, \tag{7.25}$$

$$q_w = -k_{hnf}\left(\frac{\partial T}{\partial r}\right)_{r=0}.$$

Using Eq. (7.24) in Eq. (7.25), we get the dimensionless form as follows

$$Re_s^{1/2} C_f = \frac{\rho_f}{\rho_{hnf}} \left(\frac{1}{(1 - \Phi_2)^{5/2}(1 - \Phi_1)^{5/2}} + K\right)\left(F''(0) + \frac{F'(0)}{K_1} - nKF''(0)\right), \tag{7.26}$$

$$Re_s^{1/2} C_m = \frac{\rho_f}{\rho_{hnf}} \left(\frac{1}{(1 - \Phi_2)^{5/2}(1 - \Phi_1)^{5/2}} + K/2\right)\left(G'(0) - \frac{nF''(0)}{K_1}\right), \tag{7.27}$$

$$Re_s^{1/2} N_{u_s} = -\frac{k_{hnf}}{k_f}\Theta'(0), \tag{7.28}$$

where, $Re_s = \left(\frac{u_0 e^{2s/l}}{\nu_f}\right)$ is the local Reynold number.

## 7.3 Results and discussion

The dimensionless system is solved through the numerical scheme via bvp4c technique having the dimensionless boundary conditions. Some physical parameters are defined as curvature parameter $K_1$, dimensionless stretching parameter $R_0$, stretching parameter $\alpha$, solid nanoparticle volume fraction $\Phi_2$, thermal slip parameter $\delta$ and micropolar parameter $K$.

Impacts of these physical parameters are illustrated through the Figs. $(7.2 - 7.10)$. Table 7.1 shows the comparative result with Wang [55]. It is noted that our findings align well with [55] when $\Phi_2 = \Phi_1 = S = 0$, $R_0 = 1$ and $K_1 \to \infty$ for the various values of $S$.

**Table 7.1: The comparison $F''(0)$ with our current outcomes. When $K_1 \to \infty$, $\Phi_2 = \Phi_1 = S = K = 0$ and $R_0 = 1$.**

| $\alpha$ | Wang [55] | Present Result |
|---|---|---|
| **0.0** | 1.232588 | 1.231588 |
| **0.1** | 1.14656 | 1.143556 |
| **0.2** | 1.05113 | 1.050613 |
| **0.5** | 0.71330 | 0.712510 |
| **1** | 0 | 0 |
| **2** | $-1.88731$ | $-1.868321$ |
| **5** | $-10.26475$ | $-10.25234$ |

### 7.3.1 Strong concentration ($n = 0.5$)

Tables [7.2-7.3] show the weak concentration (n = 0.5) of $Re_s^{1/2}C_m$, $Re_s^{1/2}Nu_s$ and $Re_s^{1/2}C_f$ for Yamada Ota, and Xue models for $Cu - Al_2O_3/H_2O$ and $Cu/H_2O$. These tables show the variation of the $\Phi_2$, $R_0$, $K_1$, $K$, $\alpha$, $S$ and $\delta$ on the $Re_s^{1/2}C_m$, $Re_s^{1/2}Nu_s$ and $Re_s^{1/2}C_f$ for Yamada-Ota and Xue models for $Cu - Al_2O_3/H_2O$ and $Cu/H_2O$. The values of $Re_s^{1/2}C_m$, and $Re_s^{1/2}C_f$ enhances for the large values of $\Phi_2$ while decreases the values of Nusselt numbers for higher values of $\Phi_2$ for $Cu - Al_2O_3/H_2O$ and $Cu/H_2O$ of Yamada and Ota model, and Xue model. The values of $Re_s^{1/2}C_m$, $Re_s^{1/2}Nu_s$ and $Re_s^{1/2}C_f$ are increased for the large values of $R_0$ which are revealed in Tables [7.2-7.3] for the both cases $Cu - Al_2O_3/H_2O$ and $Cu/H_2O$. These tables also depict the impact of $K$ on the $Re_s^{1/2}C_m$, $Re_s^{1/2}Nu_s$ and $Re_s^{1/2}C_f$ for the $Cu - Al_2O_3/H_2O$ and $Cu/H_2O$. It is noted that the skin friction enhances for growing the values of the $K$ but different behavior is prominent for the Nusselt number and couple stress that is decreased for the sophisticated values of $K$ in the both cases of $Cu - Al_2O_3/H_2O$ and $Cu/H_2O$. Impacts of $K_1$ on skin friction, Nusselt numbers and couple stress for the $Cu - Al_2O_3/H_2O$ and $Cu/H_2O$ are shown in These tables as well. It is depicted that the values of $Re_s^{1/2}C_m$, $Re_s^{1/2}Nu_s$ and $Re_s^{1/2}C_f$ decreases when the values of $K_1$ are increased. The impressions of $\gamma$ on the $Re_s^{1/2}C_m$,

$Re_s^{1/2}N_{u_s}$ and $Re_s^{1/2}C_f$ are also shows in these tables. In the case of injection ($S > 0$), the values of skin friction, Nusselt numbers and couple stress are increasing for the higher values of the physical parameter $S$ but opposite behavior is seen in the case of suction ($S < 0$). The impacts of $\alpha$ for $Cu - Al_2O_3/H_2O$ and $Cu/H_2O$ on the $Re_s^{1/2}C_m$, $Re_s^{1/2}N_{u_s}$ and $Re_s^{1/2}C_f$ are revealed in the these tables. The $Re_s^{1/2}C_m$ and $Re_s^{1/2}C_f$ are enhanced for the large values of stretching parameter $\alpha$ but opposite performance is seen for the $Re_s^{1/2}N_{u_s}$ when the stretching parameter $\alpha$ inceases. The effects of thermal slip parameter $\delta$ on the Nusselt number are shown in these tables, i.e., the $\delta$ increases as $Re_s^{1/2}N_{u_s}$ decreases.

**Table 7.2: Numerical results of $Re_s^{1/2}C_m$, $Re_s^{1/2}C_f$ and $Re_s^{1/2}N_{u_s}$ when $n = 0.5$.**

| | | | Yamada and Ota model | | | | Nanofluids | | | Hybrid nanofluids | | |
|---|---|---|---|---|---|---|---|---|---|---|---|---|
| $\Phi_2$ | $R_0$ | $K_1$ | $K$ | $S$ | $\alpha$ | $M$ | $Re_s^{1/2}C_f$ | $Re_s^{1/2}N_{u_s}$ | $-Re_s^{1/2}C_m$ | $Re_s^{1/2}C_f$ | $Re_s^{1/2}N_{u_s}$ | $-Re_s^{1/2}C_m$ |
| 0.005 | 0.5 | 0.5 | 0.5 | 0.4 | 0.4 | 0.4 | 0.6904 | 1.4452 | 0.9090 | 0.9123 | 0.4393 | 1.0582 |
| 0.02 | - | - | - | - | - | - | 0.8346 | 1.0257 | 0.9471 | 1.0103 | 0.3098 | 1.0788 |
| 0.04 | - | - | - | - | - | - | 0.9807 | 0.7175 | 0.9785 | 1.1086 | 0.2157 | 1.0903 |
| 0.06 | - | - | - | - | - | - | 1.0853 | 0.5383 | 0.9905 | 1.1763 | 0.1616 | 1.0861 |
| 0.04 | 0.1 | - | - | - | - | - | -0.5730 | 0.4675 | -0.4325 | -0.5468 | 0.1444 | -0.4340 |
| - | 0.3 | - | - | - | - | - | 0.0082 | 0.6253 | 0.2143 | 0.0637 | 0.1860 | 0.2522 |
| - | 0.5 | - | - | - | - | - | 0.9807 | 0.7175 | 0.9785 | 1.1086 | 0.2157 | 1.0903 |
| - | 0.5 | 0.1 | - | - | - | - | -4.2601 | 1.0117 | -1.3341 | -4.0508 | 0.3391 | -0.7362 |
| - | - | 0.3 | - | - | - | - | -0.1990 | 0.8159 | 1.7316 | -0.0828 | 0.2535 | 1.9405 |
| - | - | 0.5 | - | - | - | - | 0.9807 | 0.7175 | 0.9785 | 1.1086 | 0.2157 | 1.0903 |
| - | - | 0.5 | 0.0 | - | - | - | -0.0191 | 0.7078 | 0.1050 | -0.0659 | 0.2105 | 0.0623 |
| - | - | - | 0.5 | - | - | - | 0.9807 | 0.7175 | 0.9785 | 1.1086 | 0.2157 | 1.0903 |
| - | - | - | 1.0 | - | - | - | 2.9368 | 0.7265 | 2.1252 | 3.3934 | 0.2206 | 2.4062 |
| - | - | - | 0.5 | 0.1 | - | - | 0.7258 | 0.6586 | 0.8309 | 0.8347 | 0.2030 | 0.9250 |
| - | - | - | - | 0.4 | - | - | 0.9807 | 0.7175 | 0.9785 | 1.1086 | 0.2157 | 1.0903 |
| - | - | - | - | 0.8 | - | - | 1.3703 | 0.7868 | 1.1887 | 1.5266 | 0.2321 | 1.3247 |
| - | - | - | - | -0.1 | - | - | 0.5728 | 0.6166 | 0.7381 | 0.6704 | 0.1943 | 0.8210 |
| - | - | - | - | -0.4 | - | - | 0.3672 | 0.5512 | 0.6081 | 0.4496 | 0.1812 | 0.6754 |
| - | - | - | - | -0.8 | - | - | 0.1335 | 0.4639 | 0.4527 | 0.1995 | 0.1637 | 0.5017 |
| - | - | - | - | 0.4 | 0.0 | - | 1.9946 | 0.7035 | 1.4333 | 2.0816 | 0.2113 | 1.5446 |
| - | - | - | - | - | 0.4 | - | 0.9807 | 0.7175 | 0.9785 | 1.1086 | 0.2157 | 1.0903 |
| - | - | - | - | - | 0.8 | - | -0.0678 | 0.7300 | 0.5246 | 0.0981 | 0.2198 | 0.6338 |
| - | - | - | - | - | 0.4 | 0.0 | 0.9807 | 1.6724 | 0.9785 | 1.1086 | 0.3927 | 1.0903 |
| - | - | - | - | - | - | 0.4 | 0.9807 | 0.7175 | 0.9785 | 1.1086 | 0.3927 | 1.0903 |
| - | - | - | - | - | - | 0.8 | 0.9807 | 0.4567 | 0.9785 | 1.1086 | 0.2157 | 1.0903 |

**Table 7.3: Numerical results of $Re_s^{1/2}C_m$, $Re_s^{1/2}C_f$ and $Re_s^{1/2}N_{u_s}$ when $n = 0.5$.**

| | | | Xue model | | | | Nanofluids | | | Hybrid nanofluids | | |
|---|---|---|---|---|---|---|---|---|---|---|---|---|
| $\Phi_2$ | $R_0$ | $K_1$ | $K$ | $S$ | $\alpha$ | $M$ | $Re_s^{1/2}C_f$ | $Re_s^{1/2}N_{u_s}$ | $-Re_s^{1/2}C_m$ | $Re_s^{1/2}C_f$ | $Re_s^{1/2}N_{u_s}$ | $-Re_s^{1/2}C_m$ |
| 0.005 | 0.5 | 0.5 | 0.5 | 0.4 | 0.4 | 0.4 | 0.6904 | 1.4542 | 0.9090 | 0.9123 | 0.4719 | 1.0582 |
| 0.02 | - | - | - | - | - | - | 0.8346 | 1.0458 | 0.9471 | 1.0103 | 0.3374 | 1.0788 |
| 0.04 | - | - | - | - | - | - | 0.9807 | 0.7396 | 0.9785 | 1.1086 | 0.2376 | 1.0903 |
| 0.06 | - | - | - | - | - | - | 1.0853 | 0.5588 | 0.9905 | 1.1763 | 0.1791 | 1.0861 |
| 0.04 | 0.1 | - | - | - | - | - | -0.5730 | 0.4821 | -0.4325 | -0.5468 | 0.1582 | -0.4340 |
| - | 0.5 | - | - | - | - | - | 0.0082 | 0.6448 | 0.2143 | 0.0637 | 0.2048 | 0.2522 |
| - | 1.0 | - | - | - | - | - | 0.9807 | 0.7396 | 0.9785 | 1.1086 | 0.2376 | 1.0903 |
| - | 0.5 | 0.0 | - | - | - | - | -4.2601 | 1.0400 | -1.3341 | -4.0508 | 0.3701 | - 0.7362 |
| - | - | 0.3 | - | - | - | - | -0.1990 | 0.8404 | 1.7316 | -0.0828 | 0.2784 | 1.9405 |
| - | - | 0.5 | - | - | - | - | 0.9807 | 0.7396 | 0.9785 | 1.1086 | 0.2376 | 1.0903 |

| | | | | | | | | | | | | |
|---|---|---|---|---|---|---|---|---|---|---|---|---|
| - | - | 0.5 | 0.0 | - | - | - | -0.0191 | 0.7297 | 0.1050 | -0.0659 | 0.2319 | 0.0623 |
| - | - | - | 0.5 | - | - | - | 0.9807 | 0.7396 | 0.9785 | 1.1086 | 0.2376 | 1.0903 |
| - | - | - | 1.0 | - | - | - | 2.9368 | 0.7488 | 2.1252 | 3.3934 | 0.2428 | 2.4062 |
| - | - | - | 0.5 | 0.1 | - | - | 0.7258 | 0.6784 | 0.8309 | 0.8347 | 0.2231 | 0.9250 |
| - | - | - | - | 0.4 | - | - | 0.9807 | 0.7396 | 0.9785 | 1.1086 | 0.2376 | 1.0903 |
| - | - | - | - | 0.8 | - | - | 1.3703 | 0.8113 | 1.1887 | 1.5266 | 0.2561 | 1.3247 |
| - | - | - | - | -0.1 | - | - | 0.5728 | 0.6348 | 0.7381 | 0.6704 | 0.2132 | 0.8210 |
| - | - | - | - | -0.4 | - | - | 0.3672 | 0.5667 | 0.6081 | 0.4496 | 0.1983 | 0.6754 |
| - | - | - | - | -0.8 | - | - | 0.1335 | 0.4760 | 0.4527 | 0.1995 | 0.1784 | 0.5017 |
| - | - | - | - | 0.4 | 0.0 | - | 1.9946 | 0.7252 | 1.4333 | 2.0816 | 0.2326 | 1.5446 |
| - | - | - | - | - | 0.4 | - | 0.9807 | 0.7396 | 0.9785 | 1.1086 | 0.2376 | 1.0903 |
| - | - | - | - | - | 0.8 | - | -0.0678 | 0.7525 | 0.5246 | 0.0981 | 0.2421 | 0.6339 |
| - | - | - | - | - | 0.4 | 0.0 | 0.9807 | 1.7372 | 0.9785 | 1.1086 | 0.4394 | 1.0903 |
| - | - | - | - | - | - | 0.4 | 0.9807 | 0.7396 | 0.9785 | 1.1086 | 0.2376 | 1.0903 |
| - | - | - | - | - | - | 0.8 | 0.9807 | 0.4698 | 0.9785 | 1.1086 | 0.1628 | 1.0903 |

## 7.3.2 Strong concentration ($n = 0.0$)

Table 7.4 shows the inspiration of different parameters on the $Re_s^{1/2}C_m$, $Re_s^{1/2}N_{u_s}$ and $Re_s^{1/2}C_f$ for the Hybrid nanofluid flow. It is also discussed for the strong concentration ($n = 0.0$) for the Yamada Ota and Xue models. It is noted that the values of the $Re_s^{1/2}C_f$ are enhanced for the higher values of $\Phi_2$, but Nusselt number and couple stress are reduced when the values of the $\Phi_2$ increases for the both cases of Yamada Ota and Xue models. The impacts of $R_0$ on the $Re_s^{1/2}C_m$, $Re_s^{1/2}N_{u_s}$ and $Re_s^{1/2}C_f$ for the Yamada and Ota model, and Xue model are observed in the Table 7.4. The $Re_s^{1/2}C_m$, $Re_s^{1/2}N_{u_s}$ and $Re_s^{1/2}C_f$ are increased for the higher values of $R_0$ Yamada and Ota model as well as Xue model. The impacts of curvature parameter $K$ on skin friction, Nusselt numbers and couple stress for the Hybrid nanomaterial fluid are noted in this table as well. The values of the skin friction are increased for the large values of $K_1$, and the values of $Re_s^{1/2}N_{u_s}$ and couple stress are reduced when $K_1$ is increasing. Yamada and Ota model gains higher values of the $Re_s^{1/2}N_{u_s}$ and couple stress than that of Xue model, but reverse conduct is noted for $Re_s^{1/2}C_f$. The effects of $K$ on the $Re_s^{1/2}C_f$ Nusselt numbers and couple stress for the Hybrid nanofluid are observed in this table. Enhancing values of $K$ implies the improvment in the skin friction, Nusselt numbers and couple stress. In the case of $S > 0$ (injection), the $Re_s^{1/2}C_f$, Nusselt numbers and couple stress show the increasing behavior for the $S$ but reverse conduct is noted for the $S < 0$ (suction). The stretching parameter $\alpha$ on the skin friction, Nusselt numbers and couple stress are exhibited in this table as well. It is noted that the $\alpha$ augments with decrease in the $Re_s^{1/2}C_f$ while opposite behavior is seen for the Nusselt number and couple stress. The impacts of thermal slip parameter $M$ are depicted for

Nusselt number in the table 7.4. It is noted that Nusselt number decays for the higher values of $M$ for the both models Yamada Ota model, and Xue model.

**Table 7.4: Numerical results of $Re_s^{1/2}C_m$, $Re_s^{1/2}C_f$ and $Re_s^{1/2}N_{u_s}$ when $n = 0.0$.**

| Hybrid nanofluids ($n = 0.0$) | | | | | | | Yamada and Ota model | | | Xue model | | |
|---|---|---|---|---|---|---|---|---|---|---|---|---|
| $\Phi_2$ | $R_0$ | $K_1$ | $K$ | $S$ | $\alpha$ | $M$ | $Re_s^{1/2}C_f$ | $Re_s^{1/2}N_{u_s}$ | $Re_s^{1/2}C_m$ | $Re_s^{1/2}C_f$ | $Re_s^{1/2}N_{u_s}$ | $Re_s^{1/2}C_m$ |
| 0.005 | 0.5 | 0.5 | 0.5 | 0.4 | 0.4 | 0.4 | 3.6560 | 1.4593 | 0.8087 | 4.1398 | 0.4751 | 0.9232 |
| 0.02 | - | - | - | - | - | - | 3.7957 | 1.0506 | 0.7466 | 4.1981 | 0.3401 | 0.8540 |
| 0.04 | - | - | - | - | - | - | 3.9175 | 0.7440 | 0.6720 | 4.2297 | 0.2397 | 0.7713 |
| 0.06 | - | - | - | - | - | - | 3.9759 | 0.5628 | 0.6057 | 4.2153 | 0.1809 | 0.6977 |
| 0.04 | 0.1 | - | - | - | - | - | -0.2543 | 0.4824 | 0.6061 | -0.2254 | 0.1582 | 0.6855 |
| - | 0.5 | - | - | - | - | - | 1.2114 | 0.6468 | 0.6237 | 1.3204 | 0.2057 | 0.6935 |
| - | 1.0 | - | - | - | - | - | 3.9175 | 0.7440 | 0.6720 | 4.2297 | 0.2397 | 0.7713 |
| - | 0.5 | 0.0 | - | - | - | - | -4.2686 | 1.0400 | 1.0239 | -3.8258 | 0.3702 | 1.1873 |
| - | - | 0.3 | - | - | - | - | 2.2404 | 0.8442 | 0.8425 | 2.5756 | 0.2807 | 0.9699 |
| - | - | 0.5 | - | - | - | - | 3.9175 | 0.7440 | 0.6720 | 4.2297 | 0.2397 | 0.7713 |
| - | - | 0.5 | 0.0 | - | - | - | 0.5098 | 0.7297 | 0.6387 | 0.4484 | 0.2319 | 0.6700 |
| - | - | - | 0.5 | - | - | - | 3.9175 | 0.7440 | 0.6720 | 4.2297 | 0.2397 | 0.7713 |
| - | - | - | 1.0 | - | - | - | 11.2010 | 0.7584 | 0.6121 | 12.1948 | 0.2472 | 0.7671 |
| - | - | - | 0.5 | 0.1 | - | - | 3.2594 | 0.6833 | 0.6362 | 3.5232 | 0.2252 | 0.7293 |
| - | - | - | - | 0.4 | - | - | 3.9175 | 0.7440 | 0.6720 | 4.2297 | 0.2397 | 0.7713 |
| - | - | - | - | 0.8 | - | - | 4.9118 | 0.8149 | 0.7215 | 5.2934 | 0.2582 | 0.8289 |
| - | - | - | - | -0.1 | - | - | 2.8616 | 0.6399 | 0.6130 | 3.0956 | 0.2153 | 0.7020 |
| - | - | - | - | -0.4 | - | - | 2.3239 | 0.5718 | 0.5795 | 2.5173 | 0.2003 | 0.6625 |
| - | - | - | - | -0.8 | - | - | 1.7099 | 0.4805 | 0.5373 | 1.8576 | 0.1802 | 0.6126 |
| - | - | - | - | 0.4 | 0.0 | - | 5.2882 | 0.7312 | 0.5182 | 5.5471 | 0.2354 | 0.6092 |
| - | - | - | - |  | 0.4 | - | 3.9175 | 0.7440 | 0.6720 | 4.2297 | 0.2397 | 0.7713 |
| - | - | - | - | - | 0.8 | - | 2.4852 | 0.7557 | 0.8190 | 2.8456 | 0.2437 | 0.9257 |
| - | - | - | - | - | 0.4 | 0.0 | 3.9175 | 1.7618 | 0.6720 | 4.2297 | 0.4469 | 0.7713 |
| - | - | - | - | - | - | 0.4 | 3.9175 | 0.7440 | 0.6720 | 4.2297 | 0.2397 | 0.7713 |
| - | - | - | - | - | - | 0.8 | 3.9175 | 0.4716 | 0.6720 | 4.2297 | 0.1638 | 0.7713 |

## 7.3.3 Graphical results

Figs. (7.2-7.10) show the impacts of solid nanoparticle volume fraction of copper particle $\Phi_2$, dimension less parameter $R_0$, curvature parameter $K_1$, micropolar parameter $K$, stretching parameter $\alpha$, suction parameter ($S < 0$), injection parameter ($\gamma > 0$) and $M$ on the $\Theta(\zeta)$ for the both models Yamada Ota and Xue models while Prandtl number ($Pr = 6.2$) and solid nanoparticle of $Al_2O_3$ ($\Phi_1 = 0.1$) are fixed. Figs. (7.2-7.3) show the impact of the solid nanoparticle of copper ($\Phi_2$) on $\Theta(\zeta)$. The effects of Yamada and Ota model, and Xue model for $Cu - Al_2O_3/H_2O$ and $Cu/H_2O$ are highlighted on the $\Theta(\zeta)$. It is seen that $Cu - Al_2O_3/H_2O$ gain higher heat transfer than that of $Cu/H_2O$ for both models. Fig. (7.4) reveals the impacts of $K$ on the $\Theta(\zeta)$. It is noted that Yamada Ota model of the $Cu - Al_2O_3/H_2O$ has better heat transfer rate as compared to Xue model of the $Cu - Al_2O_3/H_2O$. It is also seen that the curvature parameter ($K$) rises for growing the $\Theta(\zeta)$. The impacts of micropolar parameter $K$ on the $\Theta(\zeta)$ are revealed in Fig. (7.5) for the Yamada Ota and Xue models of the Hybrid

nanomaterial fluid. The temperature profile decreases as micropolar parameter $(K)$ increases. Yamada and Ota model of the Hybrid nanofluid achievements greater heat transfer as compared to the Xue model of the Hybrid nanomaterial fluid. Figs. (7.6-7.7) depict the impacts of $M$ and dimensionless parameter $(R_0)$ on $\Theta(\zeta)$. It is revealed that thermal slip parameter improves as temperature profile declines. The boundary layer thickness improves as increasing the thermal slip parameter $(M)$ and dimensionless parameter $(R_0)$. Figs. (7.8-7.9) are emphasized the impressions of suction parameter $(S < 0)$, injection parameter $(S > 0)$ and stretching parameter $(\alpha)$ on the temperature function. Physical parameters $S$ and $\alpha$ are improved with the increased in the temperature profile for both models. For the Xue model of the hybrid nanomaterial fluid, the case of injection parameter $(S > 0)$ gains higher boundary layer thickness than that of suction parameter $(S < 0)$. Fig. (7.10) shows the impact of solid particle of copper $\Phi_2$ on the temperature profile. Both temperature profile as solid particle of copper $\Phi_2$ find to be increasing behavior for the Yamada and Ota model of the Hybrid nanomaterial fluid and Xue model of the Hybrid nanomaterial fluid.
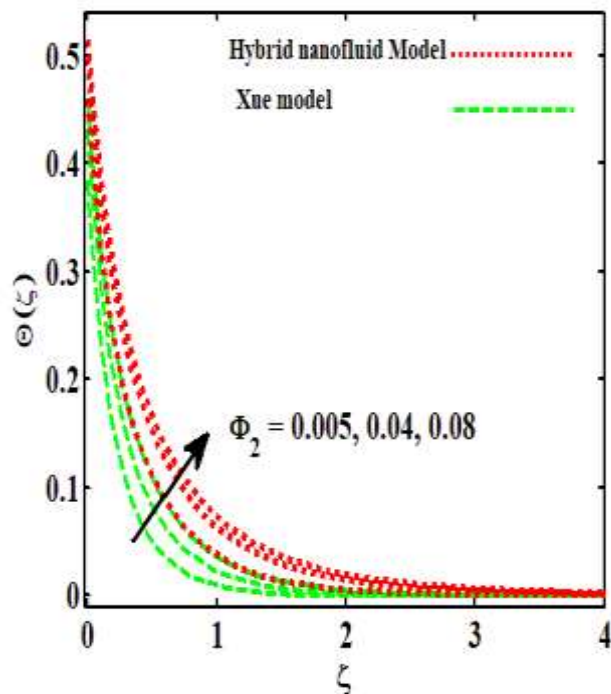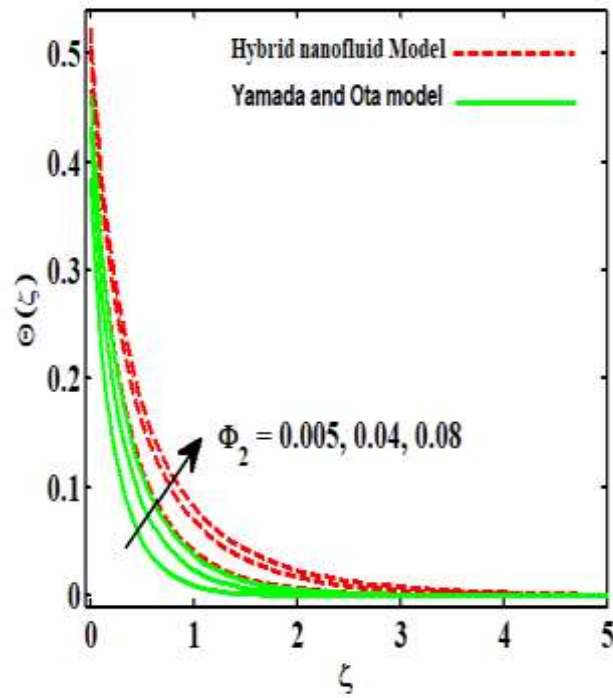
**Fig. 7.2**



80

**Fig. 7.3**



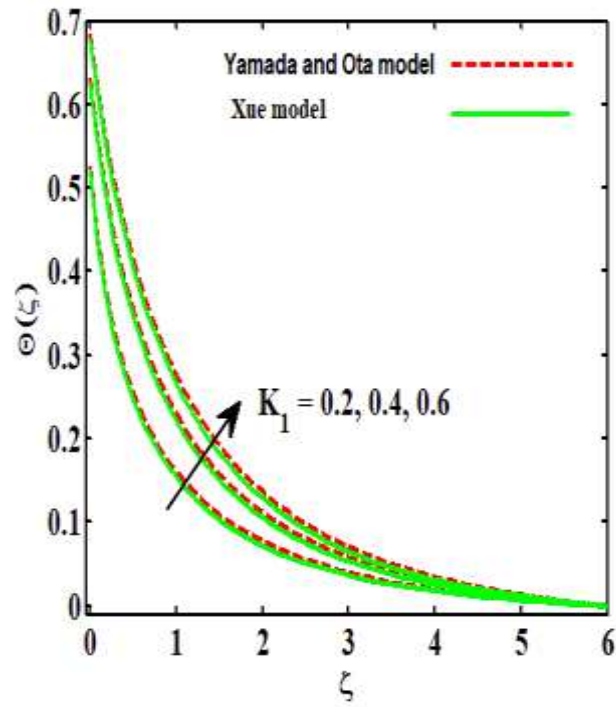**Comparative results of nanofluids and Hybrid fluids model.**
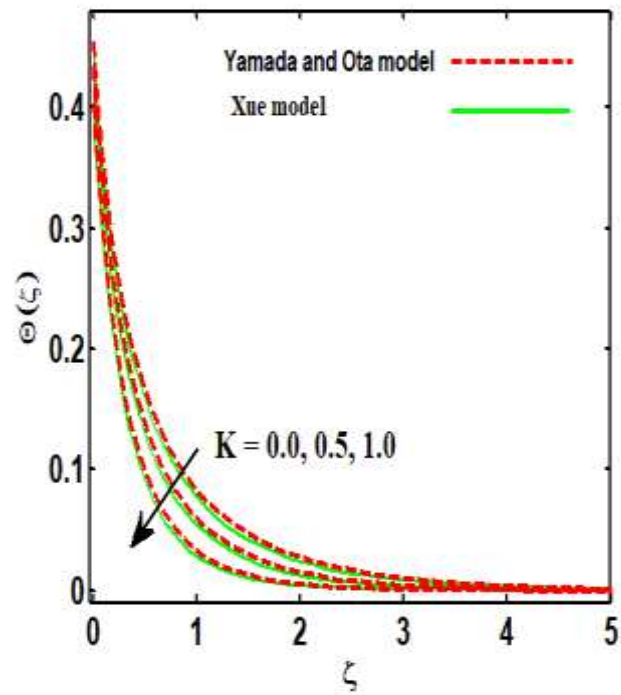
**Fig. 7.4**



**Fig. 7.5**



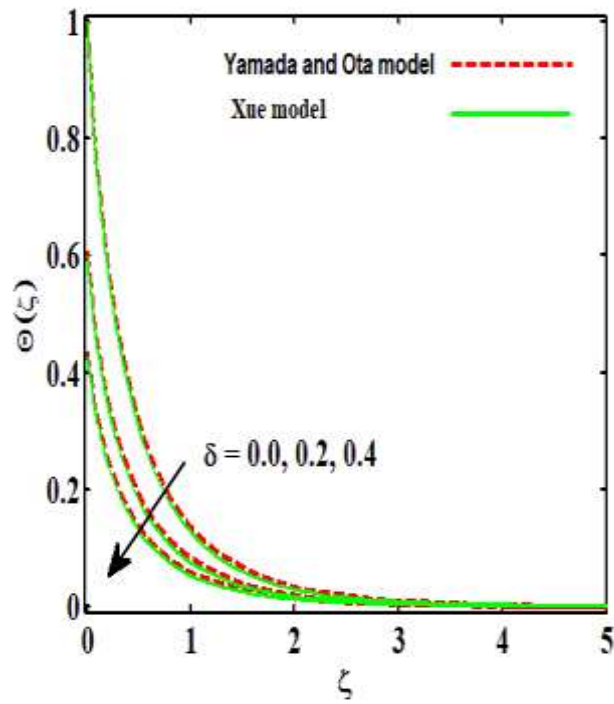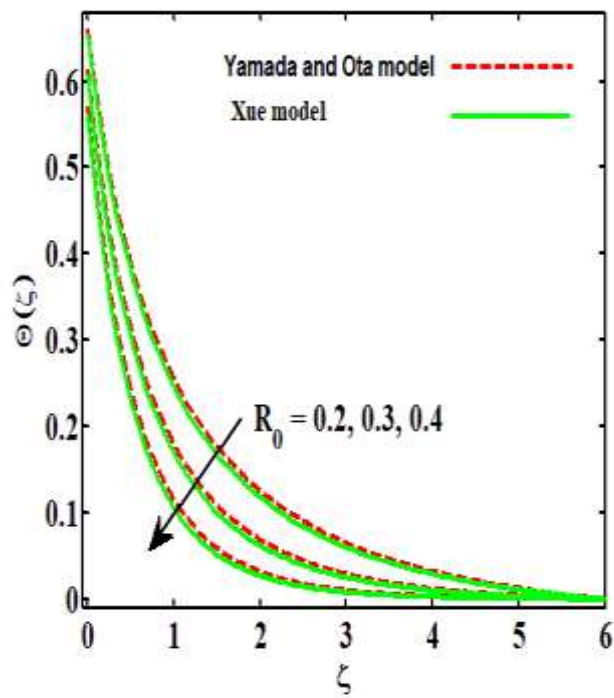**Effects of curvature parameter and micropolar parameter on $\Theta(\zeta)$.**

**Fig. 7.6**



**Fig. 7.7**



**Influence of thermal slip parameter and dimensionless parameter on $\Theta(\zeta)$.**
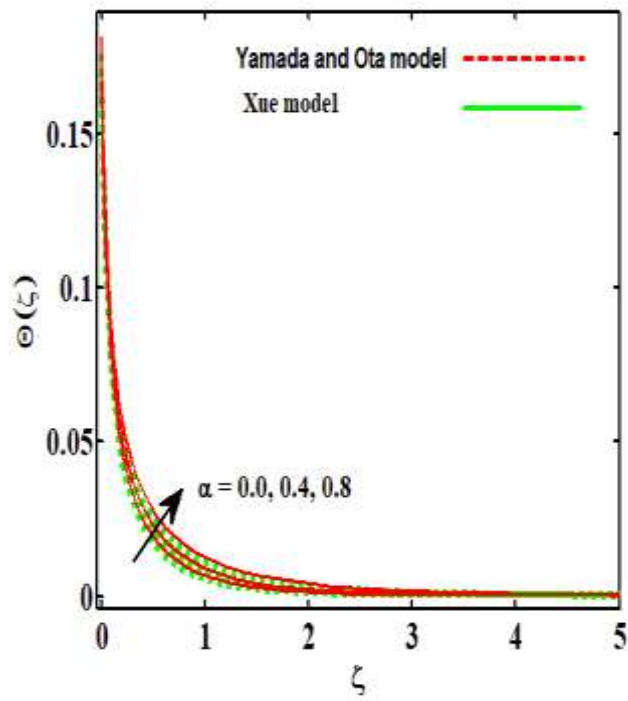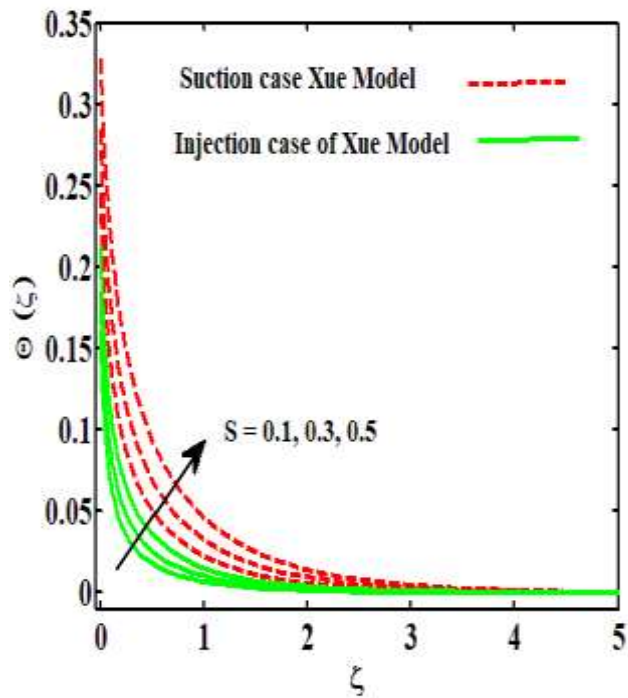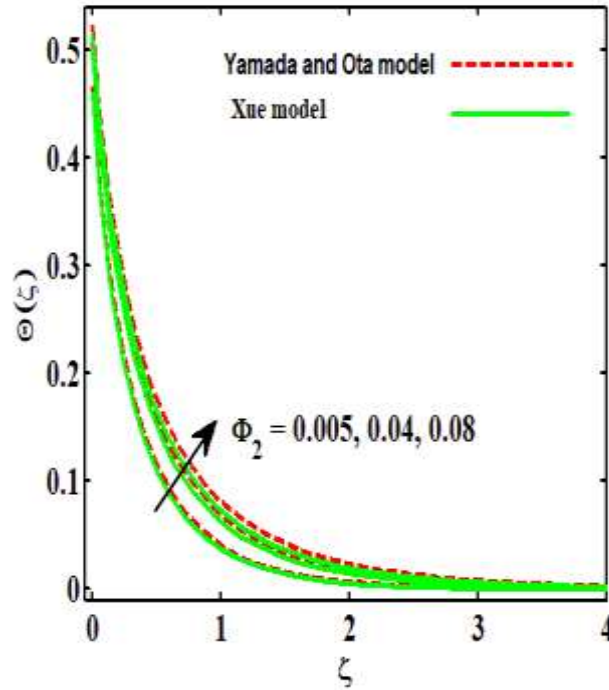
**Fig. 7.8**



**Fig. 7.9**



**Impacts of stretching parameter and $S > 0$/ $S < 0$ on $\Theta(\zeta)$.**

**Fig. 7.10**



Comparative results of Yamada and Ota model with Xui model of Hybrid nanofluids.

## 7.8 Final remarks

A steady flow of micropolar Hybrid nanofluid over permeable curved nonlinear stretching surface is analyzed. Two models of Hybrid nanofluid, namely, Yamada and Ota model, and Xue model are discussed for the above flow. For the various physical parameters, significant findings are illuminated like as solid nanoparticle volume fraction of copper particle $\Phi_2$, dimension less parameter $R_0$, curvature parameter $K$, micropolar parameter $K_1$, stretching parameter $\alpha$, suction parameter $(S < 0)$, injection parameter $(S > 0)$ and thermal slip parameter $M$. Some key points of the above discussion are:

- The Yamada and Ota model of the $Cu - Al_2O_3/H_2O$ gain higher heat transfer rate as compared to Xue model of the $Cu - Al_2O_3/H_2O$ on the $\Theta(\zeta)$.
- In the both cases, the injection parameter $(S > 0)$ gains higher thermal boundary layer thickness than that of suction parameter $(S < 0)$.
- It is perceived that the skin friction having opposite behavior to note for the Nusselt number and couple stress for the both cases of $Cu - Al_2O_3/H_2O$ and $Cu/H_2O$.
- The present review offers a clear understanding of the decay.

**Chapter 08**

**On extended version of Yamada-Ota and Xue models of hybrid nanofluid on moving needle**

## 8.1 Introductions

In this chapter, the study of extended description of Xue and Yamada-Ota models for Hybrid nanomaterial fluid is discussed and analyzed on the needle stretching surface. The temperature dependent viscosity and thermal conductivity are taken in this chapter. Two different nanoparticles are discussed, namely: $SWCNT$ and $MWCNT$ with base fluid pure water. The system under the flow assumptions are developed and dimensionlized through similarity transformations. Furthermore, the results of the dimensionless system are built through the a numerical procedure. The effects of the governing parameters are discussed through tables and graphs.
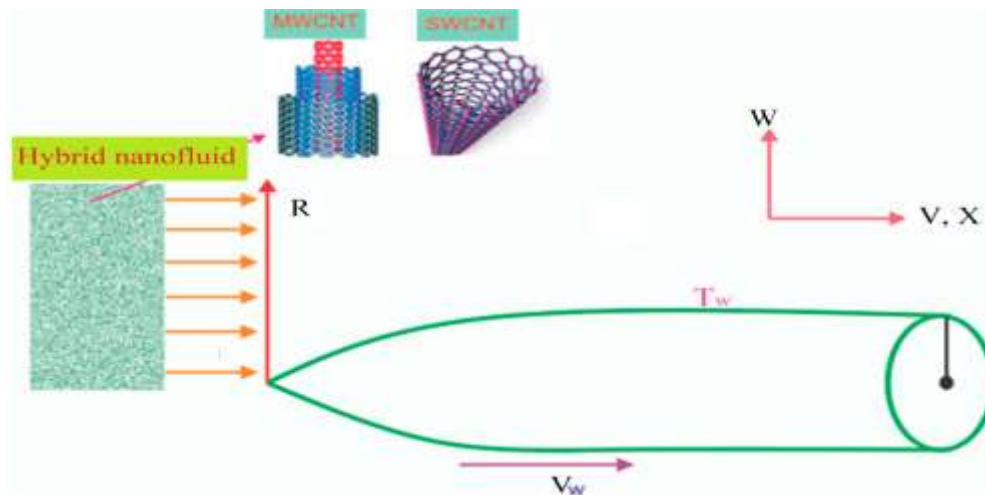


**Fig. 8.1:** Flow of Hybrid nanofluid.

## 8.2 Mathematical formulation

The Hybrid nanofluid flow of variable thermal conductivity and viscosity at thin needle are debated. Even the thin needle is engaged as a continuous movement that is revealed in Fig. 8.1. Two forms of nanoparticles are studied in the Yamada and Ota and Xue Hybrid nanomaterial fluid models. The radius of the cylinder needle is considered to be set in the horizontal direction as $R = r(X)$, where $R$ and $X$ are the radial and axial coordinates measuring the $X$-

axis from the leading edge of the needle. When the needle is assumed to become as thin, the importance of its transverse curvature is significant, while the pressure gradient is ignored in the direction of the body. In addition, constant and ambient temperatures are both considered, correspondingly $T_w$ and $T_\infty$, where, $T_w > T_\infty$. The flow model is defined as

$$\vec{\nabla}.\vec{V} = 0, \tag{8.1}$$

$$\vec{\nabla}P + (\vec{V}.\vec{\nabla})\vec{V} + \rho\left(\frac{\partial\vec{V}}{\partial t}\right) = K\vec{\nabla}\times\vec{\Omega} + \vec{\nabla}(\mu\vec{\nabla}\vec{V}) + \sigma(\vec{J}\times\vec{B}), \tag{8.2}$$

$$\rho c_p\left((\vec{V}.\vec{\nabla})\vec{T} + \left(\frac{\partial\vec{T}}{\partial t}\right)\right) = \vec{\nabla}(K\vec{\nabla}.\vec{T}). \tag{8.3}$$

By means of the boundary layer approximations, mathematical model in the form of differential equations is writen as:

$$\frac{\partial}{\partial X}(RV) + \frac{\partial}{\partial R}(RW) = 0, \tag{8.4}$$

$$\left(V\frac{\partial V}{\partial R} + W\frac{\partial V}{\partial X}\right) = \frac{\rho_f}{\rho_{hnf}}\frac{1}{R}\frac{\partial}{\partial R}\left(\mu_{hnf}R\frac{\partial V}{\partial R}\right) - \sigma_{hnf}B_0{}^2V, \tag{8.5}$$

$$\left(W\frac{\partial T}{\partial X} + V\frac{\partial T}{\partial R}\right) = \frac{1}{R}\frac{\partial}{\partial R}\left(\alpha_{hnf}R\frac{\partial T}{\partial R}\right), \tag{8.6}$$

with the boundary conditions

$$V(X,R) = V_w, \qquad W(X,R) = 0, \quad T = T_w + \lambda_1\frac{k_{hnf}}{k_f}\left(\frac{\partial T}{\partial R}\right), \quad \text{at } R \to r(X),$$

$$V(X,R) \to V_\infty, \quad T \to T_\infty, \text{ at } R \to \infty. \tag{8.7}$$

The thermo physical characteristics are defined as

$$\rho_{hnf} = \Phi_2\rho_{s_2} + \{\Phi_1\rho_{s_1} + (1 - \Phi_1)\rho_f(1 - \Phi_2)\},$$

$$(\rho C_p)_{hnf} = \Phi_2\rho(\rho C_p)_{s_2} + \left[\Phi_1(\rho C_p)_{s_1} + \{(1 - \Phi_2)(\rho C_p)_f(1 - \Phi_1)\}\right],$$

$$\mu_{hnf} = \frac{\mu_f}{(1 - \Phi_2)^{2.5}(1 - \Phi_1)^{2.5}},$$

$$\frac{\kappa_{hnf}}{\kappa_{bf}} = \frac{(n - 1)\kappa_{bf} + \kappa_{s_2} - (\kappa_{bf} - \kappa_{s_2})(n - 1)\Phi_2}{(n - 1)\kappa_{bf} + \kappa_{s_2} + (\kappa_{bf} - \kappa_{s_2})\Phi_2}, \text{where}$$

$$\frac{\kappa_{bf}}{\kappa_f} = \frac{(n - 1)\kappa_f + \kappa_{s_1} - (\kappa_f - \kappa_{s_1})(n - 1)\Phi_1}{(n - 1)\kappa_f + \kappa_{s_1} + (\kappa_f - \kappa_{s_1})\Phi_1}.$$

| Thermo-physical properties | Fluid phase (water) | SWCNT | MWCNT |
|---|---|---|---|
| $C_p(j/kg)K$ | 4179 | 425 | 796 |
| $\rho(kg/m^3)$ | 997.1 | 2600 | 1600 |
| $k(W/mK)$ | 0.613 | 6600 | 3000 |

Introducing the following axisymmetric similarity transformation as

$$\frac{T - T_\infty}{T_w - T_\infty} = \Theta(\zeta), \quad \zeta = \frac{V_0 R^2}{a v_f X}, \quad \Psi = v_f X F(\zeta). \tag{8.8}$$

Applying the above transformations, we have

$$\frac{\rho_f}{\rho_{hnf}} \left(\frac{\mu_{hnf}}{\mu_f}\right) \left[\frac{F''(\zeta)}{1 - \frac{\Theta(\zeta)}{\Theta_e}} + \frac{\zeta F''(\zeta)\Theta'(\zeta)}{\Theta_e \left(1 - \frac{\Theta(\zeta)}{\Theta_e}\right)^2} + \frac{\zeta F'''(\zeta)}{1 - \frac{\Theta(\zeta)}{\Theta_e}}\right] + F(\zeta)F'(\zeta)$$

$$- \left(\frac{\rho_f}{\rho_{hnf}}\right) MF'(\zeta) = 0, \tag{8.9}$$

$$2\alpha_{hnf}(\zeta(1 + \varepsilon\Theta(\zeta))\Theta''(\zeta) + \varepsilon(\Theta'(\zeta))^2 + (1 + \varepsilon\Theta(\zeta))\Theta'(\zeta)) + F(\zeta)\Theta'(\zeta) = 0, \tag{8.10}$$

dimensionless boundary conditions are

$$F(c) = \gamma c/2, \quad F'(c) = \gamma/2, \quad F'(\infty) = (1 - \gamma)/2,$$

$$\Theta(c) = 1 + \lambda \frac{k_{hnf}}{k_f}\Theta'(c), \qquad \Theta(\infty) = 0. \tag{8.11}$$

The velocity ratio parameter represented as $\gamma = \frac{V_w}{V_0}$. If in a flowing fluid called Blassius flow, $\gamma = 0$ reflects a needle (fixed) and when $\gamma = 1$ relates to a fixed needle flowing in a quiescent fluid called Sakiadis flow. Because the fluid and needle are travelling in a certain path whenever $0 < \gamma < 1$. If $\gamma < 0$, then free stream direction is in positive X-axis and $\gamma > 1$, then free stream direction is in the negative X-axis, while the needle moves along the positive X-direction. But, we reflected the case $\gamma \leq 1$, its mean that the free stream direction is always in the positive direction. Physical parameters are defined

$$C_f = \frac{\tau_{RX}}{\rho_{hnf} V_w^2}, \quad N_{VX} = \frac{X q_w}{k_{hnf}(T_w - T_\infty)}. \tag{8.12}$$

where, $\tau_{RX}$ is shear stress and $q_w$ is heat flux defined as

$$\tau_{rs} = \left(\frac{1}{(1 - \Phi_2)^{\frac{5}{2}}(1 - \Phi_1)^{\frac{5}{2}}}\right) \left(\frac{\partial V}{\partial R}\right)_{R=c}, \tag{8.13}$$

$$q_w = -k_{hnf} \left(\frac{\partial T}{\partial R}\right)_{R=c}, $$

$$Re_s^{1/2} C_f = \left(\frac{4\sqrt{c}}{(1 - \Phi_2)^{5/2}(1 - \Phi_1)^{5/2}}\right) F''(c), \tag{8.14}$$

$$Re_s^{1/2} N_{u_s} = -2\sqrt{c}\frac{k_{hnf}}{k_f}\Theta'(c), \tag{8.15}$$

where, $Re_X = \left(\frac{V_0 X}{v_f}\right)$ is the local Reynold number.

## 8.3 Hybrid nanomaterial fluid models

The Yamada and Ota model of nanofluid [53] and the extended Yamada and Ota model of

nanofluid into the Hybrid nanomaterial fluid are presented as.

$$\frac{k_{hnf}}{k_{bf}} = \frac{1 + \frac{k_{bf}}{k_{s_2}}\frac{L}{R}\Phi_2{}^{0.2} + \left(1 - \frac{k_{bf}}{k_{s_2}}\right)\Phi_2\frac{L}{R}\Phi_2{}^{0.2} + 2\Phi_2\left(\frac{k_{s_2}}{k_{s_2} - k_{bf}}\right)\ln\left(\frac{k_{s_2} + k_{bf}}{2k_{s_2}}\right)}{1 - \Phi_2 + 2\Phi_2\left(\frac{k_{bf}}{k_{s_2} - k_{bf}}\right)\ln\left(\frac{k_{s_2} + k_{bf}}{2k_{bf}}\right)}, \quad (8.16)$$

$$\frac{k_{bf}}{k_f} = \frac{1 + \frac{k_f}{k_{s_1}}\frac{L}{R}\Phi_1{}^{0.2} + \left(1 - \frac{k_f}{k_{s_1}}\right)\Phi_1\frac{L}{R}\Phi_1{}^{0.2} + 2\Phi_1\left(\frac{k_{s_1}}{k_{s_1} - k_f}\right)\ln\left(\frac{k_{s_1} + k_f}{2k_{s_1}}\right)}{1 - \Phi_1 + 2\Phi_1\left(\frac{k_f}{k_{s_1} - k_f}\right)\ln\left(\frac{k_{s_1} + k_f}{2k_f}\right)}, \quad (8.17)$$

here, length and radius of the nanotube are L and R. Hybrid nanomaterial fluid of Xue model is

$$\frac{k_{hnf}}{k_{bf}} = \frac{1 - \Phi_2 + 2\Phi_2\left(\frac{k_{s_2}}{k_{s_2} - k_{bf}}\right)\ln\left(\frac{k_{s_2} + k_{bf}}{2k_{bf}}\right)}{1 - \Phi_2 + 2\Phi_2\left(\frac{k_{bf}}{k_{s_2} - k_{bf}}\right)\ln\left(\frac{k_{s_2} + k_{bf}}{2k_{bf}}\right)}, \quad (8.18)$$

$$\frac{k_{bf}}{k_f} = \frac{1 - \Phi_1 + 2\Phi_1\left(\frac{k_{s_1}}{k_{s_1} - k_f}\right)\ln\left(\frac{k_{s_1} + k_f}{2k_f}\right)}{1 - \Phi_1 + 2\Phi_1\left(\frac{k_f}{k_{s_1} - k_f}\right)\ln\left(\frac{k_{s_1} + k_f}{2k_f}\right)}. \quad (8.19)$$

The significant results for different physical parameters of the above models are analyzed through a numerical scheme and the obtained results are discussed in the coming section.

## 8.4 Results and discussion

The reduced dimensionless system Eqs. (8.9-8.10) having boundary conditions (8.11) is analyzed numerically. Physical effects on the flow behavior are discussed through graphs and tables. Table 8.6 indicates the best relation with system BVP4C and system of 4th order Runge Kutta.

### 8.4.1 Solid nanoparticle effects ($\Phi_2$)

The impression of the $\Phi_2$ is distinguished on the temperature and velocity distributions which are emphasized in the Figs. 8.2 and 8.3. On the velocity and temperature profile, we describe two models, Xue and Yamada-Ota models of Hybrid nanomaterial fluid. It is prominent that the velocity profile improves with the $\Phi_2$ increments as shown in Fig. 8.2. The momentum conductivity of the hybrid nanofluid that enhances due to the rise in the thickness of the momentum boundary layer. Since the viscosity parameters of base fluid hybrid nanoparticles increases for high values of solid nanoparticles that are provided higher fluid motion resistant. The influence of $\Phi_2$ on the temperature function is shown in Fig. 8.3. With higher values of solid nanoparticle $\Phi_2$, the temperature profile declines due to the rise of thermal conductivity

of Hybrid nanomaterial fluid, thus decreased the thickness of the thermal boundary layer.
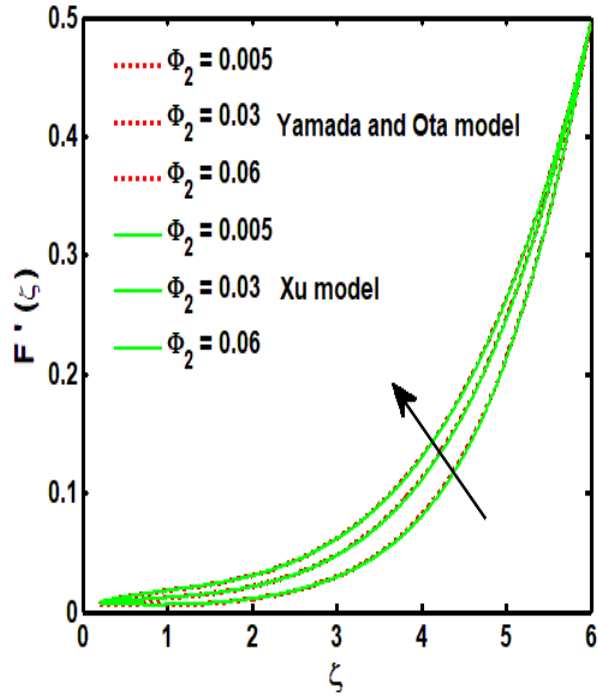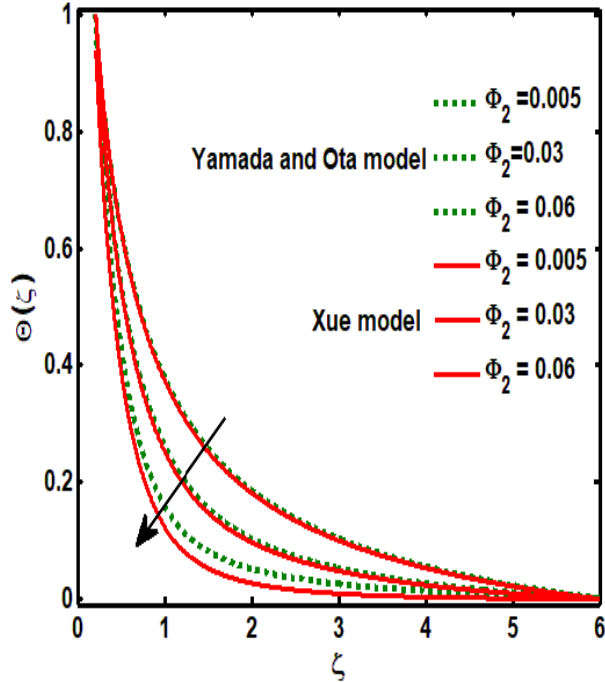
**Fig. 8.2**



**Fig. 8.3**



Influence of $\Phi_2$ on the $F'(\zeta)$ and $\Theta(\zeta)$.

Compared to the Xue model of the Hybrid nanomaterial fluid, the significant outcomes, achieve as our interest in this topic, Yamada-Ota model gains enhanced heat transfer rate. The

influences of the solid nanoparticle $\Phi_2$ on the $Re_s^{1/2}C_f$ and $Re_s^{1/2}N_{u_s}$ are seen in Table 8.1. It is seen that $Re_s^{1/2}C_f$ and $Re_s^{1/2}N_{u_s}$ decrease for the increasing in $\Phi_2$ in both cases $SWCNT - MWCNT/Water$ and $MWCNT/Water$.

**Table 8.1: Computational analysis of Xue and Yamada-Ota models of $SWCNT - MWCNT/Water$ and $MWCNT/Water$.**

| | $SWCNT - MWCNT/Water$ | | | | $MWCNT/Water$ | | | |
|---|---|---|---|---|---|---|---|---|
| | Xue model | | Yamada-Ota model | | Xue model | | Yamada-Ota model | |
| $\Phi_2$ | $Re_s^{1/2}C_f$ | $Re_s^{1/2}N_{u_s}$ | $Re_s^{1/2}C_f$ | $Re_s^{1/2}N_{u_s}$ | $Re_s^{1/2}C_f$ | $Re_s^{1/2}N_{u_s}$ | $Re_s^{1/2}C_f$ | $Re_s^{1/2}N_{u_s}$ |
| 0.005 | 0.5632 | 0.1515 | 0.5625 | 0.1450 | 0.3710 | 0.9153 | 0.3710 | 0.9109 |
| 0.02 | 0.5524 | 0.0910 | 0.5513 | 0.0854 | 0.3648 | 0.6385 | 0.3645 | 0.6293 |
| 0.04 | 0.5402 | 0.0521 | 0.5389 | 0.0481 | 0.3585 | 0.4435 | 0.3582 | 0.4337 |
| 0.06 | 0.5304 | 0.0329 | 0.5291 | 0.0300 | 0.3537 | 0.3305 | 0.3534 | 0.3214 |
| 0.08 | 0.5225 | 0.0221 | 0.5214 | 0.0201 | 0.3498 | 0.2564 | 0.3495 | 0.2482 |

## 8.4.2 Thermal slip Imapcts ($\delta$)

The effects of $\delta$ on the velocity and temperature functions are depicted in Figs. 8.4-and 8.5. The velocity profile increases with the $\delta$ which is revealed in Fig. 8.4. The Hybrid nanofluid Yamada-Ota model receives larger levels than the Hybrid nanofluid Xue model that is depicted in Fig. 8.4. The influence of $\delta$ on the temperature function is illustrated in the Fig. 8.5. For large thermal slip parameter values, the temperature profile decays. The Hybrid nanofluid Yamada-Ota model achieves heat transfer larger than the Hybrid nanofluid Xue model. It can also be interpreted that a boost in the $\delta$ induces a strict decrease in the temperature for a given value of $c$. The Yamada-Ota Hybrid nanofluid model obtains a thermal boundary layer much better than that of the Xue Hybrid nanofluid model. Table 8.2 displays the effects of $\delta$ on the $Re_s^{1/2}C_f$ and $Re_s^{1/2}N_{u_s}$. $Re_s^{1/2}C_f$ and $Re_s^{1/2}N_{u_s}$. For the $Re_s^{1/2}N_{u_s}$, the Hybrid nanomaterial fluid Xue model gains greater values than those of the Hybrid nanomaterial fluid Yamada-Ota model while the opposite results are gained for $Re_s^{1/2}C_f$.
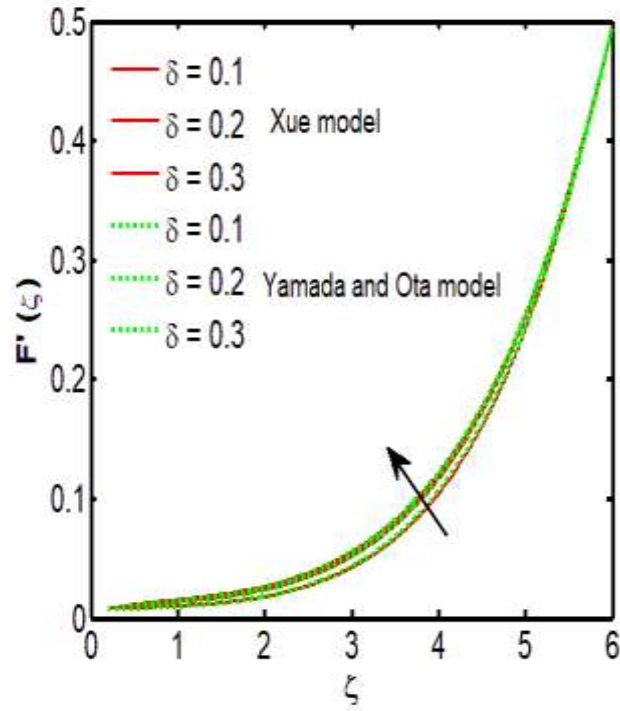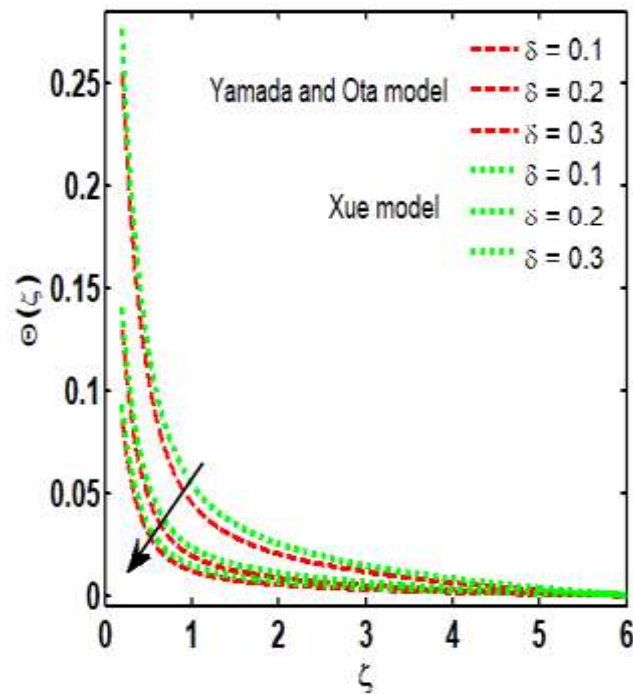
**Fig. 8.4**



**Fig. 8.5**



Influence of δ on the $F'(\zeta)$ and $\Theta(\zeta)$.

**Table 8.2: Numerical outcomes of Yamada-Ota and Xue models of $SWCNT -$ $MWCNT/Water$ and $MWCNT/Water$.**

| | $SWCNT - MWCNT/Water$ | | | | $MWCNT/Water$ | | | |
|---|---|---|---|---|---|---|---|---|
| | Xue model | | Yamada-Ota model | | Xue model | | Yamada-Ota model | |
| $\delta$ | $Re_s^{1/2}C_f$ | $Re_s^{1/2}N_{u_s}$ | $Re_s^{1/2}C_f$ | $Re_s^{1/2}N_{u_s}$ | $Re_s^{1/2}C_f$ | $Re_s^{1/2}N_{u_s}$ | $Re_s^{1/2}C_f$ | $Re_s^{1/2}N_{u_s}$ |
| 0.0 | 1.0179 | 0.2449 | 1.0291 | 0.2401 | 0.4444 | 0.6050 | 0.4455 | 0.5955 |
| 0.1 | 0.5680 | 0.0885 | 0.5655 | 0.0825 | 0.3833 | 0.5141 | 0.3831 | 0.5042 |
| 0.2 | 0.5402 | 0.0521 | 0.5389 | 0.0481 | 0.3585 | 0.4435 | 0.3582 | 0.4337 |
| 0.3 | 0.5308 | 0.0368 | 0.5299 | 0.0339 | 0.3462 | 0.3882 | 0.3460 | 0.3787 |
| 0.4 | 0.5261 | 0.0284 | 0.5255 | 0.0261 | 0.3393 | 0.3443 | 0.3391 | 0.3353 |

## 8.4.3 Impacts of magnetic field (M)

The influences of $M$ are illustrated through the Figs. 8.6 - 8.7. It is interpreted that the velocity function indicates the declined curves for different values of $M$ as exposed in Fig. 8.6. Although, the Lorentz force is connected to the $M$, the quality of the physical parameter $M$ is determined. Futhermore, the velocity of fluid declines by increasing the magnetic field. The magnetic field uses generated Lorentz force which is capable to transport liquids as an active micro-mixing technology tool in the mixing developments. The Xue model achieves thicker momentum thickness than that of the Hybrid nanofluid model of Yamada-Ota. Fig. 8.6 also indicates the effect of the magnetic field parameter on the temperature profile. The thermal thickness increases as magnetic field parameter is boosted. Table 8.3 exposes the impressions of $M$ on the $Re_s^{1/2}C_f$ and $Re_s^{1/2}N_{u_s}$ for both cases of Yamada-Ota and Xue models of Hybrid nanomaterial fluid. The $Re_s^{1/2}C_f$ surges and $Re_s^{1/2}N_{u_s}$ decays for the greater values of $M$.
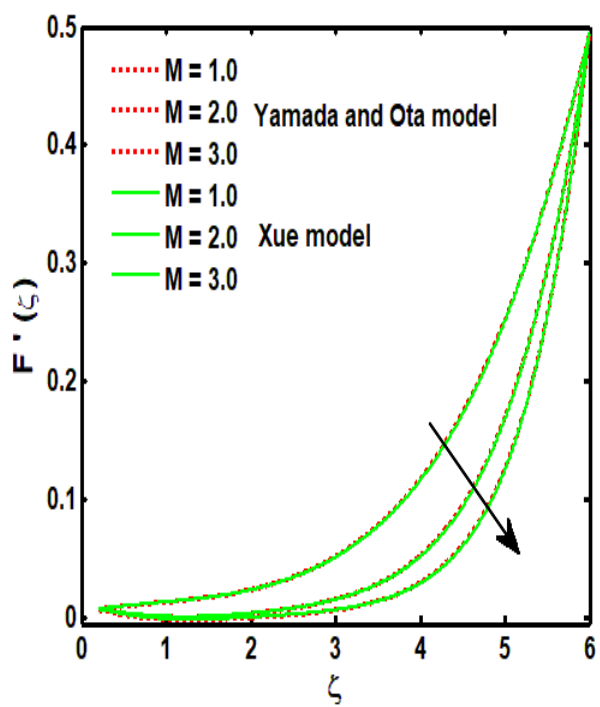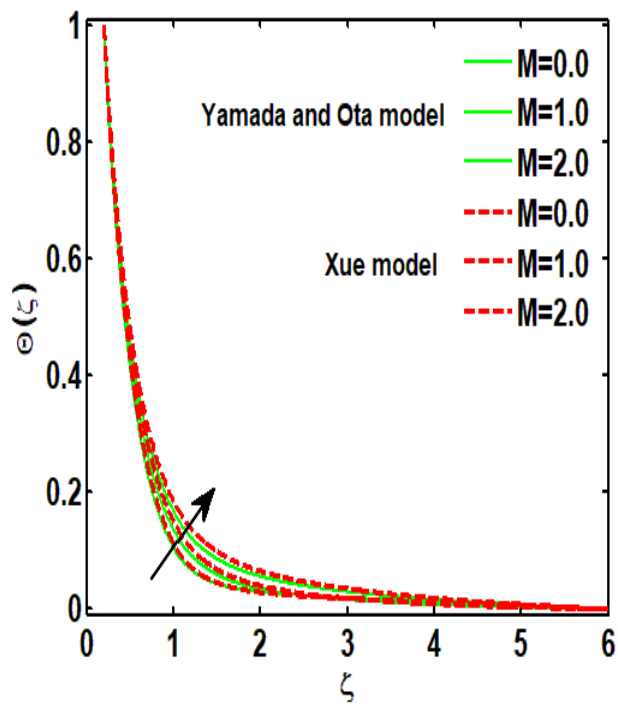
**Fig. 8.6**



**Fig. 8.7**

Influence of $M$ on the $F'(\zeta)$ and $\Theta(\zeta)$.

**Table 8.3: Numerical outcomes of Yamada-Ota model, and Xue model of $SWCNT - MWCNT/Water$ and $MWCNT/Water$.**

| | $SWCNT - MWCNT/Water$ | | | | $MWCNT/Water$ | | | |
| | Xue model | | Yamada-Ota model | | Xue model | | Yamada-Ota model | |
| M | $Re_s^{1/2}C_f$ | $R_s^{1/2}N_{u_s}$ | $Re_s^{1/2}C_f$ | $Re_s^{1/2}N_{u_s}$ | $Re_s^{1/2}C_f$ | $Re_s^{1/2}N_{u_s}$ | $Re_s^{1/2}C_f$ | $Re_s^{1/2}N_{u_s}$ |
|---|---|---|---|---|---|---|---|---|
| 0.0 | 0.0673 | 0.0527 | 0.0668 | 0.0486 | 0.0173 | 0.4787 | 0.0172 | 0.4682 |
| 0.5 | 0.3972 | 0.0523 | 0.3958 | 0.0483 | 0.2755 | 0.4489 | 0.2751 | 0.4390 |
| 1.0 | 0.5402 | 0.0521 | 0.5389 | 0.0481 | 0.3585 | 0.4435 | 0.3582 | 0.4337 |
| 1.5 | 0.6510 | 0.0520 | 0.6499 | 0.0480 | 0.4216 | 0.4402 | 0.4214 | 0.4304 |
| 2.0 | 0.7444 | 0.0519 | 0.7435 | 0.0479 | 0.4742 | 0.4378 | 0.4741 | 0.4280 |

### 8.4.4 Variable viscosity parameter effects ($\Theta_e$)

The influences of $\Theta_e$ on the velocity and temperature functions are illustrated through the Figs. 8.8 and 8.9 for the both cases of the Xue, and Yamada-Ota Hybrid nanofluid models. It is reported that for higher values of $\Theta_e$, the velocity function decreases and the temperature profile increases. This is due to the effects that horizontal rate of physical thickness reduces with an consistent increasing fluid parameter. Physically, this may be attributed to a higher temperature between the surface and the ambient fluid as well. The Xue Hybrid nanomaterial fluid model succeeds fast thermal thickness than those of the Yama-Ota Hybrid nanofluid model, but the momentum boundary layer is observed oppositely. Table 8.4 provide a comparison of $\Theta_e$ on $Re_s^{1/2}C_f$ and $Re_s^{1/2}N_{u_s}$. It is emphasized that $Re_s^{1/2}C_f$ augments while $Re_s^{1/2}N_{u_s}$ diminishes for the boost of $\Theta_e$ for the both models.
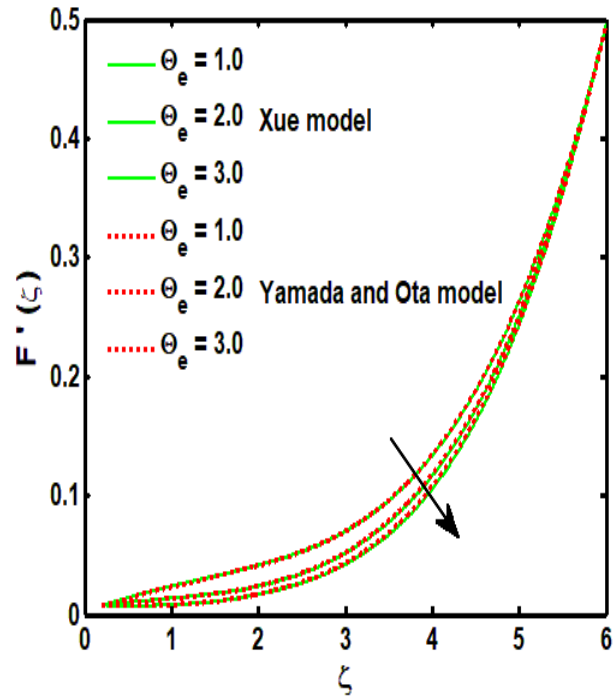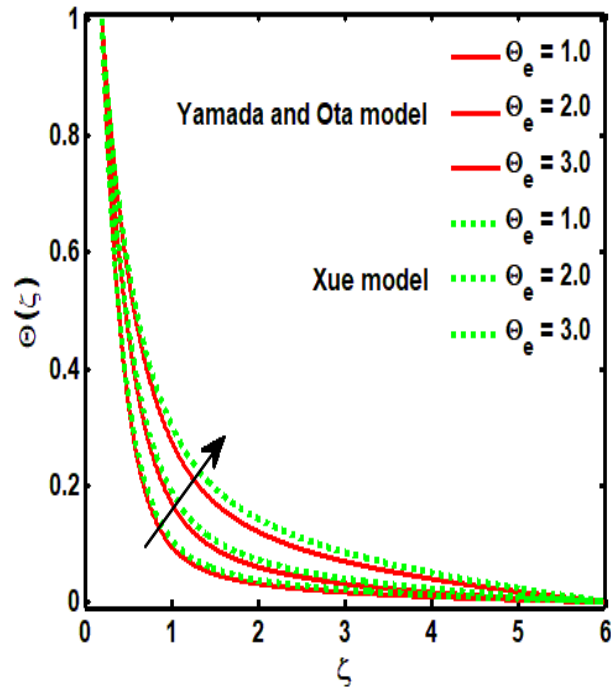
**Fig. 8.8**



**Fig. 8.9**



Influence of $\Theta_e$ on the $F'(\zeta)$ and $\Theta(\zeta)$.

**Table 8.4: Numerical outcomes of Yamada-Ota model, and Xue model of $SWCNT - MWCNT/Water$ and $MWCNT/Water$.**

| | $SWCNT - MWCNT/Water$ | | | | $MWCNT/Water$ | | | |
| | Xue model | | Yamada-Ota model | | Xue model | | Yamada-Ota model | |
| $\Theta_e$ | $Re_s^{1/2}C_f$ | $Re_s^{1/2}N_{u_s}$ | $Re_s^{1/2}C_f$ | $Re_s^{1/2}N_{u_s}$ | $Re_s^{1/2}C_f$ | $Re_s^{1/2}N_{u_s}$ | $Re_s^{1/2}C_f$ | $Re_s^{1/2}N_{u_s}$ |
|---|---|---|---|---|---|---|---|---|
| 0.01 | 0.7316 | 0.0509 | 0.5627 | 0.0467 | 0.3236 | 0.4289 | 0.3227 | 0.4195 |
| 0.5 | 0.0690 | 0.0527 | 0.0696 | 0.0486 | 0.1450 | 0.3392 | 0.0741 | 0.3319 |
| 1.0 | 0.2146 | 0.0526 | 0.2149 | 0.0485 | 0.1072 | 0.4625 | 0.1074 | 0.4523 |
| 1.5 | 0.3755 | 0.0524 | 0.3751 | 0.0483 | 0.2314 | 0.4514 | 0.2314 | 0.4415 |
| 2.0 | 0.5402 | 0.0521 | 0.5389 | 0.0481 | 0.3585 | 0.4435 | 0.3582 | 0.4337 |

## 8.4.5  Variable thermal conductivity parameter effects (ε)

The effects of thermal conductivity parameters are analyzed in the Fig. 8.10 for the both models of  Hybrid nanofluid. It is reported that for both Xue and Yamada-Ota models of Hybrid nanomaterial fluid, the temperature profile improves for enhancement in ε. The Xue hybrid nanofluid model succeeds a thermal boundary layer rather than that of the Yamada-Ota Hybrid nanofluid model. The warm thermal boundary layer is seen to generate energy, which increases the temperature profiles with the expansion in certain places in ε. Table 8.5 exposes the impressions of ε on $Re_s^{1/2}C_f$ and $Re_s^{1/2}N_{u_s}$. It is highlighted that $Re_s^{1/2}C_f$ enhances while $Re_s^{1/2}N_{u_s}$ reduces for increment of ε for all cases of Xue and Yamada-Ota models of Hybrid nanomaterial fluid.

**Fig. 8.10**



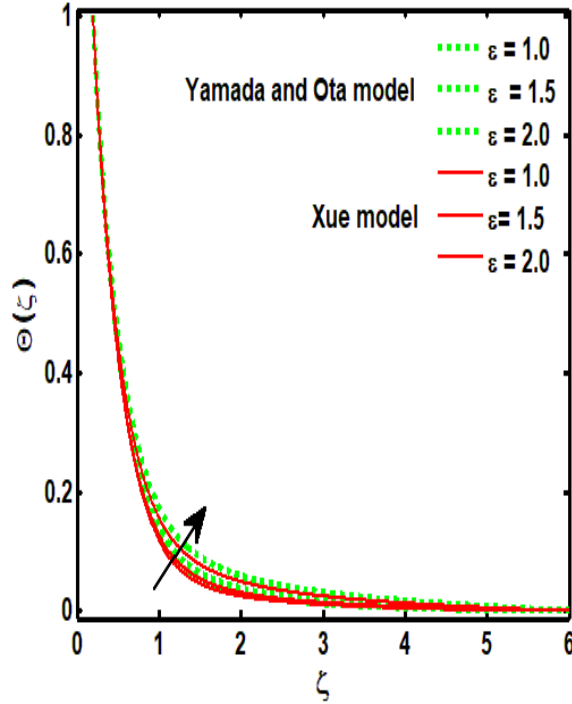Influence of ε on the $\Theta(\zeta)$.

**Table 8.5: Numerical outcomes of Yamada-Ota model, and Xue model of $SWCNT - MWCNT/Water$ and $MWCNT/Water$.**

| | $SWCNT - MWCNT/Water$ | | | | $MWCNT/Water$ | | | |
|---|---|---|---|---|---|---|---|---|
| | Xue model | | Yamada-Ota model | | Xue model | | Yamada-Ota model | |
| ε | $Re_s^{1/2}C_f$ | $Re_s^{1/2}N_{u_s}$ | $Re_s^{1/2}C_f$ | $Re_s^{1/2}N_{u_s}$ | $Re_s^{1/2}C_f$ | $Re_s^{1/2}N_{u_s}$ | $Re_s^{1/2}C_f$ | $Re_s^{1/2}N_{u_s}$ |
| 0.0 | 0.5392 | 0.0526 | 0.5380 | 0.0485 | 0.3654 | 0.4987 | 0.3649 | 0.4870 |
| 0.2 | 0.5396 | 0.0524 | 0.5384 | 0.0484 | 0.3629 | 0.4742 | 0.3625 | 0.4634 |
| 0.4 | 0.5400 | 0.0522 | 0.5387 | 0.0482 | 0.3600 | 0.4530 | 0.3597 | 0.4429 |
| 0.6 | 0.5403 | 0.0520 | 0.5391 | 0.0480 | 0.3569 | 0.4346 | 0.3566 | 0.4251 |
| 0.8 | 0.5407 | 0.0518 | 0.5394 | 0.0479 | 0.4346 | 0.4187 | 0.3535 | 0.4096 |

**Table 8.6: Comparison Runge Kutta 4th order method with bvp4c technique.**

| | BVP4C Method | | | | Runge Kutta 4th order method | | | |
|---|---|---|---|---|---|---|---|---|
| | Xue model | | Yamada-Ota model | | Xue model | | Yamada-Ota model | |
| $\Phi_2$ | $Re_s^{1/2}C_f$ | $Re_s^{1/2}N_{u_s}$ | $Re_s^{1/2}C_f$ | $Re_s^{1/2}N_{u_s}$ | $Re_s^{1/2}C_f$ | $Re_s^{1/2}N_{u_s}$ | $Re_s^{1/2}C_f$ | $Re_s^{1/2}N_{u_s}$ |
| 0.005 | 0.5632 | 0.1515 | 0.5625 | 0.1450 | 0.5589 | 0.1492 | 0.5593 | 0.1386 |
| 0.02 | 0.5524 | 0.0910 | 0.5513 | 0.0854 | 0.5496 | 0.0899 | 0.5478 | 0.0853 |
| 0.04 | 0.5402 | 0.0521 | 0.5389 | 0.0481 | 0.5369 | 0.0513 | 0.5311 | 0.0479 |
| 0.06 | 0.5304 | 0.0329 | 0.5291 | 0.0300 | 0.5291 | 0.0354 | 0.5243 | 0.0295 |
| 0.08 | 0.5225 | 0.0221 | 0.5214 | 0.0201 | 0.5187 | 0.01986 | 0.5168 | 0.0213 |

## 8.5 Final remarks

The Hybrid nanofluid flow with amagnetic field is examined at a surface of the moving needle for the Yamada-Ota, and Xue extended models. For the both models, different charactristics are compared in the above sections. The major outcomes are:

- Yamada-Ota Hybrid nanofluid model achieves higher values than that of Xue Hybrid nanofluid model for different values of $\Theta_e$ as in case of $Re_s^{1/2}C_f$.

- Yamada-Ota Hbrid nanofluid model achieves higher values than that of Xue Hybrid nanofluid model for different values of $\Theta_e$ as in case of $Re_s^{1/2}N_{u_s}$.

- $Re_s^{1/2}C_f$ and $Re_s^{1/2}N_{u_s}$ are diminished for the growing the values of $\Phi_2$ in both cases.

- The Yamada-Ota model is typically improving rapidly compared to the Hybrid nanofluid Xue model.

# References

1.  Crane, L. J. (1970). Flow past a stretching plate. *Zeitschrift für angewandte Mathematik und Physik ZAMP*, *21(4), 645-647.*

2.  Carragher, P., & Crane, L. J. (1982). Heat transfer on a continuous stretching sheet. *Zeitschrift Fuer Angewandte Mathematik und Mechanik, 62*(10),564-565.

3.  Wu, G. X. (2006). Numerical simulation of water entry of twin wedges. *Journal of Fluids and Structures*, *22(1), 99-108.*

4.  Haq, R. U., Nadeem, S., Akbar, N. S., & Khan, Z. H. (2015). Buoyancy and radiation effect on stagnation point flow of micropolar nanofluid along a vertically convective stretching surface. *IEEE Transactions on Nanotechnology, 14(1), 42-50.*

5.  Ramesh, K. (2016). Effects of slip and convective conditions on the peristaltic flow of couple stress fluid in an asymmetric channel through porous medium. *Computer Methods and Programs in Biomedicine*, *135, 1-14.*

6.  Ramesh, K. (2016). Influence of heat and mass transfer on peristaltic flow of a couple stress fluid through porous medium in the presence of inclined magnetic field in an inclined asymmetric channel. *Journal of Molecular Liquids*, *219, 256-271.*

7.  Gireesha, B. J., Mahanthesh, B., Gorla, R. S. R., & Manjunatha, P. T. (2016). Thermal radiation and Hall effects on boundary layer flow past a non-isothermal stretching surface embedded in porous medium with non-uniform heat source/sink and fluid-particle suspension. *Heat and Mass Transfer*, *52(4), 897-911.*

8.  Gireesha, B. J., Mahanthesh, B., & Krupalakshmi, K. L. (2017). Hall effect on two-phase radiated flow of magneto-dusty-nanoliquid with irregular heat generation/consumption. *Results in Physics*, *7, 4340-4348.*

9.  Mahanthesh, B. (2017). Hall effect on two-phase laminar boundary layer flow of dusty liquid due to stretching of an elastic flat sheet. *Mapana* Journal of Sciences, *16(3), 13-26.*

10. Gireesha, B. J., Mahanthesh, B., Thammanna, G. T., & Sampathkumar, P. B. (2018). Hall effects on dusty nanofluid two-phase transient flow past a stretching sheet using KVL model. *Journal of Molecular Liquids*, *256, 139-147.*

11. Gireesha, B. J., Mahanthesh, B., Makinde, O. D., & Muhammad, T. (2018). Effects of Hall current on transient flow of dusty fluid with nonlinear radiation past a convectively heated stretching plate. In *Defect and Diffusion Forum*, *387, 352-363.*

12. Shalini, G., & Mahanthesh, B. (2018). Rayleigh-Benard convection in a dusty Newtonian nanofluid with and without Coriolis force. *Journal of Nanofluids*, *7(6), 1240-1246.*

13. Ramesh, K., Tripathi, D., Bég, O. A., & Kadir, A. (2019). Slip and Hall current effects on Jeffrey fluid suspension flow in a peristaltic hydromagnetic blood micropump. *Iranian Journal of Science and Technology, Transactions of Mechanical Engineering, 43(4), 675-692.*

14. Mahanthesh, B., Shashikumar, N. S., Gireesha, B. J., & Animasaun, I. L. (2019). Effectiveness of Hall current and exponential heat source on unsteady heat transport of dusty TiO2-EO nanoliquid with nonlinear radiative heat. *Journal of Computational Design and Engineering*, *6(4), 551-561.*

15. Wakif, A., Chamkha, A., Animasaun, I. L., Zaydan, M., Waqas, H., & Sehaqui, R. (2020). Novel physical insights into the thermodynamic irreversibilities within dissipative EMHD fluid flows past over a moving horizontal riga plate in the coexistence of wall suction and joule heating effects: A comprehensive numerical investigation. *Arabian Journal for Science and Engineering*, *45(11), 9423-9438.*

16. Choi, S. U., & Eastman, J. A. (1995). Enhancing thermal conductivity of fluids with nanoparticles *(No. ANL/MSD/CP-84938; CONF-951135-29). Argonne National Lab., IL (United States).*

17. Lee, S., Choi, S. S., Li, S. A., & Eastman, J. A. (1999). Measuring thermal conductivity of fluids containing oxide nanoparticles. *Journal of Heat transfer, 121(2), 280-289.*

18. Das, S. K., Choi, S. U., Yu, W., & Pradeep, T. (2007). Nanofluids: science and technology. John Wiley & Sons.

19. Ellahi, R., Hassan, M., & Zeeshan, A. (2016). Aggregation effects on water base Al2O3— nanofluid over permeable wedge in mixed convection. *Asia-Pacific Journal of Chemical Engineering, 11(2), 179-186.*

20. Usman, M., Hamid, M., Zubair, T., Haq, R. U., & Wang, W. (2018). Cu-Al2O3/Water hybrid nanofluid through a permeable surface in the presence of nonlinear radiation and variable thermal conductivity via LSM. *International Journal of Heat and Mass Transfer, 126, 1347-1356.*

21. Sheikholeslami, M., Li, Z., & Shamlooei, M. (2018). Nanofluid MHD natural convection through a porous complex shaped cavity considering thermal radiation. *Physics Letters A, 382(24), 1615-1632.*

22. Ramesh, K. (2018). Effects of viscous dissipation and Joule heating on the Couette and Poiseuille flows of a Jeffrey fluid with slip boundary conditions. *Propulsion and Power Research*, *7(4), 329-341.*

23. Ramesh, K., Tripathi, D., & Bég, O. A. (2019). Cilia-assisted hydromagnetic pumping of biorheological couple stress fluids. *Propulsion and Power Research*, *8(3), 221-233.*

24. Zeeshan, A., Shehzad, N., Abbas, T., & Ellahi, R. (2019). Effects of radiative electro-magnetohydrodynamics diminishing internal energy of pressure-driven flow of titanium dioxide-water nanofluid due to entropy generation. *Entropy, 21(3), 236.*

25. Liu, H., Animasaun, I. L., Shah, N. A., Koriko, O. K., & Mahanthesh, B. (2020). Further discussion on the significance of quartic autocatalysis on the dynamics of water conveying 47 nm alumina and 29 nm cupric nanoparticles. *Arabian Journal for Science and Engineering, 45(7), 5977-6004.*

26. Suresh, S., Venkitaraj, K. P., Selvakumar, P., & Chandrasekar, M. (2011). Synthesis of Al2O3–Cu/water hybrid nanofluids using two step method and its thermo physical properties. *Colloids and Surfaces A: Physicochemical and Engineering Aspects, 388(1-3), 41-48.*

27. Suresh, S., Venkitaraj, K. P., Selvakumar, P., & Chandrasekar, M. (2012). Effect of Al2O3–Cu/water hybrid nanofluid in heat transfer. *Experimental Thermal and Fluid Science, 38, 54-60.*

28. Baghbanzadeh, M., Rashidi, A., Rashtchian, D., Lotfi, R., & Amrollahi, A. (2012). Synthesis of spherical silica/multiwall carbon nanotubes hybrid nanostructures and investigation of thermal conductivity of related nanofluids. *Thermochimica acta, 549, 87-94.*

29. Esfe, M. H., Arani, A. A. A., Rezaie, M., Yan, W. M., & Karimipour, A. (2015). Experimental determination of thermal conductivity and dynamic viscosity of Ag–MgO/water hybrid nanofluid. *International Communications in Heat and Mass Transfer, 66, 189-195.*

30. Hayat, T., & Nadeem, S. (2017). Heat transfer enhancement with Ag–CuO/water hybrid nanofluid. *Results in Physics, 7, 2317-2324.*

31. Muhammad, N., & Nadeem, S. (2017). Ferrite nanoparticles Ni-ZnFe2O4, Mn-ZnFe2O4 and Fe2O4 in the flow of ferromagnetic nanofluid. *The European Physical Journal Plus, 132(9), 377.*

32. Sheikholeslami, M. (2018). Application of Darcy law for nanofluid flow in a porous cavity under the impact of Lorentz forces. *Journal of Molecular Liquids, 266, 495-503.*

33. Ghalambaz, M., Doostani, A., Izadpanahi, E., & Chamkha, A. J. (2020). Conjugate natural convection flow of Ag–MgO/water hybrid nanofluid in a square cavity. *Journal of Thermal Analysis and Calorimetry*, *139(3), 2321-2336.*

34. Huminic, G., & Huminic, A. (2020). Entropy generation of nanofluid and hybrid nanofluid flow in thermal systems: A review. *Journal of Molecular Liquids*, *302, 112533.*

35. Eringen, A. C. (1964). Simple microfluids. *International Journal of Engineering Science, 2(2), 205-217.*

36. Abd-Alla, A. M., Abo-Dahab, S. M., & Al-Simery, R. D. (2013). Effect of rotation on peristaltic flow of a micropolar fluid through a porous medium with an external magnetic field. *Journal of Magnetism and Magnetic Materials, 348, 33-43.*

37. Rauf, A., Ashraf, M., Batool, K., Hussain, M., & Meraj, M. A. (2015). MHD flow of a micropolar fluid over a stretchable disk in a porous medium with heat and mass transfer. *AIP Advances, 5(7), 077156.*

38. Haq, R. U., Nadeem, S., Akbar, N. S., & Khan, Z. H. (2015). Buoyancy and radiation effect on stagnation point flow of micropolar nanofluid along a vertically convective stretching surface. *IEEE Transactions on Nanotechnology, 14(1), 42-50.*

39. Pal, D., & Mandal, G. (2017). Thermal radiation and MHD effects on boundary layer flow of micropolar nanofluid past a stretching sheet with non-uniform heat source/sink. *International Journal of Mechanical Sciences, 126, 308-318.*

40. Shah, Z., Islam, S., Gul, T., Bonyah, E., & Khan, M. A. (2018). The electrical MHD and Hall current impact on micropolar nanofluid flow between rotating parallel plates. *Results in Physics, 9, 1201-1214.*

41. Izadi, M., Mehryan, S. A. M., & Sheremet, M. A. (2018). Natural convection of CuO-water micropolar nanofluids inside a porous enclosure using local thermal non-equilibrium condition. *Journal of the Taiwan Institute of Chemical Engineers, 88, 89-103.*

42. Farooq, A. A., Tripathi, D., & Elnaqeeb, T. (2019). On the propulsion of micropolar fluid inside a channel due to ciliary induced metachronal wave. *Applied Mathematics and Computation, 347, 225-235.*

43. Rehman, K. U., Shahzadi, I., Malik, M. Y., Al-Mdallal, Q. M., & Zahri, M. (2019). On heat transfer in the presence of nano-sized particles suspended in a magnetized rotatory flow field. *Case Studies in Thermal Engineering, 100457.*

44. Rana, S., Nawaz, M., Saleem, S., & Alharbi, S. O. (2020). Numerical study on enhancement of heat transfer in hybrid nano-micropolar fluid. *Physica Scripta, 95(4), 045201.*

45. Howarth, L. (1951). CXLIV. The boundary layer in three dimensional flow.—Part II. The flow near a stagnation point. *The London, Edinburgh, and Dublin Philosophical Magazine and Journal of Science*, *42(335), 1433-1440.*

46. Dinarvand, S., Hosseini, R., Damangir, E., & Pop, I. (2013). Series solutions for steady three-dimensional stagnation point flow of a nanofluid past a circular cylinder with sinusoidal radius variation. *Meccanica, 48(3), 643-652.*

47. Navier, C. L. M. H. (1823). Mémoire sur les lois du mouvement des fluides. *Mémoires de l'Académie Royale des Sciences de l'Institut de France*, *6, 389-440.*

48. Wang, C. Y. (2006). Stagnation slip flow and heat transfer on a moving plate. *Chemical Engineering Science*, *61(23), 7668-7672.*

49. Wang, C. Y. (2002). Flow due to a stretching boundary with partial slip—an exact solution of the Navier–Stokes equations. *Chemical Engineering Science*, *57(17), 3745-3747.*

50. Sahoo, B., & Do, Y. (2010). Effects of slip on sheet-driven flow and heat transfer of a third grade fluid past a stretching sheet. *International Communications in Heat and Mass Transfer*, *37(8), 1064-1071.*

51. Abbas, Z., Naveed, M., & Sajid, M. (2016). Hydromagnetic slip flow of nanofluid over a curved stretching surface with heat generation and thermal radiation. *Journal of Molecular Liquids*, *215, 756-762.*

52. Noghrehabadi, A., Pourrajab, R., & Ghalambaz, M. (2012). Effect of partial slip boundary condition on the flow and heat transfer of nanofluids past stretching sheet prescribed constant wall temperature. *International Journal of Thermal Sciences*, *54, 253-261.*

53. Yamada, E., & Ota, T. (1980). Effective thermal conductivity of dispersed materials. *Wärme-und Stoffübertragung*, *13(1-2), 27-37.*

54. Xue, Q. Z. (2005). Model for thermal conductivity of carbon nanotube-based composites. *Physica B: Condensed Matter*, *368(1-4), 302-307.*

55. Wang, C. Y. (2008). Stagnation flow towards a shrinking sheet. *International Journal of Non-Linear Mechanics*, *43(5), 377-382.*

Theoretical analysis ofhybrid nanofluid flow by various stretching surfaces Abbas .

by Nadeem turnitin

From DRSM (DRSM L)

- Processed on 04-Mar-2021 10:47 PKT
- ID: 1523857908
- Word Count: 19330

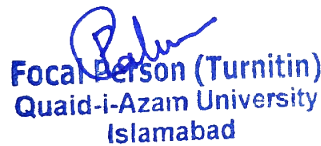Similarity Index
16%
Similarity by Source

Internet Sources:
    10%
Publications:
    13%
Student Papers:
    2%

Focal Person (Turnitin)
Quaid-i-Azam University
Islamabad

## sources:

**1** 1% match (Internet from 23-Jan-2021)
https://www.scilit.net/articles/search?offset=0&q=reference_ids%3A%28110732472%29

**2** < 1% match (Internet from 16-Jan-2021)
https://doaj.org/article/c21863d0aab04f5ea5ce3266af1c1a8d

**3** < 1% match (Internet from 05-Oct-2017)
http://prr.hec.gov.pk/Thesis/2927S.pdf

**4** < 1% match (publications)
Wang, C.Y.. "Stagnation flow on a plate with anisotropic slip", European Journal of Mechanics - B/Fluids, 2013.

**5** < 1% match (publications)
Wang, C.Y.. "Stagnation slip flow and heat transfer on a moving plate", Chemical Engineering Science, 200612

**6** < 1% match (publications)
Saeed Dinarvand, Reza Hosseini, Ebrahim Damangir, Ioan Pop. "Series solutions for steady three-dimensional stagnation point flow of a nanofluid past a circular cylinder with sinusoidal radius variation", Meccanica, 2012